

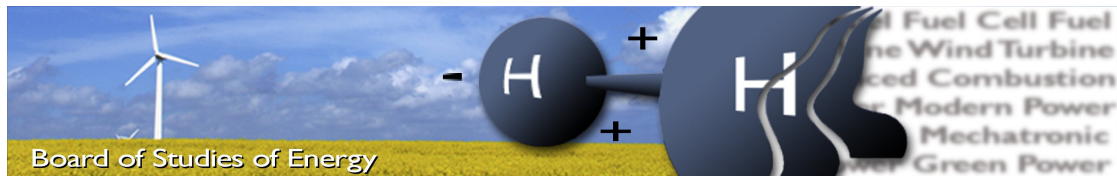
Development, Modelling and Implementation of an Electrical Drivetrain for a Go-Kart

Student Project Report
M.Sc. Energy Engineering - PED2-840

Group PED2-840
Jörgen Beer
Simon Jæger Nielsen
Mohamad Yamen Saad
Jesper Milver Nielsen
Edi Matijevic
Sakaria Omar Ahmad



AALBORG UNIVERSITY
STUDENT REPORT
Department of Energy Technology
May 2018



Title: Development, Modelling and Implementation of an electrical drivetrain for a Go-Kart
Semester: PED2 - M.Sc. Energy Engineering
Semester theme: Control of Power Electronic Systems
Project period: 06.02.18 to 28.05.18
ECTS: 15
Supervisor: Erik Schaltz and Enrique Rodriguez Diaz
Project group: PED2-840

Jörgen Beer

Simon Jæger Nielsen

Mohamad Yamen Saad

Jesper Milver Nielsen

Edi Matijevic

Sakaria Omar Ahmad

SYNOPSIS:

In today's modern world, electrical cars are becoming field of interest in the car industry. This is due to the advantages of using electrical drives compared to regular combustion engines. A crucial part of designing a electrical vehicle is the design and implementation of power electronics and motor drives. This project is build around designing inverter and the drive for a 7.3 kW, 24 V_{rms} induction motor which will be used to drive a small Go-Kart. Implementation and design of the hardware and software is done through simulation, test and validation. At the end, a 2-level inverter was designed and tested using different methods. The inverter is controlled by a MCU using space vector pulse width modulation technique.

Pages, total: 116

Appendix: 22

By accepting the request from the fellow student who uploads the study group's project report in Digital Exam System, you confirm that all group members have participated in the project work, and thereby all members are collectively liable for the contents of the report. Furthermore, all group members confirm that the report does not include plagiarism.

Contents

List of Abbreviations	VII
1. Project Formulation	1
1.1. Introduction	1
1.1.1. Initial problem	1
1.2. Problem analysis	2
1.3. Scope and project objectives	3
1.3.1. Methodology	3
1.4. System architecture	4
1.4.1. Block Definition	4
1.4.2. User interface	5
1.5. System requirements	6
1.5.1. Functional requirements	6
1.5.2. Performance requirements	6
1.6. Constraints	7
2. System analysis	8
2.1. Induction machine	8
2.2. Transmission	9
2.3. Encoder	10
2.4. Main supply batteries	11
2.4.1. Battery Testing	11
2.4.2. Approximation of Driving time	13
3. Modelling	17
3.1. Reference frame	17
3.2. Model of the Induction machine	18
3.2.1. Encoder representation	20

3.2.2. Motor model verification	21
3.3. Estimating the load profile	23
4. Motor drive design	25
4.1. Vector Control	25
4.1.1. Indirect Field Oriented Control of IM	26
4.1.2. The torque equation in indirect Field Oriented Control (FOC) . .	27
4.1.3. Slip estimation in indirect FOC	29
4.1.4. Determining the currents reference	30
4.1.5. PI controller design	32
4.1.6. Motor controller verification	34
4.2. Conclusion on the motor and the controller Model	35
5. Modulation methods	36
5.1. SPWM	36
5.2. Third harmonic injection PWM	37
5.2.1. Space vector modulation	38
5.3. Investigation of Total Harmonic Distortion (THD)	40
5.4. Conclusion on modulation	41
6. Software Implementation	42
6.1. Implementation of modulation	42
6.2. Microcontroller Unit (MCU)	44
6.2.1. Connection to MCU	45
6.2.2. Communication with MCU	45
7. Inverter hardware	50
7.1. Introduction and requirements	50
7.2. Concept selection	51
7.2.1. MOSFETs vs. IGBT	52
7.2.2. Package types	53
7.2.3. Chosen concept	55
7.3. Design and Choices	55
7.3.1. A modular approach	56
7.3.2. Phase leg	56

Chapter Contents

7.3.3. Thermal design	59
7.3.4. Gate drive	62
7.3.5. DC-Link Capacitor bank	67
7.4. Simulation	69
7.5. Test and verification	72
8. Additional hardware	81
8.1. DC Chopper	81
8.1.1. Controller circuit design for DC chopper	82
8.1.2. Components selection	84
8.1.3. Layout design	84
8.1.4. DC Chopper Test	85
8.2. Interface board	85
8.2.1. Supply	85
8.2.2. Main supply voltage measurement	86
8.2.3. Inverter output current measurement	87
8.2.4. Torque pedal command	89
8.2.5. Signal scaling	89
9. System Test and Validation	90
9.1. Conclusion on system validation test	92
10. Conclusion	93
11. Future work	94
Bibliography	I
A. appendix	III
A.1. Schematics and PCB-layout	III
A.1.1. Wiring diagram	IV
A.1.2. Modular Inverter Phase	V
A.1.3. Gate drive	VIII
A.1.4. DC Chopper	XI
A.1.5. Interface board	XIII

Chapter Contents

A.1.6. Current measurement board	XVII
A.2. Mechanics	XX
A.3. Calculation	XXII
A.3.1. Calculating I_{dRef}	XXII

List of Abbreviations

MOSFET	Metal Oxide Semiconductor Field Effect Transistor	52
IGBT	Insulated Gate Bipolar Transistor.....	52
BJT	Bipolar Junction Transistor.....	67
SOC	State Of Charge.....	13
MCU	Microcontroller Unit	IV
FOC	Field Oriented Control	IV
MTTF	Mean Time To Failure.....	69
ESR	Equivalent Series Resistance.....	69
ADC	analog-to-digital converter.....	46
GPIO	general-purpose input/output.....	46
eQEP	enhanced quadrature encoder pulse	48
PWM	pulse-width modulation.....	46
SPWM	Sinusoidal PWM	36
THIPWM	Third Harmonic Injection PWM.....	36
SVPWM	Space Vector PWM.....	36
SMD	Surface-mounted device.....	54
DUT	Device under Test	72
THD	Total Harmonic Distortion	IV
DSP	Digital signal processor	72
IC	Integrated circuit	66
BJT	Bipolar junction transistor.....	67

1. Project Formulation

This project is made at Aalborg University at the Master of Science program in Energy Engineering. The purpose of the project is to look into control and drive of an induction machine used in an electric Go-Kart. The main focus will be the hardware implementation for the inverter and the software to control the drive system.

1.1. Introduction

Classic Go-Karts, powered by combustion engines are race- and joy ride Go-Karts for closed courts. The sound of a roaring engine combined with the smell of gasoline can be very attractive to some people, but has certain problems at indoor race tracks. Firstly, the use of combustion engines at indoor environments set high requirements for building ventilation to get rid of the dangerous emitted carbon-mono-oxide gasses and secondly may be very loud due to echos inside the building.

As an alternative, electric engines offer a number of advantages; Obviously they have no exhaust fumes and are more quiet than combustion engines. This provides solutions to the two problems found for classic Go-Karts. While some people may miss the sound and smell from the classic Go-Kart, the electric motor has an extra advantage that may further improve the race experience. Namely that electrical machines can produce high torque at low rotational speeds. In comparison combustion engines can not go below their idling speed without stopping and requires a certain speed before producing a good level of torque. An electric Go-Kart can hence be made to have a much higher initial acceleration than the classic Go-Kart.

1.1.1. Initial problem

What is necessary to implement to be able to fully replace the traditional combustion engine in a Go-Kart with an electrical machine allowing bi-directional power flow?

1.2. Problem analysis

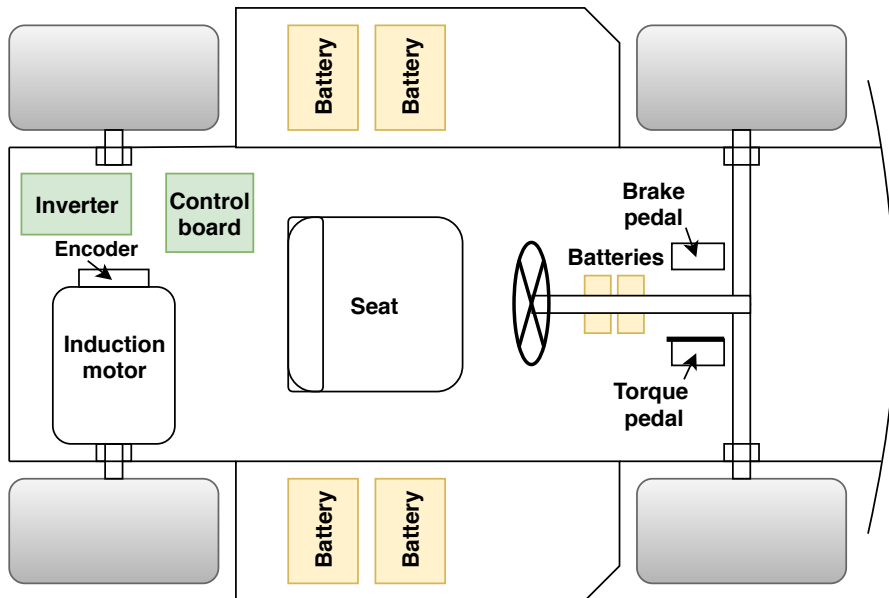


Figure 1.1.: Overview of the given Go-Kart platform

Seen on Figure 1.1 an overview of the given Go-Kart platform is shown. The green areas indicate the parts that has to be replaced, the yellow parts indicates where the source batteries will be located and the rest is given by the university as part of the platform. The given machine is an squirrel cage induction machine, and this will be taken into consideration regarding design choices.

For an induction machine of this type it is not possible to determine the exact rotor currents which makes it complex to determine the rotational speed of the rotor without an encoder.

The machine is a Sauer Danfoss machine with a rated power of 5.3 kW (7.3 kW for 60 minutes) normally used to drive the hydraulic system on a forklift. The machine has a rated voltage of 24 V which makes the current relatively high to reached the rated power. This has to be taking into consideration for both hardware design and control.

1.3. Scope and project objectives

The main scope of the project is to create a working electric Go-Kart based on the supplied platform and induction motor. In details, this splits up in the following objectives:

- System: Go-Kart platform
 - Driving forward
- Unit: Develop a three-phase inverter:
 - Driving the supplied induction motor at full power
 - Facilitate bidirectional power flow allowing regenerative breaking
- Unit: Develop an induction motor controller that:
 - Provides stable dynamic torque control
 - Operates sensored (using an encoder)
- Unit: Safety:
 - Safety stop button disconnects the battery from the system

1.3.1. Methodology

To obtain all the project objectives the following procedure will be followed:

1. Validate the design through simulation
2. Validate the design through hardware implementation and unit test
3. Validate the complete system in a controlled environment
4. Integrate the system to the Go-Kart and validate requirements

1.4. System architecture

1.4.1. Block Definition

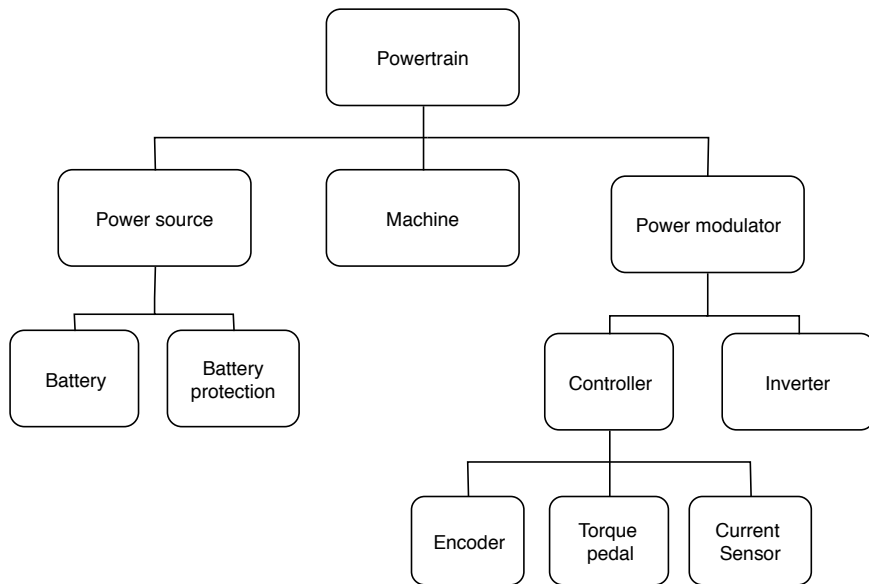


Figure 1.2.: Block Definition Diagram

The Go-Kart consists of mechanical parts in form of e.g. chassis, gear and hydraulic brakes, and an electrical powertrain. The electric powertrain will forward also be referred to as the "system". The system contains three main blocks, a power source, power modulator and a machine. By dividing these blocks into inherited sub-blocks each of the sub-blocks can be tested individually and the functionality can be verified. This method is useful in the process of test and validation.

The **Power source** consists of a battery pack and a voltage sensor to measure the under-voltage level of the battery pack.

The **Power modulator** consists of an inverter, which makes it possible to control the power flow in two directions, allowing regenerative breaking for the Go-Kart. It also consists of a controller, used for controlling the gate drivers.

The **Machine** is a squirrel cage induction machine.

1.4.2. User interface

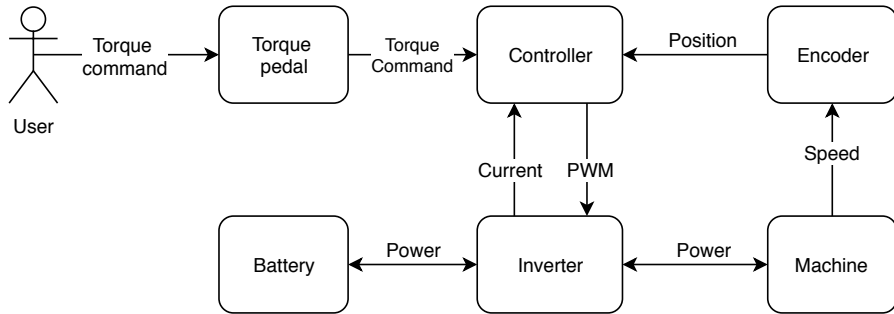


Figure 1.3.: Domain model

For racing purposes a high acceleration is needed and it is therefore of interest to implement a torque controller. To start the system the user is pressing the torque pedal producing a torque command, which is send from the potentiometer in the torque pedal to the controller.

The controller is using the torque command to determine the reference voltage for PWM output for the inverter to supply the needed current.

The encoder will give the position of the machine to the controller of the position machine. This information is used to determine the speed of the rotor. A current feedback to the controller is giving information about the applied torque on the rotor, because it is directly proportional to the current.

1.5. System requirements

1.5.1. Functional requirements

Req.#	Description
1.1	The system shall be manually controlled by user
1.2	The system shall be able to control bi-directional power flow
1.3	The system shall be able to supply sufficient torque to overcome the load torque
1.4	The power source shall be possible to disconnect in case of emergency
1.5	The system shall turn off the power output when the battery is depleted

Table 1.1.: Functional requirements

1.5.2. Performance requirements

Req.#	Description	Specs.	Unit	Type
2.1	Mechanical output power	≤ 7.3	kW	a
2.2	Minimum usage time of mixed driving*	10	min.	b
2.3	Minimum top speed	30	km/h	b

*Mixed driving is understood as an undefined number of accelerations, decelerations, turns, etc.

Table 1.2.: Performance requirements

All type "a" performance requirements given for the system. All type "b" requirements are for the system integrated in the Go-Kart as complete electrical powertrain system for a Go-Kart. Requirement 2.1 is based on the peak power output of the machine. Requirement 2.2 and 2.3 is chosen as a minimum success criteria for the system integrated in the the platform.

1.6. Constraints

Class	Description	Type
Economic	3000 kr	-
Material	Platform	Go-Kart chassis
Material	Gear	24/40 ratio
Material	Machine	Induction machine
Material	Potentiometer	Slide potentiometer
Material	Batteries	4 x 12V Lead-acid
Material	Encoder	Incremental encoder

Table 1.3.: Project constraints

A approximately budget of 3000 kr was given to project along with components for the electric Go-Kart to minimise the over-all cost. Design choices will be based on these budget- and material constraints.

2. System analysis

2.1. Induction machine

The induction machine provided by the university is an TSA170-210-038 Sauer Danfoss squirrel cage induction machine, with the given parameters seen in Table 2.1.

Parameter	Symbol	Value	Unit
Rated power	P_n	5.3 (7.3 for 60 min)	kW
Rated voltage	U_n	24	V
Rated current	I_n	189	A
Rated frequency	f_n	58	Hz
Rated shaft speed	n_n	1685	rpm
Efficiency	η	88.7	%
Power factor	PF	0.76	
Pole pairs	p_{pairs}	2	
Stator resistance	R_s	2.5	$\text{m}\Omega$
Rotor resistance	R_r	2.69	$\text{m}\Omega$
Magnetising inductance	L_m	0.38	mH
Stator leakage inductance	L_{ds}	31.16	μH
Rotor leakage inductance	L_{dr}	31.16	μH

Table 2.1.: "TSA170-210-038 Sauer Danfoss" Rated parameters

The induction machine is an asynchronous machine, which means that the rotor is rotating with a different speed compared to the stator field. This is due to the fact that the rotor field is generated by an EMF which induces a current in the closed loop of the shorted squirrel cage. This happens when experiencing a change in the magnetic field. At synchronous speed, the rotor will experience a constant magnetic field and hence decrease in speed until the field is changing.

The rated peak current:

$$I_{Pn} = I_n \cdot \sqrt{2} = 267.49 \text{ A} \quad (2.1.1)$$

The rated torque is:

$$T_n = \frac{P_n}{\omega_n} = 30 \text{ Nm} \quad (2.1.2)$$

Where ω_n is the motor rated speed in rad/sec

The synchronous speed is:

$$n_s = \frac{60 \cdot f_n}{p_{pairs}} = 1740 \text{ [rpm]} \quad (2.1.3)$$

And the rated slip in percentage:

$$\text{Slip} = \frac{n_s - n_n}{n_s} \cdot 100 = 3.325 \% \quad (2.1.4)$$

2.2. Transmission



Figure 2.1.: Transmission

The transmission for the Go-Kart was given and includes two sprockets connected through a chain. From the given transmission a gear ratio can be calculated. The number of teeth on the wheel axle sprocket is counted to be 40 and 24 for the rotor axle sprocket.

$$G_r = \frac{\text{teeth}_{\text{wheel}}}{\text{teeth}_{\text{rotor}}} = \frac{40}{24} = 1.66 \quad (2.2.1)$$

Knowing the rated rotor speed for the motor and the gear ratio, the rated wheel axle speed can be calculated, see Equation 2.2

$$n_{\text{axle}} = \frac{n_{\text{rated}}}{G_r} = \frac{1685}{1.66} = 1040 \text{ rpm} \quad (2.2.2)$$

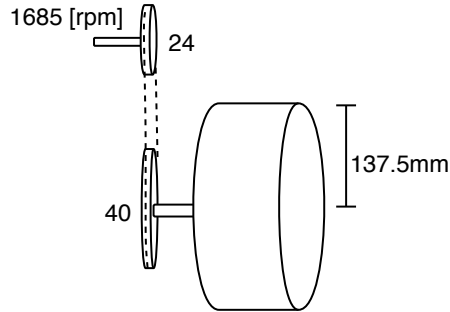


Figure 2.2.: Transmission overview

In Figure 2.2 the sketch of the gearing setup is shown with the given parameters. By knowing the radius of the wheel and the speed of the axle, the theoretically maximum speed of the can be calculated.

$$n_{\text{kart}} = \frac{2\pi \cdot r_{\text{wheel}} \cdot n_{\text{axle}} \cdot 60}{1000} = \frac{2\pi \cdot 0.1375 \cdot 1040 \cdot 60}{1000} = 54.12 \text{ km/t} \quad (2.2.3)$$

2.3. Encoder

An encoder is a sensor device capable of capturing linear or rotational displacement. Displacement information can be used to determine rotor position or rotational speed.

There are different types of encoders, but in this project, an incremental encoder was provided by the university and no further types will be explained.

The incremental encoder is from Scancon encoders [1] and consist of three tracks generating three separate signals, which makes it possible to detect the rotational direction as well. Besides track A and B, used for determining speed and rotational direction, Z is used to determine the starting position of the shaft.

Parameter	Value
Supply voltage	4.5-30 V
Output signal	Differential 6-channels A,B,Z,-A,-B,-Z
Pulses per revolution	2048 pulses/rev
Internal resistance	2.8 mΩ
Housing diameter	50 mm

Table 2.2.: Scancon incremental encoder parameters. [1]

The encoder has six channels and is capable of producing differential signals. Only three of the channels are needed to ensure that the controller can determine speed, position and rotational direction of the rotor. A comparison of two pulses from the outputs can be used to determine rotational direction of the rotor. Depending on which of the A- and B-signal is leading, a rotational direction is obtained.

2.4. Main supply batteries

2.4.1. Battery Testing

The batteries which will be used to power the machine are also provided by the university. These lead-acid batteries are called YellowTop produced by Optima and have been used in earlier projects together with the same machine that is used in this project. The inverter is designed based on the motor and since the motor is rated for 24 V_{AC} or around 36 V_{DC} , only three out of the four batteries in series are required to power the Go-Kart.

Parameter	Value	Unit
Nominal voltage	12	V
Rated capacity	55	Ah
Cranking Amps	870	A
Internal resistance	2.8	mΩ
Weight	19.9	kg

Table 2.3.: Optima YellowTop parameters [2]

The parameters of the batteries are listed in the Table 2.3. Each value is for a single battery.

Since the batteries have been used before and stored afterwards for a unknown period of time, it is necessary to test the batteries by performing cycles of discharging and charging. By that the condition of the batteries regarding their capacity can be determined and the battery with the lowest capacity can be identified. During discharging they will be discharged to the lower voltage limit of 9 V and during charging until a limit of 14.7 V. The batteries are tested individually using the charger "Turnigy MEGA 400W v.2" which is tracking the charge in mAh. The results of the test are shown in Figure 2.3.

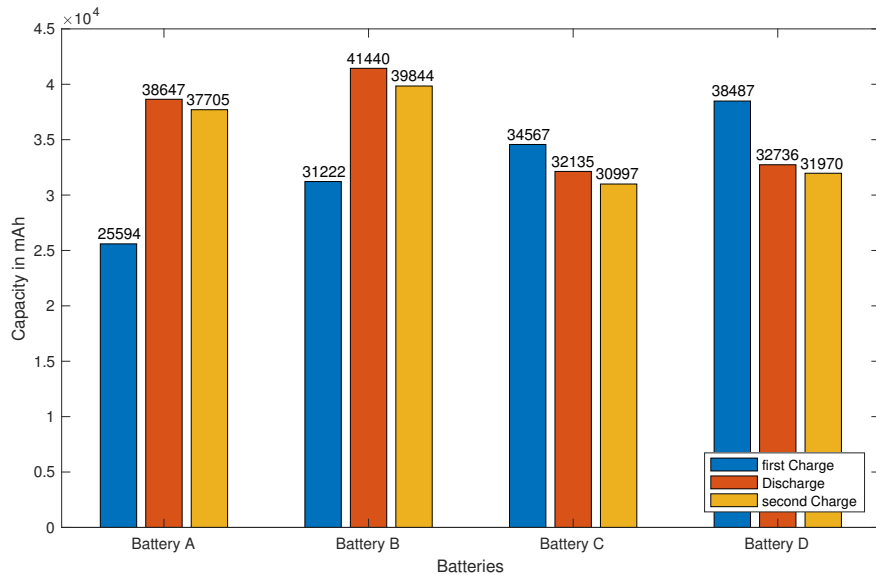


Figure 2.3.: Charge and Discharge test of all batteries

The bars in Figure 2.3 are showing the capacity in mAh which have been charged or discharged before reaching the given limit.

The values for the first charge are very different compared to the second measurements. That is due to the fact that the batteries were stored and the State Of Charge (SOC) during the storage was unknown. The discharge and second charge values are measured in relation to a known reference SOC and thereby will be considered.

From these values it can be concluded, that the batteries have very different capacities. During the discharge the values vary more than $9000 mAh$ which is about 16% of the original rated capacity of the batteries. Next to that all batteries have a significant lower charge than the original $55 Ah$. The test shows that battery C has the lowest capacity of all and thereby it will be left out.

The measured discharge-values for battery A, B and D can now be considered as the capacity of the main batteries.

2.4.2. Approximation of Driving time

Understanding battery behaviour is crucial as the batteries are an important part of the system. The batteries main role is to provide constant source of energy for driving. Therefore it is necessary to determine, next to the battery capacity, the resulting estimated driving time.

The battery capacity has already been measured and the values can be found in Figure 2.3. These values can be used to calculate an estimated driving time for a certain discharge current. In order to consider the voltage of the battery during the discharge, the driving time is estimated using a model of the battery. The purpose of the model is not simulating a driving situation but to plot the voltage level of the battery over time.

A battery can be ideally represented by a voltage source which is providing a constant voltage and a resistor representing the internal resistance of the battery (Figure 2.4).

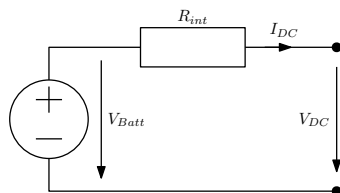


Figure 2.4.: Simple Model of the Battery

This simple model of a battery is able to show the voltage drop over the internal resistor R_{int} , but it is not able to show the change of voltage over time due to the SOC. Therefore it is necessary to use a more advanced model. SimuLink is providing a generic battery model which is considering the SOC calculating the voltage level. Therefore it will be used to plot the estimated driving time for different currents. The structure of this model is shown in Figure 2.5.

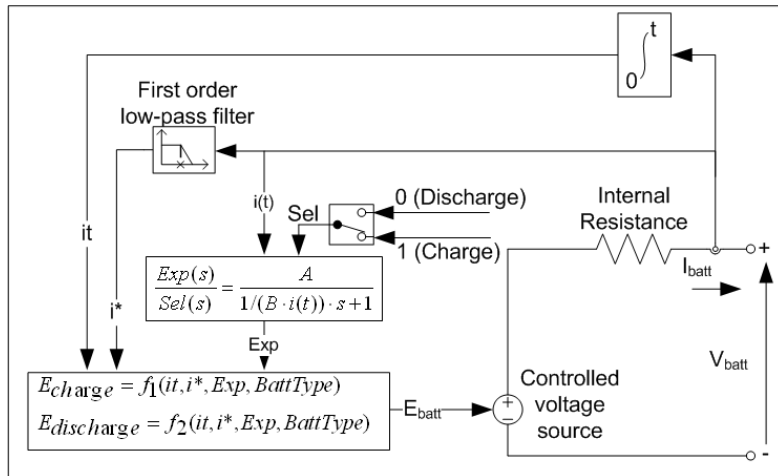


Figure 2.5.: Generic battery model in Simscape [3]

This model consists of a controlled voltage source and an internal resistance which is similar to Figure 2.4 except the fact that generic model has a variable voltage source. The value of the controlled voltage source, which corresponds to V_{Batt} , is depending on different parameters like the current I_{DC} , the battery type and the state of charging or discharging. For a lead-acid battery the following equations are used for charging mode (Equation 2.4.1) and discharging mode (Equation 2.4.2).

$$E_{charge} = E_0 - K \cdot \frac{Q}{Q - i_t} \cdot i^* - K \cdot \frac{Q}{Q - i_t} + \text{Laplace}^{-1} \left(\frac{\text{Exp}(s)}{\text{Sel}(s)} \right) \quad (2.4.1)$$

$$E_{discharge} = E_0 - K \cdot \frac{Q}{i_t + 0.1 \cdot Q} \cdot i^* - K \cdot \frac{Q}{Q - i_t} + \text{Laplace}^{-1} \left(\frac{\text{Exp}(s)}{\text{Sel}(s)} \cdot \frac{1}{s} \right) \quad (2.4.2)$$

The equations are given by Mathworks to explain the Figure 2.5 [3]. The parameters need to be set according to the battery characteristics or they are already implemented in the model as constants.

- E_0 is the rated voltage, in V
- $Exp(s)$ is the exponential zone dynamics, in V
- $Sel(s)$ represents the battery mode
- K is polarization constant, in $A\text{h}^{-1}$
- i^* is low frequency current dynamics, in A
- i_t is extracted capacity, in Ah
- Q is maximum battery capacity, in Ah

The parameter $Exp(s)$, K and i^* are values which are internally calculated in the model[3]. They are based on constants and the fact that it is a lead-acid battery. These values are already implemented in the battery model. Only E_0 and Q need to be configured according to the available battery datasheet and the capacity measurement. The parameter of i_t represents the drawn current which will be assumed for the plot.

$$I = \frac{P_{motor}}{\eta \cdot \sqrt{3} \cdot V_{AC}} \quad (2.4.3)$$

$$I = \frac{7.3 \text{ kW}}{0.88 \cdot \sqrt{3} \cdot 24 \text{ V}} = 199.56 \text{ A} \quad (2.4.4)$$

The calculation using Equation 2.4.3 is giving an approximated maximum current for running with full power. Therefore the values of 50 A, 100 A and 200 A for i_t are chosen to be plotted to approximate the driving time for different conditions up to full power. During driving the drawn current will not be constant since the Go-Kart is accelerating and braking. In this case the profile of the current is highly depending on the race-circuit and the driver, but in order to make a general assumption of a possible driving time the current can be assumed to be constant. The resulting plot is showing how the battery voltage is changing over time (Figure 2.6).

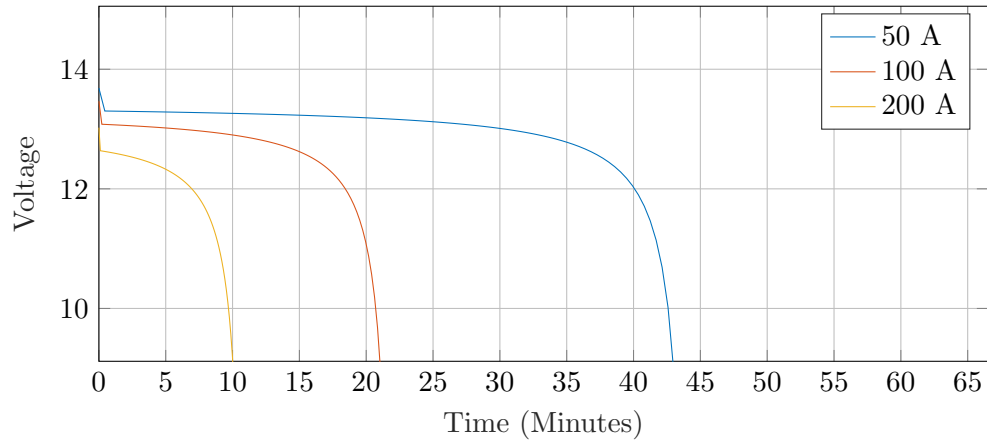


Figure 2.6.: Discharge characteristics of a single battery

It can be seen in Figure 2.6 that the battery voltage is decreasing fast at the end of the driving time. The drop-out voltage is set to 9 V and thereby the x-axis crossing is giving the maximum driving time.

In Conclusion of the plot the aim of 10 minutes of driving time can be obtained when the average drawn current is maximum 200 A. Since the current is assumed constant the time values may not be understood as an exactly prediction of driving time.

3. Modelling

3.1. Reference frame

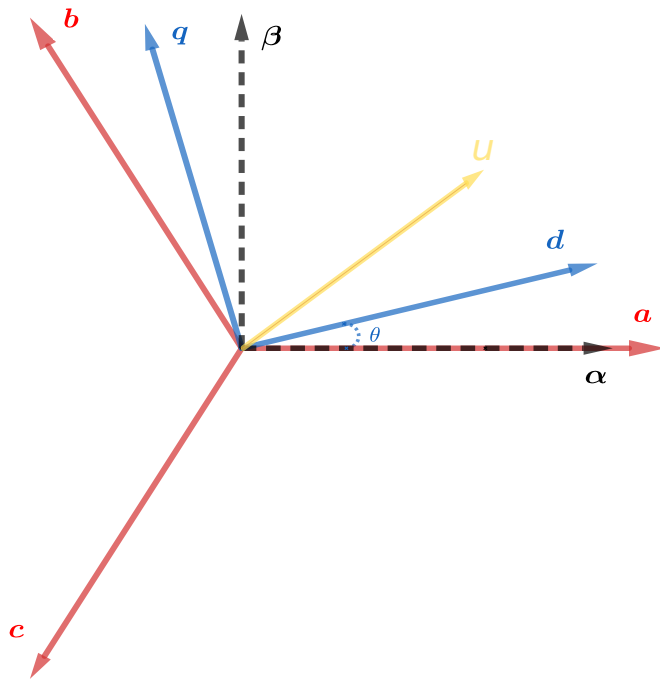


Figure 3.1.: Reference frames

When dealing with a 3-phase induction machine it is complicated to model each phase independently. The IM can instead be simplified by transforming the three phases into a single space vector. This space vector is rotating in a abc-reference frame and there by rotating in reference to the three phase vectors. By aligning a 2-dimensional reference frame to the *a*-vector in abc domain, the vector is now rotating in reference to two axes instead of three. This new reference frame is called the $\alpha\beta$ - reference frame. To simplify the system even further a rotating reference frame is introduced. By making the reference

frame rotate in the same speed as the space vector, the space vector is seen as a DC in reference to the rotating frame. This rotating frame is called a dq-reference frame, see Figure 3.1.

By assuming the phases to be balanced, meaning 120° divided, the zero component can be neglected and only the d- and q will be found.

$$\begin{bmatrix} u_d \\ u_q \end{bmatrix} = \frac{2}{3} \cdot \begin{bmatrix} \cos(\theta) & -\cos(\theta + \pi/3) & -\sin(\theta + \pi/6) \\ -\sin(\theta) & \sin(\theta + \pi/3) & -\cos(\theta + \pi/6) \end{bmatrix} \cdot \begin{bmatrix} u_a \\ u_b \\ u_c \end{bmatrix} \quad (3.1.1)$$

Equation 3.1 shows the transformation matrix used for changing the reference frame from a 3-phase (abc-frame) into a rotating 2-phase reference frame (dq-frame).

3.2. Model of the Induction machine

The induction machine will both react, for bi-directional power flow, as a motor and a generator. For modelling the induction machine will first be modelled as a motor and thereby be referred to as an induction motor. For a motor model, the following voltage equations, Equation 3.2.1 to Equation 3.2.4 can be used [4].

$$u_{ds} = R_s \cdot i_{ds} + p\lambda_{ds} - \omega_\theta \cdot \lambda_{qs} \quad (3.2.1)$$

$$u_{dr} = R_r \cdot i_{dr} + p\lambda_{dr} - (\omega_\theta - \omega_r)\lambda_{qr} \quad (3.2.2)$$

$$u_{qs} = R_s \cdot i_{qs} + p\lambda_{qs} + \omega_\theta \cdot \lambda_{ds} \quad (3.2.3)$$

$$u_{qr} = R_r \cdot i_{qr} + p\lambda_{qr} + (\omega_\theta - \omega_r)\lambda_{dr} \quad (3.2.4)$$

[4]

u :	Voltage	L_m :	Magnetisation inductance
i :	Current	λ :	Flux
R :	Resistance	ω_θ :	Synchronous speed
L_l :	Leakage inductance	ω_r :	Rotor shaft speed
p :	Derivative		

The induced flux is depending on the slip between the synchronous speed of the stator

and the speed of the rotor. This relationship can be shown by re-writing the rotor voltage equation Equation 3.2.2 and isolating the rotor flux as in Equation 3.2.5.

$$\lambda_{dr} = \int (u_{dr} + (\omega_\theta - \omega_r)\lambda_{qr} - R_r \cdot i_{dr}) dt \quad (3.2.5)$$

Because the system is torque controlled, the controller has to control the current which is proportional to the torque.

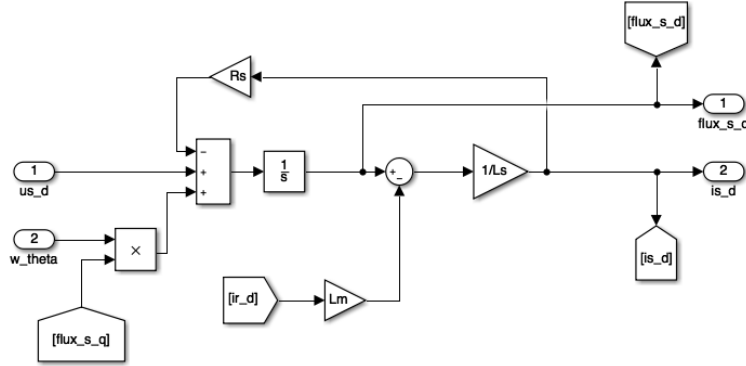


Figure 3.2.: Dynamic model of the rotor current

In Figure 3.2 a dynamic model based on Equation 3.2.6 is constructed. Having the voltage as an input and knowing the machine parameters given in Table 2.1 the four equations can be connected into a complete model of the currents and the flux in the induction machine.

When constructing the model some assumptions and considerations have to be made. For a squirrel cage induction machine the rotor bars are shorted, therefore, there is no voltage across the rotor hence the term can be disregarded from the model. Regarding the inductance's, the leakage- and magnetisation inductance for the stator and rotor can be seen as a single inductance by added them together ($L_{ls} + L_m = L_s$). By re-writing the voltage- and flux equations the expressions for the currents can be derived as shown in Equation 3.2[4].

$$i_{ds} = \int \frac{(u_{ds} + \omega_\theta \cdot \lambda_{qs} - R_s \cdot i_{ds}) - L_m \cdot i'_{dr}}{L_s} dt \quad (3.2.6)$$

$$i_{dr} = \int \frac{(u_{dr} + (\omega_\theta - \omega_r) \cdot \lambda_{qr} - R_r \cdot i_{ds}) - L_m \cdot i'_{ds}}{L_r} dt \quad (3.2.7)$$

$$i_{qs} = \int \frac{(u_{qs} - \omega_\theta \cdot \lambda_{ds} - R_s \cdot i_{qs}) - L_m \cdot i'_{qr}}{L_s} dt \quad (3.2.8)$$

$$i_{qr} = \int \frac{(u_{qr} - (\omega_\theta - \omega_r) \cdot \lambda_{dr} - R_r \cdot i_{qs}) - L_m \cdot i'_{qs}}{L_r} dt \quad (3.2.9)$$

3.2.1. Encoder representation

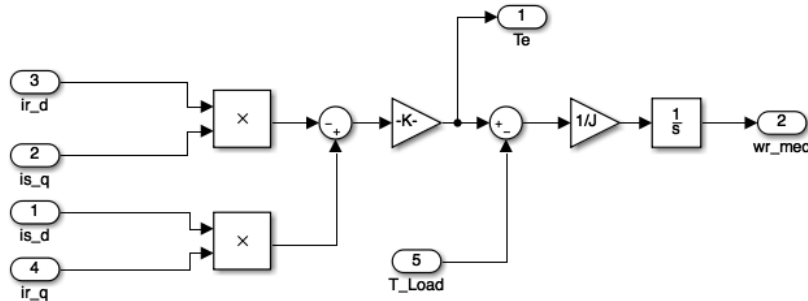


Figure 3.3.: Mechanical model of an IM

To represent the mechanical shaft speed measurement from the encoder, the mechanical equation for the induction machine can be used along with newtons second law of motion.

$$\tau_e = \frac{3}{2} \cdot p_{pairs} \cdot L_m (i_{qs} \cdot i_{dr} - i_{ds} \cdot i_{qr}) \quad (3.2.10)$$

$$\tau_e - T_{load} = J(s \cdot \omega_{mec}) \quad (3.2.11)$$

Equation 3.2.10 is giving the instantaneous rotor shaft torque τ_e with the stator- and rotor currents as input variables.

By comparing the applied torque with the load torque, the angular velocity of the rotor

shaft can be derived by applying newtons second law, see Equation 3.2.11. The viscous friction in the motor can be determined by a no-load test. This is due to the fact that the torque applied, at no-load, is the torque needed to overcome the viscous friction. This load is neglected due to the lag of no-load test data.

3.2.2. Motor model verification

In order to verify the induction motor model, two test will be conducted.

The first test is a No-load test to verify if the motor will rotate at the synchronous speed, $n_s = 1740$ rpm, the results of that test is shown in Figure 3.6 which correspond to the synchronous speed n_s .

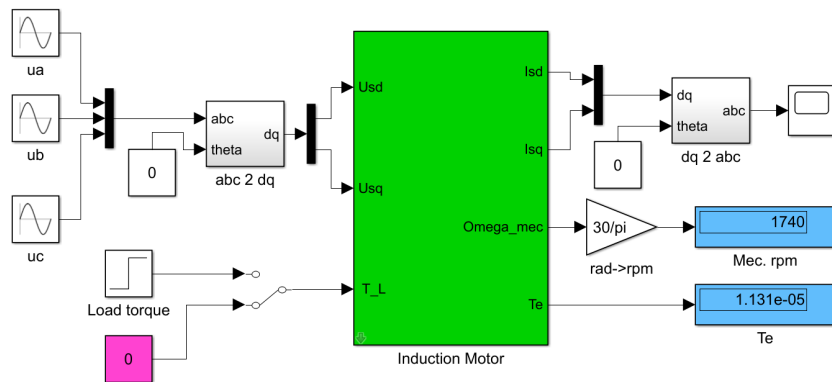


Figure 3.4.: No-load test

The second test can be done by supplying the motor model with the rated voltage, and applying the rated torque, $T_n = 30$ Nm as a step input. The motor model is expected to response by rotating at the rated speed, $n_n = 1685$ rpm. The stator current should also be equal to the rated peak current of the motor $I_{Pn} = 267$ A.

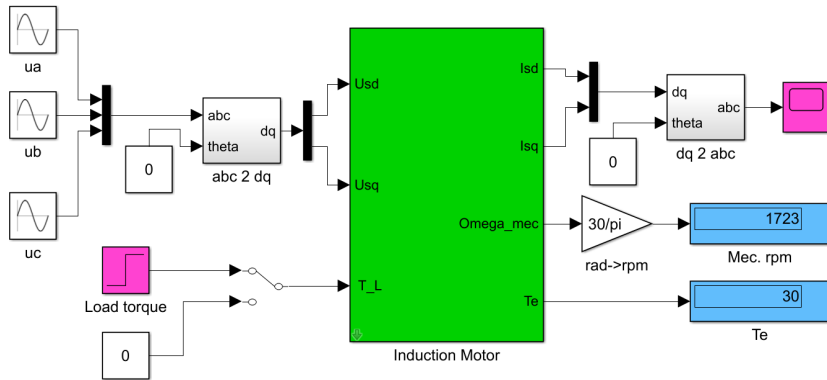


Figure 3.5.: Rated torque test

Figure 3.2.2 is showing the first test where the motor is in $\alpha \beta$ - reference frame. This is due to the motor being tested without controller. The controller gives the angle needed to transform into dq-reference frame, but because it is not included $\theta = 0$.

The speed result is shown in Figure 3.2.2, and is displayed in "Mec.rpm". The result shows a difference in speed compared to the rated speed n_n . The same applies for the current, shown in Figure 3.6. The peak of the stator current wave forms, shows a difference from the rated current I_{Pn} .

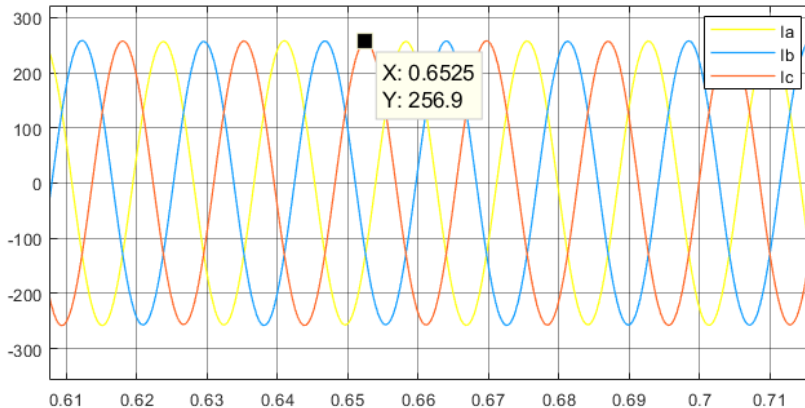


Figure 3.6.: The stator current wave forms in the first test

That small difference between the results and the expected values could be a result of inaccurate motor parameters. The model is tested in the same way for a different motor,

giving the expected values for that given motor. This shows that the model is constructed in the correct way and the functionality of it is thereby verified.

3.3. Estimating the load profile

The load profile describes the relation between the load torque and the corresponding speed. This can be done by deriving a mathematical model for the Go-Kart, describing all the forces which is applied on the Go-Kart.

Those forces are rolling resistance force, F_{rr} , aerodynamic force and F_{ad} , hill climbing force, F_{hc} [5].

A flat road is assumed, and the climbing resistance is thereby neglected. The total force will then be:

$$F_t = F_{rr} + F_{ad} \quad (3.3.1)$$

The rolling resistance force is calculated as shown in Equation 3.3.2[5]

$$F_{rr} = C_{rr} \cdot m \cdot g \quad (3.3.2)$$

Where $C_{rr}=0.0015$ [5] is the rolling resistance coefficient for rubber tires and asphalt, $m = 233$ is the total mass including motor, chassis and driver, g is the gravitational acceleration which in Denmark is equal to $9.815 \frac{m}{s^2}$ [6].

The aerodynamic drag force, F_{ad} is calculated as shown in Equation 3.3.3 [5]

$$F_{ad} = 0.625 \cdot A \cdot C_d \cdot v^2 \quad (3.3.3)$$

A is the drag reference area which is the cross sectional area of the car with a driver and is assumed to be approximately 0.5 m^2 , $C_d = 0.27$ [5] is the coefficient of drag and v is the velocity.

By substituting the parameter, the total force in terms of the velocity will be as shown in Equation 3.3.4.

$$F_t = 34.3 + 0.0843 \cdot v^2 \quad (3.3.4)$$

Converting the total forces to torque can be done in the following equation:

$$\tau_{load} = F_t \cdot \frac{r_{wheel}}{G_r} = 2.8 + 0.006 \cdot v^2 \quad (3.3.5)$$

Where $r_{wheel} = 0.1375$ m is the wheel radius and $G_r = 1.66$ is gear ratio which is given section 2.2

To converter form displacement velocity, v to rotational velocity, ω

$$v = \omega \cdot r_{wheel} \quad (3.3.6)$$

Then Equation 3.3.5 will be:

$$\tau_{load} = 2.8 + 0.0001 \cdot \omega \quad (3.3.7)$$

4. Motor drive design

There are many control methods that can be used to control the Induction Motor such as scalar control and vector control. Scalar control is easy and cheap to implement, but it has a low dynamic performance because of slow torque response to transients, while vector control operates with fast response and it is robust in transients because it controls the motor currents[7].

As mentioned in subsection 1.4.2 important to use a controller with a fast torque response to get a high acceleration, therefore vector control will be used in the project, due to its high dynamic properties.

4.1. Vector Control

The idea behind the vector control comes from the DC motor which is easy to control, due to its design, keeping the field flux perpendicular to the armature flux.

The result of this orthogonality is that these two fluxes will not be affected by each other and the field flux will be independent of the armature current, then by changing the armature current, the torque can be changed independently of flux.

The same principle is applied in the vector control in induction motor by decoupling the field components into two independent currents; the flux-producing current and the torque-producing current. The decoupling can be done in the controller by keeping 90 electrical degrees between the field components [4] and [7].

4.1.1. Indirect Field Oriented Control of IM

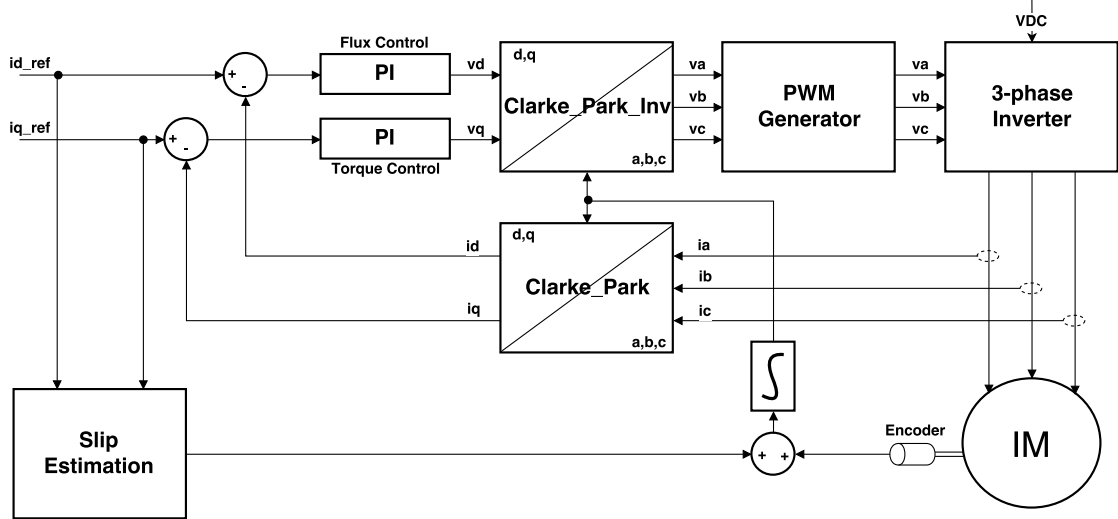


Figure 4.1.: Indirect Field Oriented Control of IM structure [4]

As described in section 4.1 the field oriented vector control regulates the stator current vector. To implement this, the instantaneous AC current in each phase should be measured as shown in Figure 4.1.

These measurements are in 3-phase stationary frame, and it will be very complicated if three AC current regulators used to control the stator current vector, therefore the measurements are feeding the "Clarke Park" transformation block which is used to transfer the 3-phase stationary frame into 2-phase rotational frame (d,q), then the stator current vector will have only two DC components: i_q is the current which produces torque, and i_d is the current which produces the rotor flux as will be derive in subsection 4.1.2. By having the DC components, the AC controller becomes simple and similar to a DC motor controller, and it is possible to use the conventional controller typologies as PI controller by using i_{dref} and i_{qref} as a reference for each control loop, i_{dref} and i_{qref} , the values of these references will be calculated in subsection 4.1.4.

The controllers output will be the stator voltage signals in dq-reference frame, therefore they should convert back to 3-phase stationary frame by using "Clarke Park inverse", the results will be three voltage signals, those signals will be used in the "PWM Generator" and "3-phase Inverter" to produce 3-phase voltage the will supply the motor.

”PWM Generator” and ”3-phase Inverter” will be explained in details in chapter 5 and chapter 7 respectively.

In both ”Clarke Park” and ”Clarke Park inverse”, the current space vector position is needed, this position can be obtained from integrating the sum of the rotor shaft speed from the Encoder and the slip speed as will be explained in subsection 4.1.3.

4.1.2. The torque equation in indirect FOC

Field oriented control is a torque control method, where the torque in the induction motor is produced as the result of the interaction between the rotor- and stator currents [4]. Hence, the torque equation can be expressed by means of the stator and rotor current in dq-reference frame as the following equation [4]:

$$\tau = \frac{3}{2} \cdot p_{pairs} \cdot L_m \cdot (i_{qs} \cdot i_{dr} - i_{ds} \cdot i_{qr}) \quad (4.1.1)$$

Where p_{pairs} is the pole pairs and L_m is the magnetisation inductance.

Equation 4.1.1 can easily be transferred to a vector form by using the following relation:

$$(i_{qs} \cdot i_{dr} - i_{ds} \cdot i_{qr}) = Im(\bar{i}_{dqs} \cdot \bar{i}_{dqr}^*) \quad (4.1.2)$$

Where \bar{i}_{dqr}^* refers to the conjugate of the rotor current on dq reference frame and Im is the imaginary part of a complex number.

The torque equation will then become[4]:

$$\tau = \frac{3}{2} \cdot p_{pairs} \cdot L_m \cdot Im(\bar{i}_{dqs} \cdot \bar{i}_{dqr}^*) \quad (4.1.3)$$

Since the rotor bars are short circuited, and it is very difficult to measure it, but that current can be represented by the rotor flux which given by the following equation [4]:

$$\bar{\lambda}_{dqr} = (L_{lr} + L_m) \cdot \bar{i}_{dqr} + L_m \cdot \bar{i}_{dqs} \quad (4.1.4)$$

By solving for \bar{i}_{dqr} , and substitute it in Equation 4.1.3, then excluding the real part, it is possible to get rid of the rotor current term from the torque equation as shown the

following equation[4]:

$$\tau = \frac{3}{2} \cdot p_{pairs} \cdot \frac{L_m}{L_r} \cdot Im \cdot (\bar{i}_{dqs} \cdot \bar{\lambda}_{dqr}^*) \quad (4.1.5)$$

Where $L_r = L_{lr} + L_m$. Thus, the torque in the induction motor is also produced as the result of the interaction between the rotor flux and stator current.

The induction motor equation in dq based on the arbitrary reference frame, but to implement the indirect FOC, d-axis must be aligned with the rotor flux, $\bar{\lambda}_{dqr}$ [4].

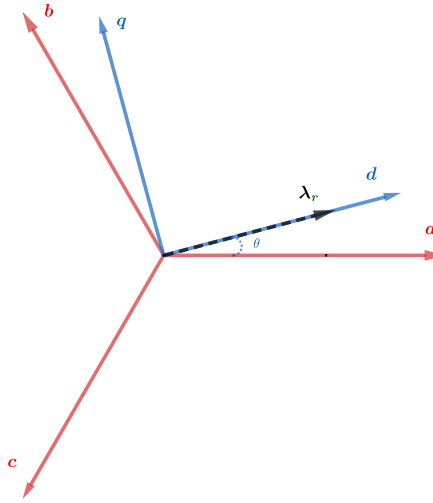


Figure 4.2.: The reference frame in indirect FOC

Hence, there is no component for $\bar{\lambda}_{dqr}$ on the q-axis, and

$$\bar{\lambda}_{dqr} = \lambda_{dr} = \lambda_r \quad (4.1.6)$$

Where λ_r is the magnitude of the rotor flux vector.

The torque equation can be simplified in scalar form as shown in the following equation [4]:

$$\tau = \frac{3}{2} \cdot p_{pairs} \cdot \frac{L_m}{L_r} \cdot i_{qs} \cdot \lambda_r \quad (4.1.7)$$

Therefore, now in this special reference frame where d-axis must be aligned with the rotor flux, the torque is determined by the stator current in q-axis, i_{qs} and the rotor d-axis

flux, λ_r .

And the torque could be proportional to i_{qs} , if λ_r is forced to be constant, then it is possible to control the motor torque by regulating i_{qs} .

4.1.3. Slip estimation in indirect FOC

As explained in subsection 4.1.2 for the indirect FOC, the d-axis must be aligned with the rotor flux, $\bar{\lambda}_{dqr}$. The rotor field rotates at the synchronous speed, while rotor shaft doesn't rotate at synchronous speed because of the slip in the induction motor, therefore, the rotor flux position is not directly linked to the rotors physical position [4].

By using the measured rotor shaft speed from the encoder and estimating the slip speed, the synchronous speed can be calculated.

And by integrating the synchronous speed, the rotor flux position can be obtained.

In order to estimate the slip speed, the induction motor rotor equations Equation 3.2.4, Equation 3.2.2 is used. Where the fluxes are:

$$\lambda_{dr} = (L_{lr} + L_m)i_{dr} + L_m \cdot i_{ds} \quad (4.1.8)$$

$$\lambda_{qr} = (L_{lr} + L_m)i_{qr} + L_m \cdot i_{qs} \quad (4.1.9)$$

The voltage across the rotor wires is equal to zero because the squirrel cage is a short circuit and the rotor flux on q-axis is also equal to zero as explained in subsection 4.1.2, then the induction motor rotor equations will be:

$$0 = R_r \cdot i_{dr} + p\lambda_{dr} \quad (4.1.10) \qquad \lambda_{dr} = L_r \cdot i_{dr} + L_m \cdot i_{ds} \quad (4.1.12)$$

$$0 = R_r \cdot i_{qr} + (\omega_\theta - \omega_r)\lambda_{dr} \quad (4.1.11) \qquad 0 = L_r \cdot i_{qr} + L_m \cdot i_{qs} \quad (4.1.13)$$

By isolating Equation 4.1.13 for i_{qr} then substituting in Equation 4.1.11, the slip speed equation can be calculated [4]:

$$S\omega_e = \frac{R_r}{L_r} \cdot \frac{L_m \cdot i_{qs}}{\lambda_{dr}} \quad (4.1.14)$$

Where $S\omega_e = (\omega_\theta - \omega_r)$ is the slip speed.

In steady state, the derivative p is equal to zero, so $i_{dr} = 0$ in Equation 4.1.10, Equation 4.1.12 will be:

$$\lambda_{dr} = L_m \cdot i_{ds} \quad (4.1.15)$$

Therefore a relation between stator d-axis current and rotor flux is obtained, by substituting it in Equation 4.1.14, a formula for the slip speed in steady state will be achieved [4]:

$$S\omega_e = \frac{R_r}{L_r} \cdot \frac{i_{qs}}{i_{dr}} \quad (4.1.16)$$

4.1.4. Determining the currents reference

The flux control reference, i_{dRef}

As explained in subsection 4.1.2 the λ_r must be constant to achieve proportional relation between i_{qs} and the motor torque.

In order to hold λ_r constant, the i_{ds} should be a constant according to Equation 4.1.15. That constant will be equal to the reference value, i_{dRef} for the flux control loop as shown in Figure 4.1

In order to calculate i_{dRef} , the induction motor equations in dq-reference frame is used. Because it is a reference value, it is possible to write the equations in steady state, meaning that all derivative terms will disappear, then by representing the equations in a vector form, using $f_{dq} = f_d + j \cdot f_q$, which is shown in Equation 4.1.20.

$$\bar{u}_{dqs} = R_s \cdot \bar{i}_{dqs} + j \cdot \omega_\theta \bar{\lambda}_{dqs} \quad (4.1.17)$$

$$\bar{u}_{dqr} = 0 = R_r \cdot \bar{i}_{dqs} + j \cdot (\omega_\theta - \omega_r) \cdot \bar{\lambda}_{dqs} \quad (4.1.18)$$

$$\bar{\lambda}_{dqs} = L_{ls} \cdot \bar{i}_{dqs} + L_m \cdot (\bar{i}_{dqs} + \bar{i}_{dqr}) \quad (4.1.19)$$

$$\bar{\lambda}_{dqr} = L_{lr} \cdot \bar{i}_{dqr} + L_m \cdot (\bar{i}_{dqs} + \bar{i}_{dqr}) \quad (4.1.20)$$

Since the rotor current, \bar{i}_{dqs} can not be measured, it will be isolated from Equation 4.1.20

then substituted it into Equation 4.1.19, then the following equation can be obtained:

$$\bar{\lambda}_{dqs} = \left(L_s - \frac{L_m^2}{L_r} \right) \cdot \bar{i}_{dqs} + \frac{L_m}{L_r} \cdot \bar{\lambda}_{dqr} \quad (4.1.21)$$

The flux vector in the stator, $\bar{\lambda}_{dqs}$ value can be calculated from Equation 4.1.17 by using the motor rated parameters from Table 2.1, then it is very simple to calculate $\bar{\lambda}_{dqr}$ in Equation 4.1.21.

As mentioned in Equation 4.1.6 that, the $|\bar{\lambda}_{dqs}|$ is equal to λ_r , because there is no component for $\bar{\lambda}_{dqs}$ on the q-axis.

Finally i_{dRef} can be calculated as the following:

$$i_{dRef} = \frac{\lambda_r}{L_m} = 222.14 \text{ A} \quad (4.1.22)$$

The detailed calculation is in subsection A.3.1

The torque control reference, i_{qRef}

In the Go-Kart, the driver can control the Go-Kart speed by changing the motor torque. That can be done by pressing the torque pedal in the Go-Kart, but in order to change the motor torque, the i_{qRef} value which is representing the torque command in the torque control loop as shown in Figure 4.1 should be change because the i_{qs} is proportional with motor torque as it was concluded in subsection 4.1.2.

Even though i_{qRef} is not constant value as i_{dRef} , this value should be limited by the motor rated current.

In order to determine the maximum value for i_{qRef} , the motor rated torque $T_n = 30 \text{ Nm}$ should be used as torque limit.

It can be calculated from Equation 3.2.10 by solving for i_{qs} :

$$i_{qs} = i_{qRef} = \frac{2 \cdot T_n \cdot L_r}{3 \cdot p_{pairs} \cdot L_m \cdot \lambda_r} = 128.3 \text{ A} \quad (4.1.23)$$

And in the same way $i_{qs} = 168 \text{ A}$

4.1.5. PI controller design

In order to make sure that the flux and torque control loops are stable and have a fast response for the reference value, a proper controller should be designed.

To do that, a transfer function describing the relationship between input and output of the plant for both control loops should be determined.

The plant for both control loops is an induction motor where the input is the stator voltage and the output is the stator current as shown in Figure 4.1.

An approximation is used by eliminating all the terms that contain the rotor current and the motor speed in the motor equations to obtain a transfer function for both loops. The induction motor dynamics are complex, but can then be described as a transfer function with a stator voltage as input and a stator current as an output by using an approximation. Both the interaction between the stator- and the rotor currents and the speed can change the motor electrical characteristics. The eliminated terms can be considered as disturbance in the control loop. The motor equations will then after approximation become:

$$u_{ds} = i_{ds}(R_s + pL_s) \quad (4.1.24)$$

$$u_{qs} = i_{qs}(R_s + pL_s) \quad (4.1.25)$$

By applying Laplace transformation, two identical first order transfer functions can be obtained in the frequency domain:

$$G_d(s) = \frac{I_{ds}}{U_{ds}} = \frac{\frac{1}{R_s}}{\frac{L_s}{R_s} \cdot s + 1} = \frac{K_{DC}}{\tau_d \cdot s + 1} \quad (4.1.26)$$

$$G_q(s) = \frac{I_{qs}}{U_{qs}} = \frac{\frac{1}{R_s}}{\frac{L_s}{R_s} \cdot s + 1} = \frac{K_{DC}}{\tau_q \cdot s + 1} \quad (4.1.27)$$

Where U_{ds} and U_{qs} are inputs, I_{ds} and I_{qs} are outputs, K_{DC} is the DC gain and τ_d and τ_q are time constant.

Since the two transfer functions are identical, only one controller will be designed.

By substituting the motor parameter, the transfer function will be:

$$G(s) = \frac{371.7}{0.15 \cdot s + 1} \quad (4.1.28)$$

K_{DC} is relatively big value, therefore the plant will have a fast response just by closing the control loop and using a unity proportional gain, K_p .

In order to make sure that the steady state error is eliminated, an integration gain, K_i , should be used.

The PI controller transfer function by choosing $K_p = 1$ and $K_i = 1$, is given by the following equation [8]:

$$G(s)_{PI} = \frac{s + 1}{s} \quad (4.1.29)$$

In order to identify the system stability in the closed loop, the gain margin and the phase margin for the open loop system, $G(s) \cdot G(s)_{PI}$ is checked in a frequency response plot "Bode plot" [8] as shown in Figure 4.3

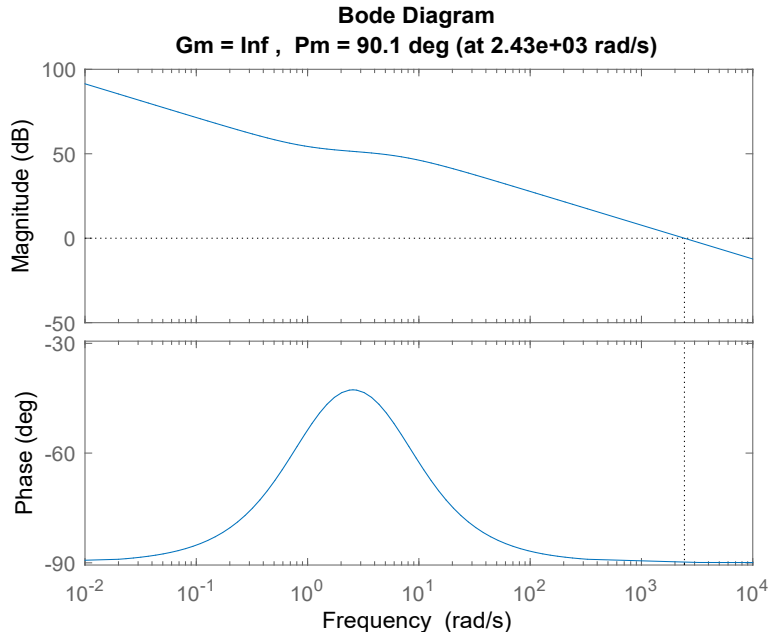


Figure 4.3.: The open loop system, $G(s) \cdot G(s)_{PI}$ bode plot showing the gain margin, Gm and the phase margin, Pm

The figure is showing that the gain margin is higher than 8 dB and the phase margin is higher than 50° , which indicates that the system in close loop is stable according to the relative stability criteria [8]. A step input is then applied on the close loop system to check the close loop step response as shown in Figure 4.4

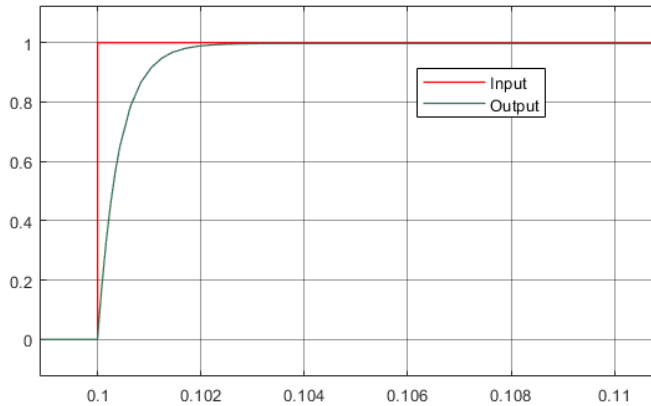


Figure 4.4.: A plot for closed-loop step response

The plot is showing a very fast response as expected due to the plants high DC gain.

4.1.6. Motor controller verification

The motor controller is reacting on a torque command, and is controlling the input for the motor to supply the command torque. To verifying the motor controller, a torque command is given and the output torque of the motor should correspond to the command.

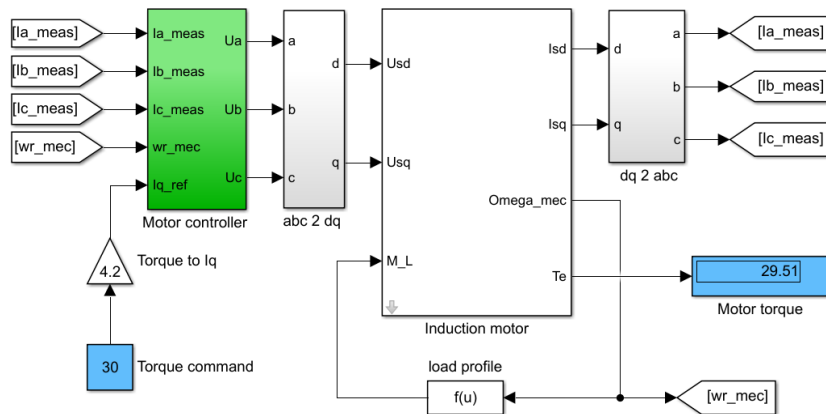


Figure 4.5.: A Torque command is applied on the motor throw the controller

In Figure 4.5 the setup is shown, given a 30 Nm torque command and respond with a motor output torque of 29.51 Nm. This shows the the controller is behaving as intended and the functionality is thereby verified.

4.2. Conclusion on the motor and the controller Model

Due to the time limitation, all the investigation was only the machine as motor, where a model for the motor and its control was implemented and verified by simulation. More investigation about the machine as generator can be done as future work.

5. Modulation methods

Pulse width modulation for three phase inverters, is a method for switching transistors to generate a AC output from a DC source by using digital gate pulses to control the states of the transistors. Different methods has been used over time, but the most generally used are Sinusoidal PWM (SPWM), Third Harmonic Injection PWM (THIPWM) and Space Vector PWM (SVPWM) [9].

5.1. SPWM

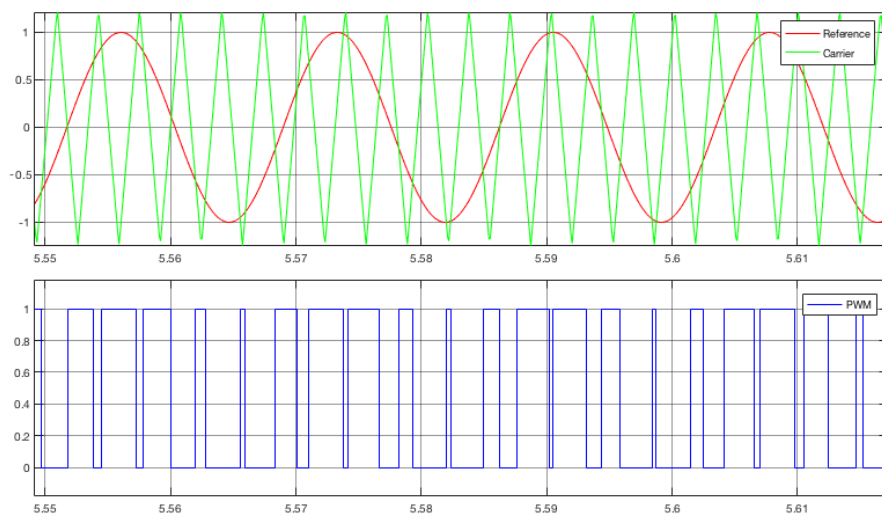


Figure 5.1.: SPWM

Sinusoidal pulse width modulation is a modulation technique that construct a pulse width modulated gate signal by comparing a sinusoidal wave (The reference) with a triangular wave (The carrier), as can be seen in Figure 5.1. When the amplitude of the reference signal is higher than the carrier signal, a high pulse is generated and kept high until the

reference is below again. As shown in Figure 5.1 the instant of switching is determined by the intersection points for the carrier and the reference. This method is the simplest compared to THIPWM and SVPWM, but has some disadvantages such as higher total harmonic distortion and lower DC voltage utilisation for the output [9].

$$V_{out} = \sqrt{3} \cdot \frac{V_{in}}{2} = 0.866 \cdot V_{in} \quad (5.1.1)$$

The maximum output line to line voltage (in the linear range) for SPWM is as shown in Equation 5.1[10] only 86.6% of the RMS input voltage. The voltage can be increased by overmodulation, with the cost of getting higher harmonic distortion. The lower voltage makes it problematic to make a motor run at rated power, but a full utilisation of the DC input will never be possible due to the forward voltage drop of the transistors.

5.2. Third harmonic injection PWM

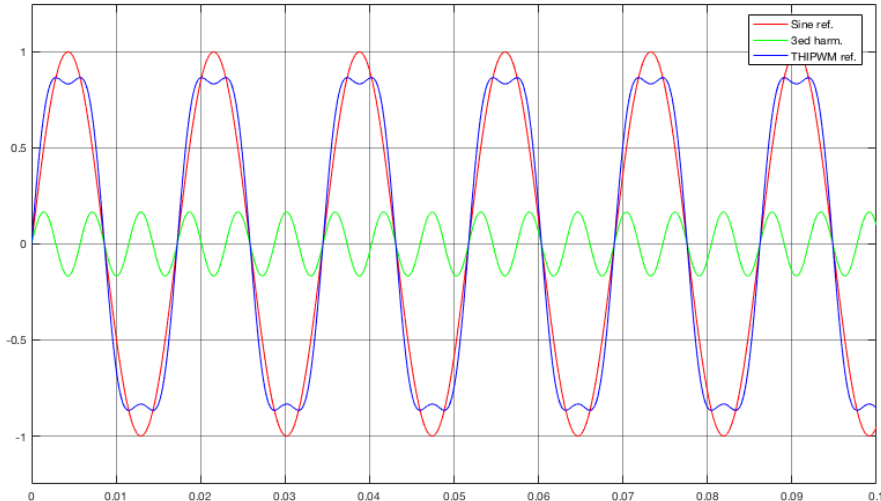


Figure 5.2.: THIPWM reference signal

When injecting the third harmonic of the reference signal, shown on Figure 5.2, it will not change the line to line voltage directly, due to equal injection in all the three signals and the line to line voltage is given as $V_{ab} = V_{an} - V_{bn}$. However the effect of injecting a third harmonic to the reference does not have a direct effect on the maximum line

to line output due to the lowering of the reference peak voltage, which is lowering the modulation index. The modulation index is the ratio between the peak of the carrier and the reference signal. A low modulation index makes it possible to increase the line to line voltage without adding extra harmonic distortion and avoiding going into overmodulation. By injecting the third harmonic of the reference with 1/6 of the magnitude to each of the reference signals gives up to around 15% increase of the line to line voltage [10]. For pulse width modulation the reference signal is compared with a triangular wave as for SPWM, the only difference is the modification of the reference signal.

5.2.1. Space vector modulation

Space vector modulation is a modulation technique that uses the space vector representation of the phase voltages to determine the switching sequence. For a 3-phase converter six gates are used to form sinusoidal output for a 3-phase inverter, three high-side gates and three low-side gates. For each of the phase legs the high-side and low-side cannot be on at the same time, due to the case of shoot-through, so the low-side is controlled opposite to the high-side. Due to this, only three gate signals need to be constructed. For each of the three gates the number of states are two (ON and OFF). The total number of states for the gates are $2^3 = 8$ states. Each of the states are represented by a vector, where the vectors V_0 and V_7 are zero vectors, because either all three high-side gates are on or all low-side are on, making the voltage between them zero. The rest of the vectors $V_1 - V_6$ are voltage vectors. By applying the vectors in different time periods a voltage reference can be constructed, which is going to rotate with a fixed magnitude, see Figure 5.4 and Figure 5.1.

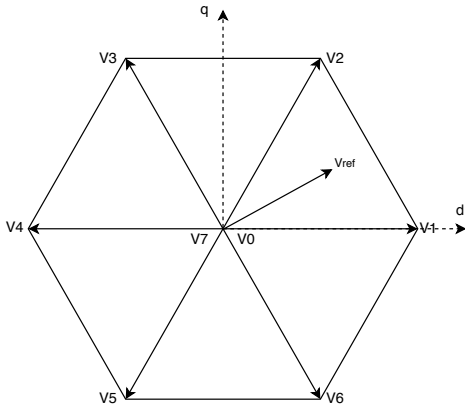


Figure (5.4) Switching sequence diagram

Vectors	States		
	a	b	c
V0	0	0	0
V1	1	0	0
V2	1	1	0
V3	0	1	0
V4	0	1	1
V5	0	0	1
V6	1	0	1
V7	1	1	1

Table (5.1) Switching states

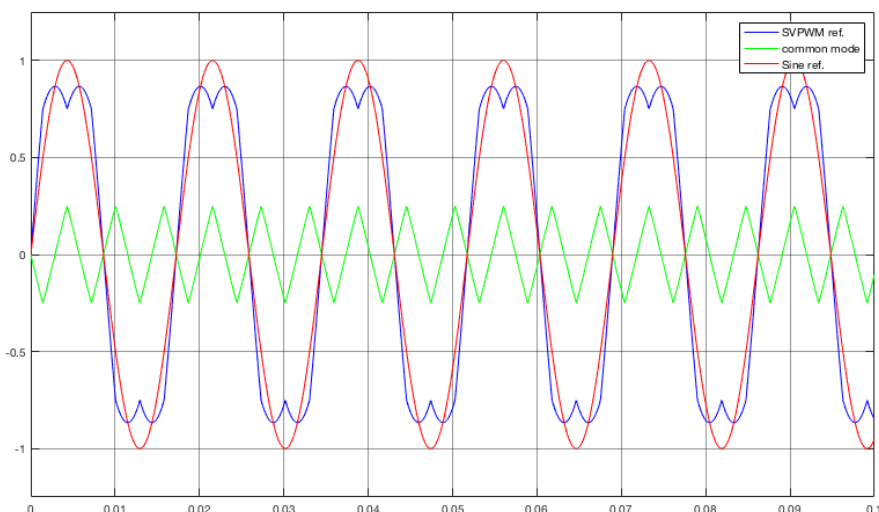


Figure 5.5.: Space vector PWM

In practical the zero vectors can be implemented by making a carrier based SVPWM. This can be constructed by a triangular waveform, added as a common mode voltage, with a peak to peak of half of the sinusoidal reference peak and triple frequency, making the reference signal a rump signal, as seen in Figure 5.5. The magnitude of the triangular

wave is calculated using Equation 5.2.1.

$$V_{cm} = \frac{\max(V_a, V_b, V_c) + \min(V_a, V_b, V_c)}{2} \quad (5.2.1)$$

This will give a signal with a lower peak for the signals Figure 5.5. The lower peaks makes it possible to increase the output line to line voltage up to 15% as for THIPWM, but giving a lower harmonic distortion [10].

5.3. Investigation of THD

By using the induction machine parameters given in Table 2.1 the machine phases can be represented as three RL loads. By using the three mentioned modulation techniques to control the switching of an inverter the total harmonic distortion can be found.

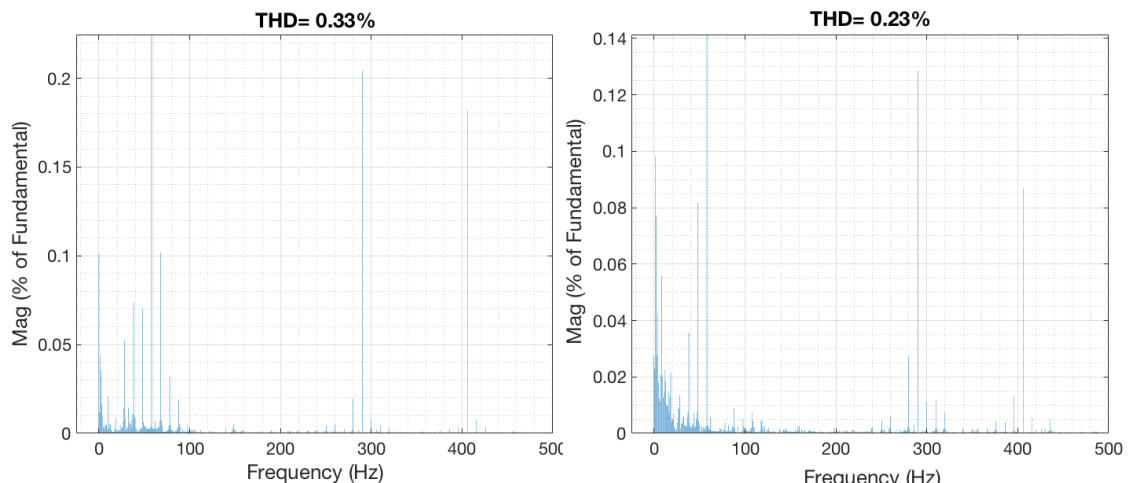


Figure (5.7) SPWM THD

Figure (5.8) THIPWM THD

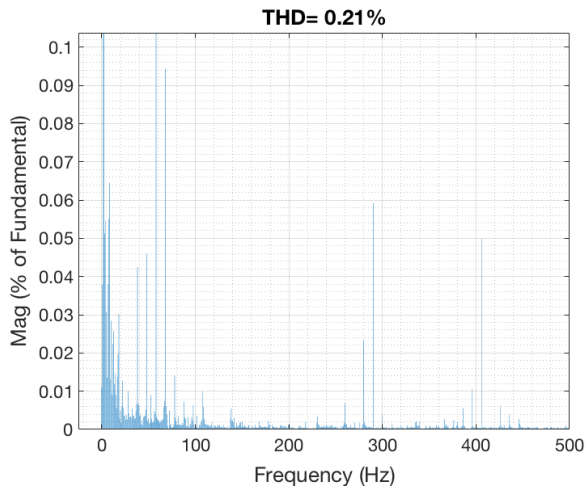


Figure 5.9.: SVPWM THD

As shown on Figure 5.7 to Figure 5.9, the THD is low. This is due to induction machine working as a filter and reduces the harmonics. The difference in harmonics distortion for the modulation techniques are no longer significant and this affect by using any of the methods is very little.

5.4. Conclusion on modulation

The two best of the mentioned methods for modulation are the SVPWM and the THIPWM. By looking at the harmonics, the SVPWM is generally giving the lowest total harmonic distortion of the two[9]. By adding the induction machine as a load, the difference in harmonics distortion is not significant. The better utilisation of the DC voltage by using either THIPWM or SVPWM is of greater importance. SVPWM is chosen as the preferable modulation technique.

6. Software Implementation

6.1. Implementation of modulation

The output of the controller is three voltage reference signals. These three signals are compared to the same triangular carrier signal, giving three different modulation patterns one for each of the phases. Only three signals are needed for the gate drivers to control the switches. To generate the LS gate signals a the HS signals are inverted, making it possible to control each phase leg with a single gate signal per phase.

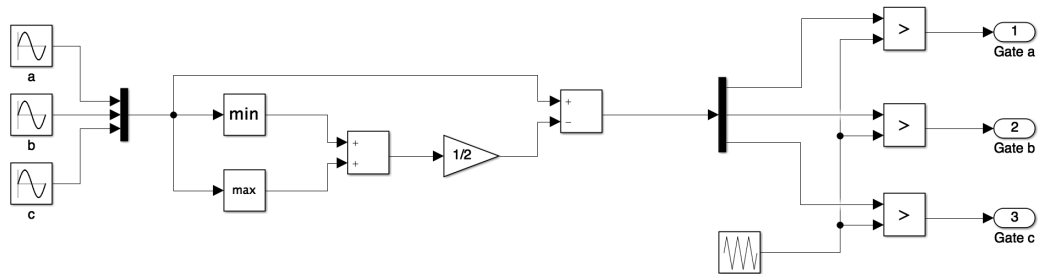


Figure 6.1.: SVPWM analytically implementation

As seen in Figure 6.1 the Equation 5.2.1 is implemented to determine the magnitude of the triangular common mode signal by using the "min" and "max" functions in simulink. The output signal, when adding the min and max, becomes a triangular wave with tripled frequency compared to the sinusoidal reference, see Figure 6.2. The logic comparison with the carrier is implemented to show the output, but will be replaced by a ePWM block made by Texas Instruments. The block is using the internal clock cycles of the MCU to generate the PWM output.

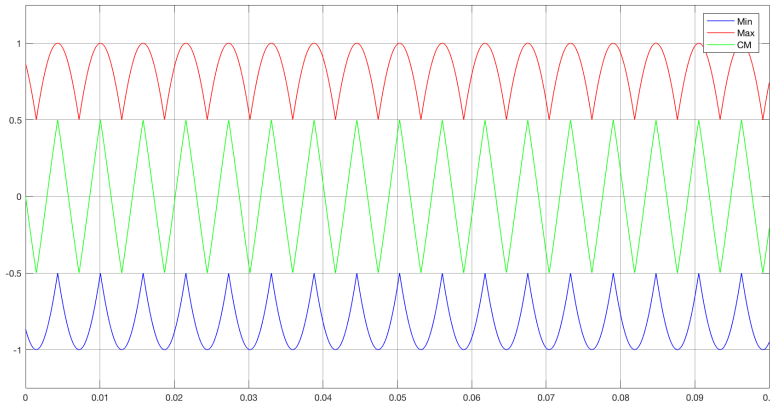


Figure 6.2.: Construction of triangular signal

This triangular signal is then divided in half and subtracted from the sinusoidal reference, generating the ramp signal reference. The new reference signal is then compared with a triangular wave, by using the rational operator (greater than). This constructs the three needed gate signals as shown in Figure 6.3.

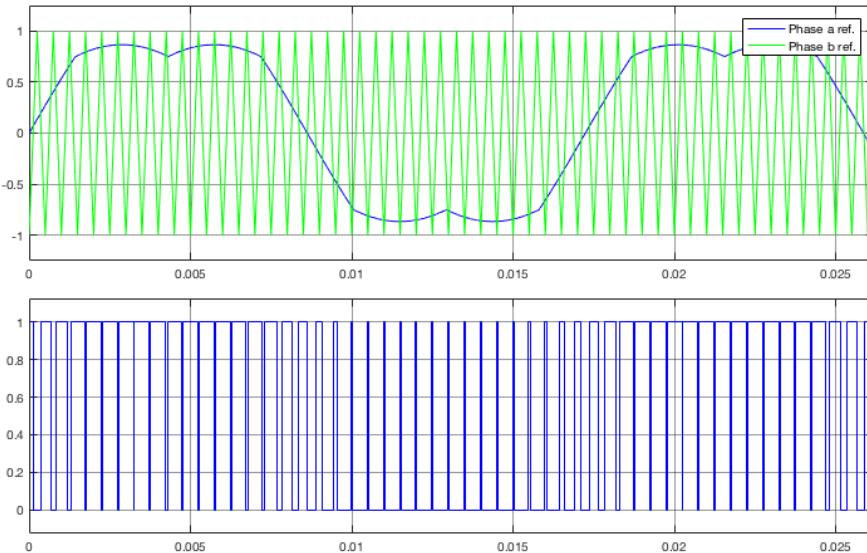


Figure 6.3.: SVPWM Gate signal

To verify the PWM sequence is correct and is generating the space vector, the signals are fed to a 3-phase convert in simulink and by transforming the output phase voltages into $\alpha\beta$ -reference frame a space vector trajectory can be plotted as seen in Figure 6.4.

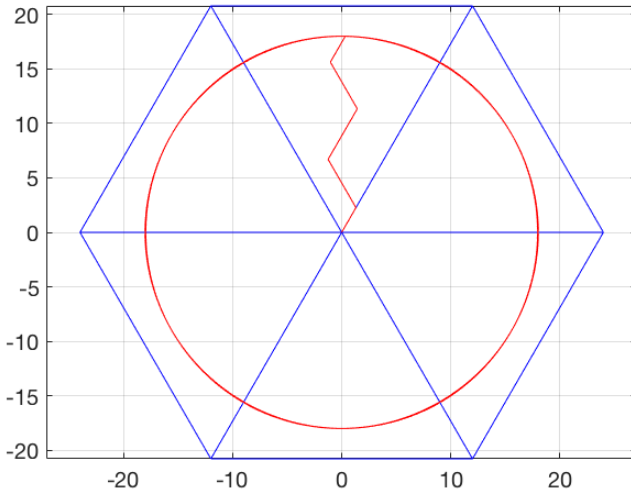


Figure 6.4.: Space vector trajectory

The trajectory shows a close to perfect circle, which means that the space vector is correctly generated.

6.2. MCU

In order to run the control software, which is shown in chapter 4, on the Go-Kart the microcontroller "TMS320F28075" from Texas Instruments will be used. It is mounted on a board which is called "Piccolo F28075 controlCARD" (Figure 6.5). This MCU is going to be placed on the interface board which provides all necessary input signals and output connections.



Figure 6.5.: Image of the MCU "Piccolo F28075 controlCARD"

This MCU is directly connected to the interface-board by using the HSEC8-Connector which can be seen at the lower edge of the MCU in Figure 6.5. This Connector is supplying the MCU with 5 V as well.

6.2.1. Connection to MCU

Mathwork is providing an Add-on Hardware Support Package for SimuLink to communicate with the "F28075 MCU". This Add-on makes it possible to compile the SimuLink model and directly convert the code into C-code. The C-Code will be automatically uploaded to the MCU by Code Composer Studio. The whole procedure is done by the Add-on within SimuLink. This makes it possible and convenient to build the control software purely in SimuLink. By simply connecting the MCU via USB cable the software can be compiled and uploaded to the MCU.

6.2.2. Communication with MCU

In order to connect the controller-scheme, which is made in SimuLink, to the inputs and outputs it is necessary to use different interface blocks. These blocks directly configure the MCU and enable the register to set the correct settings of the GPIO-pins. These blocks and the configuration of them is explained in the following part.

GPIO

The general-purpose input/output (GPIO)-block is used for a basic digital output. The purpose is to transform a boolean signal within SimuLink into a digital signal on a specified pin. According to the state of the signal, the pin has a potential of either 0 V or 3.3 V.

The GPIO-block only needs to be configured by determine the port number respectively pin number of the used pin.

PWM

The pulse-width modulation (PWM)-block is used to provide the gate-driver with switching signals. As explained in chapter 5 the controller provides a rump shaped reference signal which needs to be transformed into a pulse width modulated signal consisting of on and off states. The PWM-block is realising this modulation by creating the triangular carrier-signal and comparing it to the reference signal.

The input of this block is chosen to be the duty cycle in percentage which means than the reference signal needs to be between zero and one. Thereby, the generated space vector signal, which is the input, needs to be shifted up and scaled to fit in the range. The second input of the PWM-block is the period width of the carrier signal in clock cycles. This parameter defines up to which value the up-down counter is counting to produce the triangular signal of the carrier. This value directly determine the switching frequency of the inverter.

The output of this block is a digital signal like the GPIO-signal which providing the gate signal as seen in the lower graph of Figure 5.1.

The PWM-block is implemented three times, once for each phase leg. The carrier signal of the three blocks are directly synchronised by the settings to ensure that the switching instances are the same. One of the PWM-blocks is configured to provide a trigger signal to the ADCs when the carrier signal is reaching the top of the triangular form. The implementation for the triggering is explained in the following part.

ADC

The analog-to-digital converter (ADC)-block is used to convert the analog signal on the input of the MCU into a digital signal that can be used in the controller. The input

signals coming from the current and voltage measurement sensors consists of a voltage signal between 0 V and 3.0 V. By using a 12-bit sampling the ADC is making a linear conversion of the signal into a number between 0 and 4095. The number can be converted into the needed unit-system according to the given sensors. This way the output is a digital number in Ampere or Volt depending on the measurement.

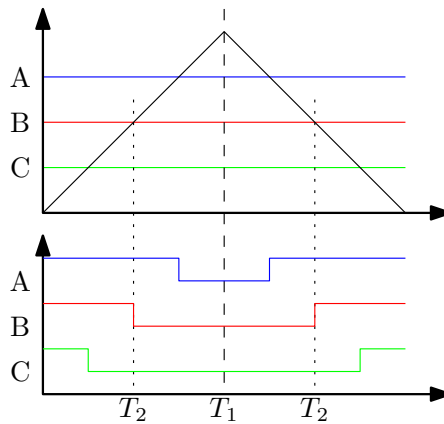


Figure 6.6.: three phased modulation scheme of one carrier period

The Figure 6.6 shows the reference signals A, B and C with the carrier signal in the upper figure and the result of the modulation comparison in the lower figure.

In order to get the accurate value of the sampling, the measurement moment of the ADC needs to be outside the switching moments of the duty cycle (T_2 for phase B). Otherwise overshoots could distort the value of the measurement. To prevent from that the value needs to be measured in the middle of each active time of the duty cycle (T_1). That ensures that the measurement can not be taken at a switching moment (T_2). The moment in the middle of an active time of the duty cycle is equal to tip of the triangular carrier signal.

By getting a trigger signal for this specific moment from the PWM the ADCs can be configured to sample at the right time (T_1).

The MCU only has three ADCs available and therefore it is necessary to use them for more than one signal by multiplexing. That means that two pins will be connected to one ADC which is sampling them after each other. For the current measurement it is very important that the values are exact because these values are used to control the machine. Thereby the three ADCs for the current measurements are triggered by the

PWM. The torque input and the DC-voltage measurement can be sampled at a different time instant. Therefore the current measurement is triggering these after finishing its sample. After this second measurement the ADC is waiting for the next trigger signal from the PWM.

eQEP

The block for enhanced quadrature encoder pulse (eQEP) will be used to interpret the signal from the encoder in order to calculate the speed in rpm from the given position that the encoder is measuring on the rotor.

As mentioned in section 2.3 the encoder provides three signals A, B and Z which are showing the pulses. The structure of the signals is shown in Figure 6.7.

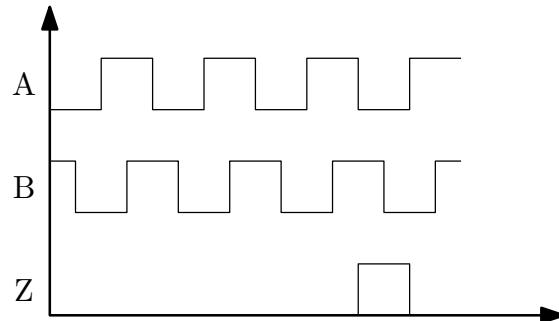


Figure 6.7.: Structure of the encoder signals A, B and Z

If signal A is running leading signal B (as in Figure 6.7) the rotor is turning clockwise. The rotational direction is available as an output from the eQEP-block. The signal Z shows one pulse for every revolution. It is used during the calculation to reset the counter that is counting the pulses.

For the signals A and B each period represents one pulse. By that each rising flank is triggered per pulse. The time between the pulses can be measured and with the known 2048 pulses per revolution the speed in rpm can be calculated.

The eQEP-block is providing the calculation of the time between two pulses as an output of the block. This signal is further on used to calculate the speed.

To configure the block, one of the eQEP-modules need to be specified to define the pins.

MCU Software scheme

All the blocks that have been described are needed in order to connect the hardware to the controller in SimuLink. By joining these blocks together the software frame for the controller corresponds to the Figure 6.8.

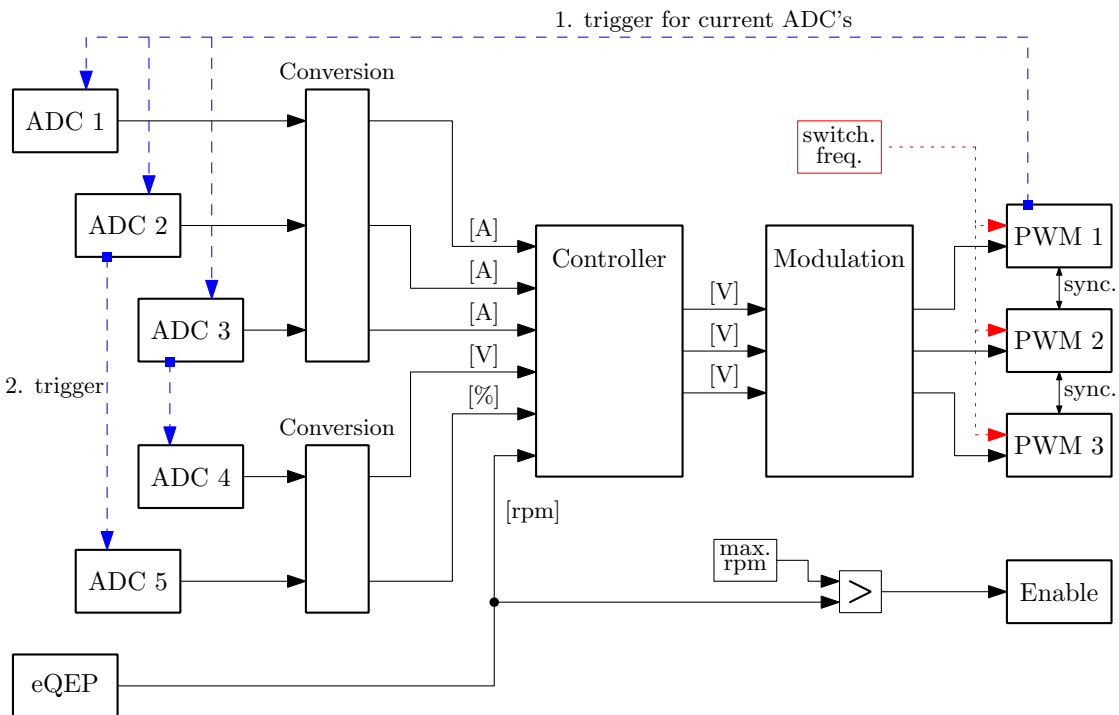


Figure 6.8.: combined scheme of the MCU blocks

The general structure of this scheme is going from the inputs on the left side via processing of the signal in the center to the outputs on the right.

The blue dashed lines show the triggering between the PWM and ADC-blocks and the red dotted lines show the configuration of the PWM with the switching frequency. The Enable output is calculated by comparing the measured rpm-value to a chosen maximum rpm-value. The conversion-blocks are representing the conversion from the giving value of the ADCs into the needed unit based value which is shown in square brackets.

7. Inverter hardware

This chapter presents the developed inverter first with the selection of concept, design and simulation, then implementation, test and validation and finally conclusion.

7.1. Introduction and requirements

When designing for high power and high current applications it is important to consider not only the circuit design, but also thermal management, circuit layout and the parasitic elements. These topics must all be covered in order to have a good functional product. The following sections will investigate the requirements and possible concept solutions for the inverter.

It has been chosen to run the motor at the 60 min. power rating of 7.3 kW. Based on this and the system specifications the inverter phase currents can be derived as:

$$V_{motor\ rated} = 24 \text{ V}_{\text{rms}} \quad (7.1.1)$$

$$P_{motor} = 7300 \text{ W} \quad (7.1.2)$$

$$S_{motor} = \frac{P_{motor\ rated}}{PF_{motor} \cdot \eta_{motor}} = 10915 \text{ VA} \quad (7.1.3)$$

$$I_{phase} = \frac{S_{inverter}}{\sqrt{3} \cdot V_{motor\ rated}} = 263 \text{ A}_{\text{rms}} \quad (7.1.4)$$

$$I_{pk} = \sqrt{2} \cdot I_{phase} = 371 \text{ A} \quad (7.1.5)$$

Switching high currents results in high losses, and a low switching frequency is desired. However, considering the application for the inverter is a Go-Kart, and that a low frequency could produce an audible tone, a switching frequency of 20 kHz is preferable. The system must be designed to operate within the range noted in Table 7.1, and a decision for the switching frequency must be made based on switching losses.

The system efficiency must be designed with a high efficiency to ensure sensible use of the battery capacity and reasonable size of cooling system.

Parameter	Symbol	Value	Unit	Condition
Output power	S_{out}	10.9	kVA	
Switching frequency	f_{sw}	3 - 20	kHz	
Efficiency	η	>90	%	At full output power
DC link nom	V_{DC}	36	V	
DC link max	$V_{DC \ max}$	45	V	
DC link min	$V_{DC \ min}$	27	V	
DC link ripple	$V_{DC \ pkpk}$	2	Vpp	
Output current nom	$I_{Out \ nom}$	263	Arms	
Output current peak	$I_{Out \ pk}$	371	A	

Table 7.1.: Inverter requirements

7.2. Concept selection

The chosen topology for the inverter is a 2-level topology, in other words the inverter is able to produce two output voltage levels. The 2-level inverter consists of three half-bridges connected to a DC-link. The half-bridge is composed by two switches for each phase, which is turned on and off for each period. The schematic for the topology is shown in Figure 7.1

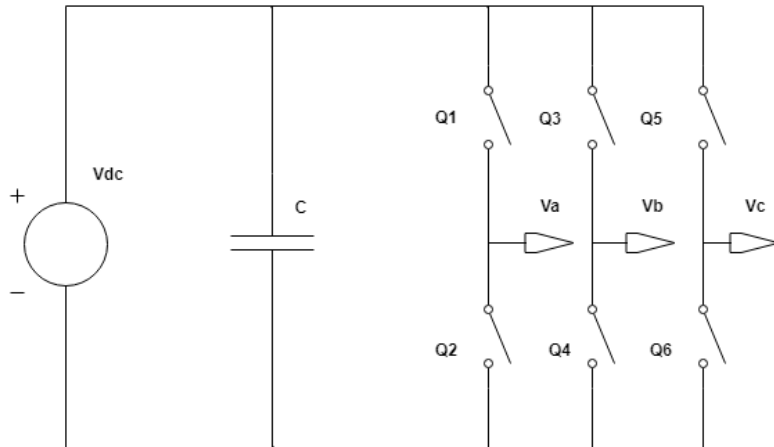


Figure 7.1.: Schematic of 3-phase 2-level inverter

The switches are driven by a pulse width modulation (PWM), which turn on the high side switch and turn off the low side switch simultaneously. To prevent the two switches

to turn on at the same time, a dead-time is integrated in the switching transition.

Advantages and disadvantages of the 2-level inverter topology [11]

Advantages

- Simple circuit topology
- Small size of the DC capacitors
- Reduction of the price, compared to a 3-level inverter

Disadvantages

- Higher harmonic distortion, compared to a 3-level inverter
- Higher losses than a 3-level inverter

The design of the 2-level inverter consists of choosing a switch, that is suitable for the application, as well as a gate driver for the switch. Thereby the thermal design is made, to ensure a functional operation. Nevertheless, the layout of the circuit is designed, to minimise parasitic elements and prevent failure in the circuit.

7.2.1. MOSFETs vs. IGBT

The Insulated Gate Bipolar Transistor (IGBT) is a high current and high voltage applications device. The IGBT can be considered a combination of a Bipolar Junction Transistor (BJT) and a Metal Oxide Semiconductor Field Effect Transistor (MOSFET), where the insulated gate technology is from a MOSFET and the output characteristics of a BJT. The output characteristics of an BJT, makes the IGBT beneficial in high voltage application, since a small voltage drop will almost be neglectable compared to the total losses. Nevertheless, this result is more significant in low voltage operation since it is more substantial compared to the overall losses.

A MOSFET is low voltage and low power device, where the operation voltage is typically ($< 250V$)[12]. Due to MOSFETs high input gate resistance, it has a fast switching time, which make it good for fast switching application, since it results in a reduction of the switching losses.

A limitation for the MOSFET can be the drain current(I_d) capability. This problem can be neglected, since a parallel connection of MOSFETs can be done safely, due to the positive temperature coefficient and thereby reach a higher drain current capability. The MOSFET is more efficient at lower current levels, compared to the IGBT, but in the region of extreme high current, the IGBT is better, since the voltage drop across the MOSFET drain-source resistance, is higher than the gate emitter diode voltage drop for the IGBT. The relationship between the power losses and the current for the MOSFET and IGBT is shown in Figure 7.2

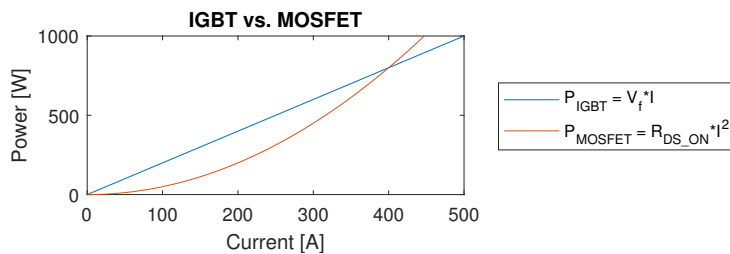


Figure 7.2.: IGBT and MOSFET losses vs. current

The MOSFET is the ideal switch for high frequency and high current application, compared to the IGBT, where this devices is preferred to be used under low frequency condition. Since our requirement for the switching frequency is between 3kHz-20kHz, with low voltage and high current, MOSFETs are ideal design choice for the given application. The prerequisites for the selected component is compliance with system requirements.[13]

7.2.2. Package types

Choosing a specific MOSFET or IGBT for an inverter application, not only the device parameters is important, but also device package. Both the device parameters and the package have directly impact on performance. The package choice is a critical part of the circuit layout and introduces certain parasitic components.

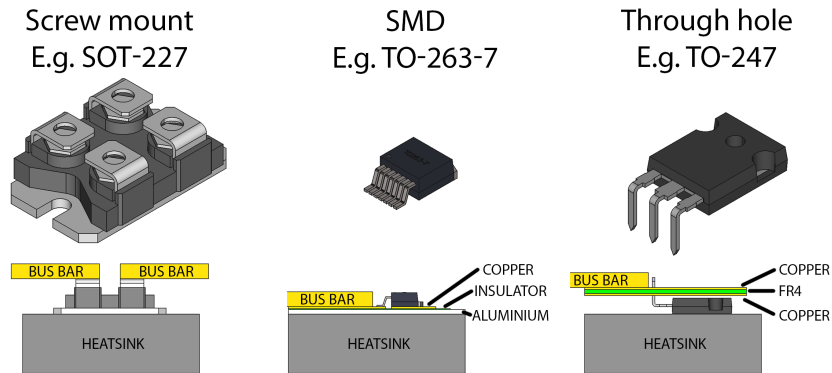


Figure 7.3.: Comparison of SOT-227, TO-263-x and TO-247

	Screw mount	SMD	Through hole
Heat sink coupling	Very good	Medium	Good
Conductor	Bus bar	PCB + Bus bar	PCB + Bus bar
Possible PCB layers	-	1	1-8
Footprint	Large	Small	Medium
Expected parasitics	Medium	Very low	Low

Table 7.2.: Peripheral considerations for MOSFET package type

For instance, the thermal coupling of a SOT-227 to the heat sink is much better than a Surface-mounted device (SMD) or through hole layout due to the direct coupling and large surface area. Apart from being bulky, a larger footprint potentially means larger current loops. This results in more parasitic inductance. For switching applications this can cause problems with EMI within own and other circuits, but also with switching as will be described later in section 7.3.4.

When it comes to device parasitics, SMDs are usually the best due to the short legs. In comparison to through hole and specially screw mount components, SMD devices usually have lower parasitic values. This is due to the shorter and often increased number of legs. This means lower losses (lower R_{DS_ON}) and better switching (lower gate loop inductance). Through hole designs however have the advantage over a SMD solution that they allow the use of multi-layer boards which makes PCB layouts much simpler.

7.2.3. Chosen concept

For this project a 2-level inverter topology has been chosen as a trade-off between simplicity of control and harmonics. As the application is battery powered, reflected harmonics are of less concern. Further, MOSFET technology has been chosen over IGBT due to the superior conduction efficiency for the given current range. To keep the footprint and parasitic inductances to a minimum, SMD packages must be used. This requires the use of Aluminium core boards, which makes thermal coupling to the heat sink very efficient.

7.3. Design and Choices

Based on the choice of concept a 2-level inverter has been designed. Figure 7.5 shows the design of a single phase, shown in details in subsection A.1.2. The following subsections goes through the design choices and considerations, first for the phase leg with selection of MOSFETs, then the gate driver design and finally DC-link. It should be noted that it should here be noted that the gate driver has been designed as a daughter board, while the phase leg and DC-link is placed on a single sided Aluminium board.

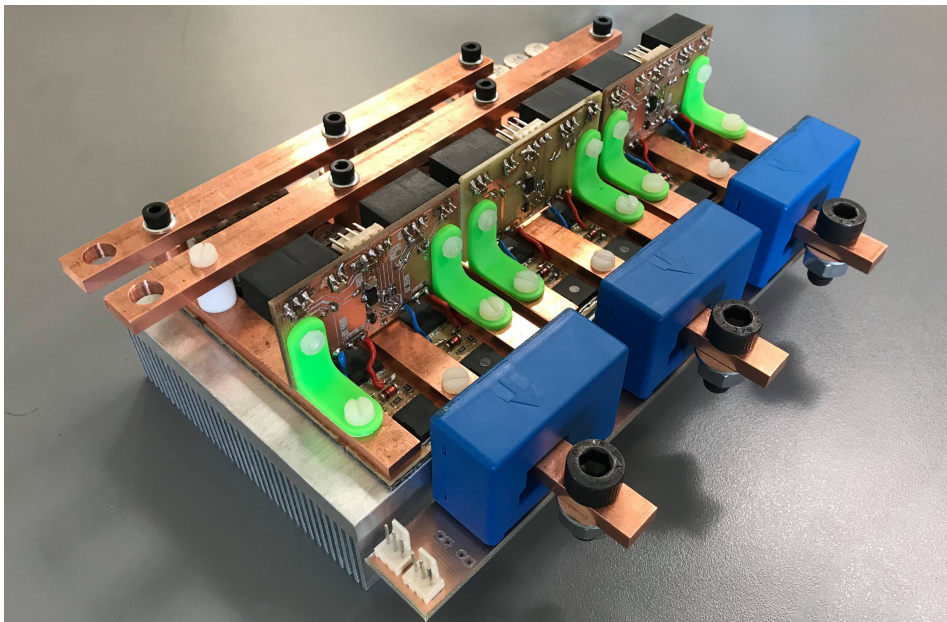


Figure 7.4.: The finished module based inverter, with current transducers attached.

7.3.1. A modular approach

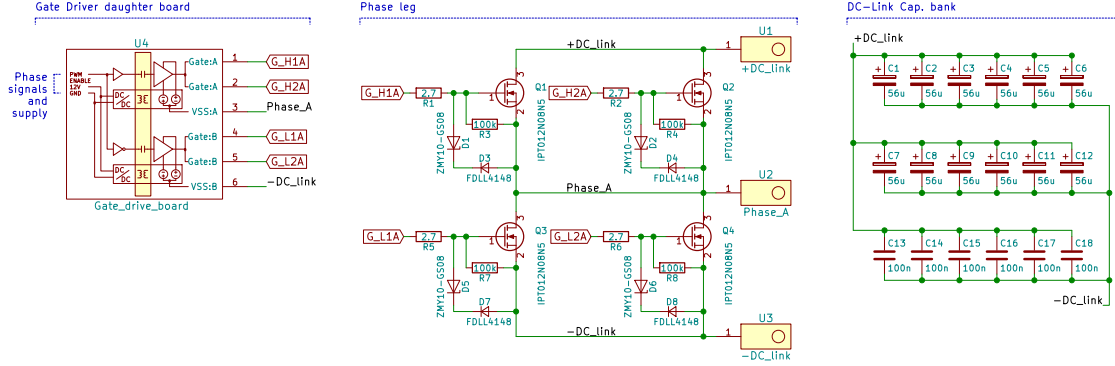


Figure 7.5.: Schematic of single phase. See subsection A.1.2 for full schematic.

Developing hardware means making choices often compromising between factors. Apart from functional requirements, project management must be considered as well. Sufficient time must be allocated for testing and redesign to ensure project success.

Designing an inverter can be done as a single three-phase system or three identical single-phase systems, also known as a modular design. Choosing a modular design can be beneficial for testing as the lower number of system elements makes troubleshooting faster. In addition, the cost of redesigning is reduced as fewer components are required per iteration.

A three-phase system on the other hand can be expected to have a smaller footprint and will have a reduced assembly time and potentially lower cost for a large scale production. However, for this project a modular design has been chosen based on time plan and budget considerations.

7.3.2. Phase leg

A 2-level phase leg is simply a half bridge, consisting of a low- and high side switching device. The initial step of designing this is selecting the specific devices. From the concept it is required to use SMD MOSFETs.

The selection process starts by evaluating a number of candidate devices to the inverter requirements from Table 7.1. From the system requirements it is stated that the inverter bridge must operate for a voltage of 36 V and a maximum current of 371 A. The

requirement is the comparison parameter, which decide the switches selection for the inverter.

MOSFET selection

The MOSFET for the inverter is selected according to the inverter requirement, where different devices are compared, based on the key parameters in Table 7.3 [14]

Parameter	MOSFET's				Unit
	AUIRFS3006-7P	IPT007N06N	IPT012N08N5	AUIRF7749L2TR	
Drain-source voltage (v_{ds})	60	60	80	60	V
Drain current (Id at T=100°)	207	300	279	243	A
Drain-source on-resistance ($R_{DS,ON}$ at T=100)	2.25	1	1.4	1.65	mΩ
Gate Charge (Q_g)	300	287	233	275	nC
Package	D2Pak 7 pin	pg-hsot-8-1	pg-hsot-8-1	DirectFET	
Thermal resistance junction-case (R_{thJC} max)	0.4	0.4	0.4	0.44	°C/W

Table 7.3.: MOSFET selection

Channel

MOSFETs can be define as two types, where the structure of the silicon inside the switch, define the if it is n- or p-type. The difference between the two types of MOSFET is defined by the applied voltage to turn on the switch, where a p-type is turn on by a negative voltage and a positive voltage for the n-type. The n-type is beneficial compared to the p-type, where it has a higher mobility and longer life time, due to the carriers in the n-type is electron compared to the p-type, where there is holes. [15]

Voltage and current ratings

The drain-source breakdown voltage rating (V_{DS}) must be chosen carefully. If it is exceeded the device goes into avalanche mode which may cause significant damage to the device. Thereby is it importance to choose a V_{DS} which is sufficiently higher than the operation voltage, considering a safety margin for voltage spikes as a result of parasitic loop inductance and switching high currents. However, MOSFETs with higher V_{DS} rating usually have a higher $R_{DS,ON}$, which result in an increase in conduction losses. Based on the nominal voltage, an estimated 60 V rating is required. It should however be investigated by SPICE simulation if it is sufficient.

Based on a search by distributors as Farnell and RS-Online a current rating above 300 A can not be reached in a single device package. This is solved by using parallel devices, which is possible due to the positive temperature coefficient of R_{DS_ON} as described earlier. However, as will be described in section 7.3.4 a good safety margin is required, so a rating above 200 A continuous current and above 400 A pulsed current should be selected.

Drain-source on resistance

The drain- source ON resistance also known as R_{DS_ON} , is an important parameter since it dictates the conduction losses for the MOSFET. The R_{DS_ON} value depends on the gate to source voltage (V_{GS}) and temperature, hence it is necessary to choose a R_{DS_ON} common temperature as reference point when comparing between datasheets. The R_{DS_ON} parameter has a direct impact on the system efficiency, due to the conduction losses of the MOSFET. Based on the system requirement, the conduction losses are the dominating losses, which make the R_{DS_ON} value an favourable parameter for comparison. From Figure 7.6 it can be seen that IPT007N06N[16] and IPT012N08N5[17] are the devices with lowest conduction losses, but due to the IPT012N08N5's higher power capability it is better to withstand the parasitic transient [18]. The loss calculation from Figure 7.6, is based on the equation in subsection 7.3.3.

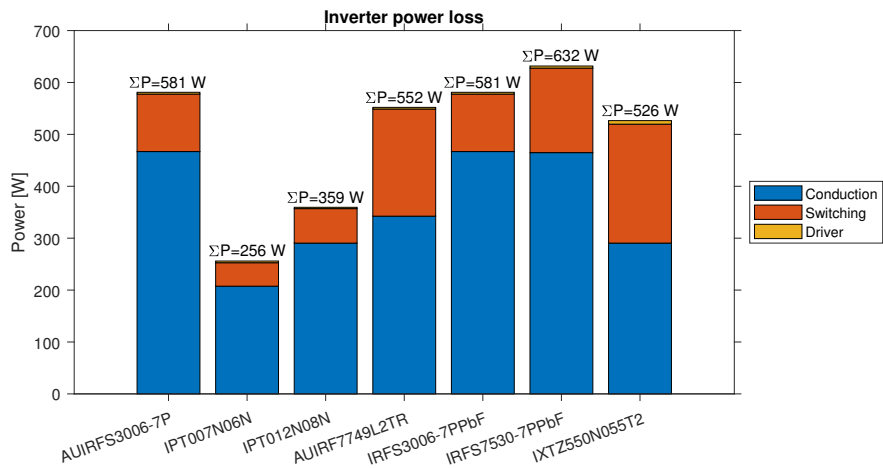


Figure 7.6.: Comparison of the losses for the MOSFET selection

Gate charge

The Gate charge parameter describes the energy it takes for the device to be in conduction mode. For high switching application, the gate charge has a significant impact on the switching losses, and thereby it is preferable to choose a MOSFET with a low gate charge as it will reduce the switching losses. From Figure 7.6 it can be seen that the switching losses are not significant compared to the conduction losses, which make the gate charge parameter less important for this application.

Package

The type of package for the MOSFETs must meet the electrical- and thermal requirements for the system. The layout of the printed circuit board makes the SMD technology preferable, compared the through-hole packages, to ensure proper solder between the PCB and the device. The package of the chosen MOSFET is PG-HSOF-8-1, which is a part of the HSOF package family.

Chosen component

Based on the above mentioned design parameters for IPT007N06N[16] and IPT012N08N5[17], they are the most suitable MOSFETs, due the low R_{Dson} and package layout, which make it advantageous for the system. Since the IPT012N08N5[17] has a higher drain-source voltage V_{ds} capability, it can ensure a safety margin for the transient that occurs in the turn on and off transition of the MOSFETs.

7.3.3. Thermal design

In the thermal design of the MOSFETs, it is important to ensure that the device is operating below the maximum junction temperature. The MOSFETs are generating the majority of the heat, thereby it is important to calculate the power loss, to ensure the reliability of the device.

Heatsink selection

To determine the size of the heatsink, the power dissipation of the MOSFETs must be evaluated. The power dissipation of the device consists of the conduction-, switching- and diode reverse recovery losses, but since the diode losses are small compared to the

total loss, it can be neglected. The losses are calculated from a single MOSFET, but by including the total amount of switches in the inverter, the total thermal resistance of the inverter circuit can be calculated. The MOSFETs behave as a resistor during the conduction mode, thereby the average conduction losses can be calculated from the following equation[19].

$$P_{con} = R_{DS(on)} \cdot \left(\frac{I_{rms}}{n_{parallel}} \right)^2 = 24.2092 \text{ W} \quad (7.3.1)$$

The current, I_{rms} is the rms current the device is conducting, which is 263 A. The drain-source on resistance ($R_{DS,ON}$) for the MOSFET IPT012N08N5 is 1.4 mΩ. The switching losses for the turn off and on transition of the MOSFETs can be calculated as the sum of the turn on E_{onM} and off E_{offM} energy. The switching losses are calculated using Equation 7.3.2 - Equation 7.3.4[19].

$$E_{onM} = V_{dc} \cdot \frac{I_{Don}}{n_{parallel}} \cdot \frac{(t_r + t_f)}{2} \cdot Q_{rr} \cdot V_{dc} \quad (7.3.2)$$

$$E_{offM} = V_{dc} \cdot I_{Don} \cdot \frac{(t_r + t_f)}{2} \quad (7.3.3)$$

$$P_{sw} = (E_{onM} + E_{offM}) \cdot f_s = 5.4222 \text{ W} \quad (7.3.4)$$

Where $V_{dc} = V_{ds}$ (drain-to-source voltage) and is it considered to be the nominal voltage of the battery is 36 V. The current $I_{Don} = I_{peak}$, which again is the peak current. Q_{rr} is the gate charge, where the maximum charge value of the MOSFET is chosen. t_r and t_f is the rise and fall time of the MOSFETs and f_{sw} is the switching frequency which is 20 kHz, for the worst case scenario. The total losses of the one MOSFET can be conclude as the following.

$$P = P_{con} + P_{sw} = 29.6314 \text{ W} \quad (7.3.5)$$

$$P_{total} = 29.6314 \cdot 12 = 355.5768 \text{ W} \quad (7.3.6)$$

$$\eta_{inverter} = \frac{\frac{P_{motor}}{\eta_{motor}}}{\frac{P_{motor}}{\eta_{motor}} + P_{total}} \cdot 100 = 95.89\% \quad (7.3.7)$$

The P_{motor} is 7.3 kW and the η_{motor} is 0.88%, which gives a overall efficiency of the inverter to be 95.89%. Before determining the size of the heatsink, the temperature of

the MOSFET without the heatsink needs to be calculated, to determine whether there is need of a heatsink or not.

$$T_J = P \cdot R_{thJA} + T_a = 1210.25^\circ\text{C} \quad (7.3.8)$$

R_{thja} is the thermal resistance from junction to ambient, which is 40 K/W, P is the total power loss pr. MOSFET's, which is find in Equation 7.3.5. T_a is the ambient temperature, defined as 25°. The junction temperature is 1210.25 °, which exceeds the maximum temperature for the MOSFETs which is 175°, therefore a heatsink is necessary for the system to achieve a functional operation.

The thermal resistance for the heatsink is calculated for the operation temperature of 100°, to ensure that the junction temperature does not exceed the maximum T_j . The thermal resistance of the inverter circuit is describe as following.

$$R_{thJA} = R_{thJC} + R_{thCS} + R_{thSC} + R_{thCI} + R_{thIA} + R_{thAP} \quad (7.3.9)$$

- R_{thJA} Thermal resistance from junction to ambient
- R_{thJC} Thermal resistance from junction to case
- R_{thCS} Thermal resistance from case to solder paste
- R_{thSC} Thermal resistance from solder past to copper
- R_{thCI} Thermal resistance from copper to insulation pad
- R_{thIA} Thermal resistance from insulation pad to aluminium
- R_{thAP} Thermal resistance from aluminium to thermal paste

$$R_{thSA} = \frac{T_j - T_a}{P} - R_{thJC} - R_{thCS} - R_{thSC} - R_{thCI} - R_{thIA} - R_{thAP} \quad (7.3.10)$$

$$R_{thSA} = 1.6748/12 = 0.139^\circ\text{C}/\text{W} \quad (7.3.11)$$

The thermal resistance of the heatsink should be smaller then the thermal resistance of the inverter circuit, to ensure a reliable thermal performance. The chosen heatsink is a 890SP-02000-A-100, which has a thermal resistance of 0.07°C/W. For the thermal performance of the heatsink, a Papst type 3312 fan will be connected to apply airflow across the heatsink.

7.3.4. Gate drive

The design choice of using an Infineon IPT012N08N5 as the switching MOSFET, and the requirement of using two devices in parallel determines the design boundaries for the gate driver.

Briefly covered, a traditional gate driver is a circuit connected between the gate and source terminals of a MOSFET or IGBT. It is used to transition the device between the on- and off-state by charging or discharging the gate capacity. The transition rates, known as fall- and rise time depends on the rate of charge and discharge. To obtain the lowest switching losses as per subsection 7.3.3 a fast transition time is desired. The required gate driver peak current can be approximated based on Equation 7.3.4.

$$I_{Gate} = \frac{Q_g}{t} \quad (7.3.12)$$

, where Q_g is the gate charge and t the desired fall- or rise time. The current is then limited to this by the gate resistor, which is selected based on Equation 7.3.4.

$$R_{Gate} = \frac{V_{high} - V_{low}}{I_{Gate}} - R_{int} \quad (7.3.13)$$

However, for applications with parallel devices and high current switching, designing a gate driver requires considering more than switching losses.

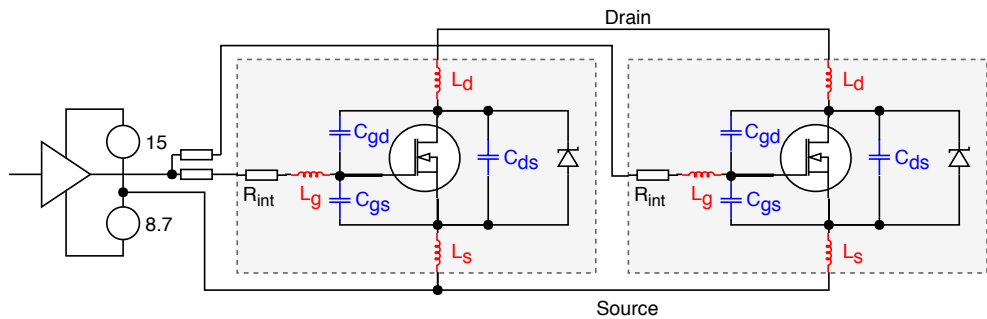


Figure 7.7.: Critical path where ringing may occur unless sufficiently damped

Figure 7.7 shows two parallel connected N-channel MOSFETs, driven by a single gate driver through individual gate resistors. If they were ideal devices, i.e. identical and

without parasitic elements, driving them would not differ from driving a single device. This is however not the case and the problems must be managed to ensure good switching characteristics.

Parallel device considerations

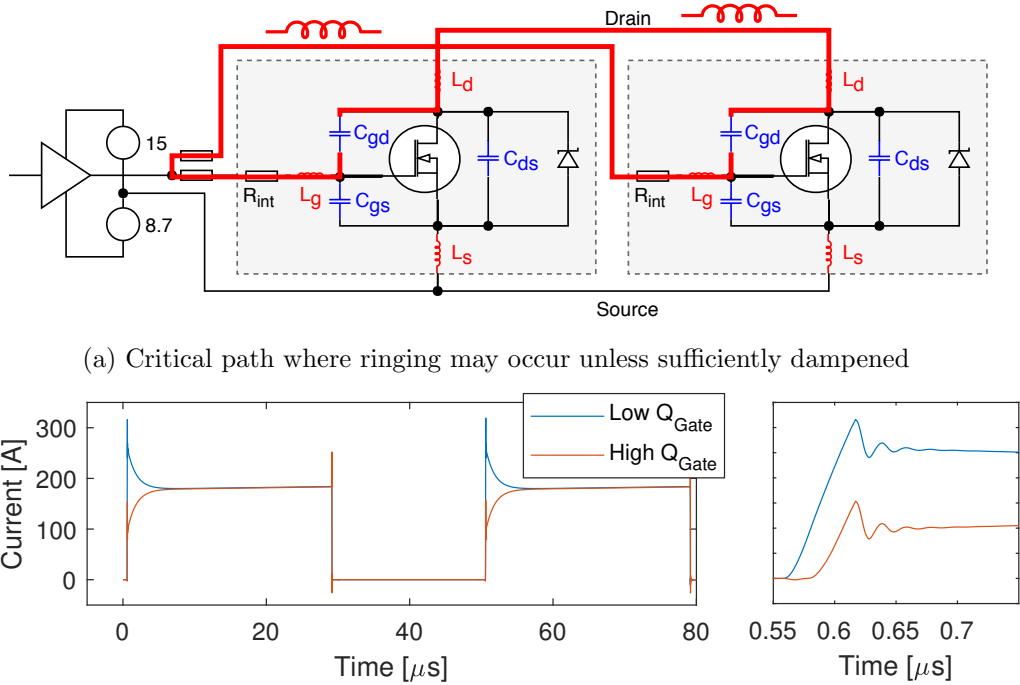


Figure 7.8.: Parallel connection considerations

Figure 7.8a shows why it is critical to use individual gate resistors. If not, the Miller capacitance, C_{gs} of each MOSFET would be directly connected in parallel through the drain terminals of each device. Together with the parasitic drain- and trace inductances this forms a resonant tank, only damped by the internal resistance of the gates. To prevent this, individual gate resistors are used. It would be ideal to use large value resistors, but this would slow down the switching, thus increasing switching losses. More importantly, it would increase the unbalance in turn-on times between the devices. The unbalance arises from the unavoidable difference in C_{gs} - and gate threshold values. The result is that the device which is turned on first, will draw a larger initial current than the other as shown in Figure 7.8b.

High current considerations

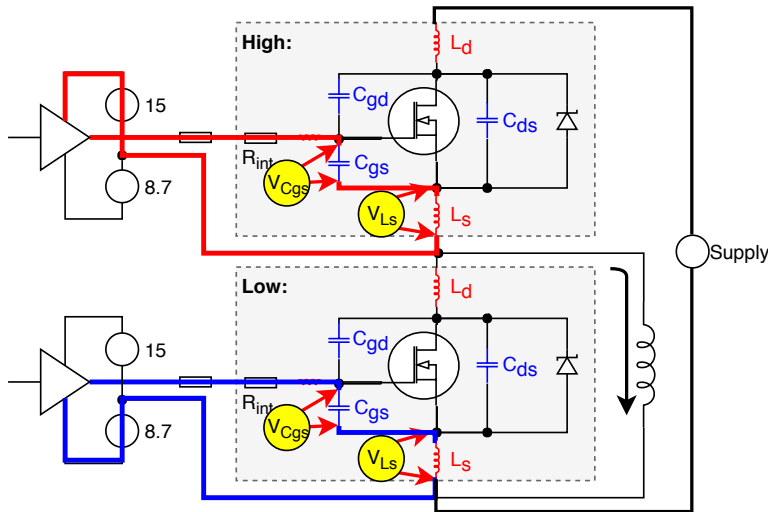


Figure 7.9.: Minimal source inductance is critical for good switching characteristics

In switching, high current applications it is critical to minimise the amount of source inductance. Due to the high rate of change in current during the switching transition, a significant voltage will build up over the parasitic inductances in the loop.

From Figure 7.9 it is clear that a voltage across the source inductances, V_{Ls} will affect the voltage across the gate-source capacitance, C_{gs} . Depending on the direction of current, the voltage will either add to- or subtract from the applied gate-source voltage. If the phase current is positive and the low side device is fully turned off - Turning on the high side device will create a positive voltage across the high side source inductance. The simulated effect of this, investigated in section 7.4 is shown in Figure 7.10.

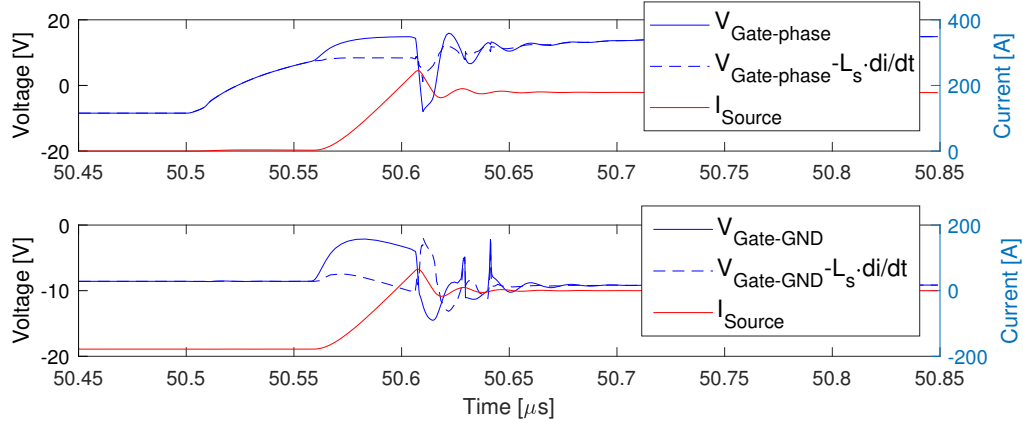


Figure 7.10.: High side MOSFET during high current transition

By subtracting the inductor voltage ($V_{Ls} = L_s \cdot di/dt$) from the gate-source voltage, reveals that V_{Cgs} is slightly discharging during turn-on. Similar for the low side device a decrease is shown, but also a large brief increase after the reverse recovery peak in the source current just after $50.61 \mu s$. This shows that using a negative off-voltage for the gate driver may be required to prevent a parasitic turn on of a low side device.

Gate drive requirements

Requirements for the gate driver, must be set in order to design and pick specific components. In order to reduce the risk of parasitic turn on, a positive and negative rail is required for each gate drive. As the high side supply will float with the phase voltage, separate isolated supplies are required.

A bipolar DC/DC converter, MGJ2D241509SC from Murata with a +15 V, -8.7 V has been chosen for each gate drive, due to simplicity of implementation, considering the time frame of the project.

Having selected the voltage, the current requirement must be set. As this will dictate the gate resistor, a compromise must be made. On the one side, a large resistive value is required to damp the parallel connected miller capacities in the parallel devices. On the other side, a low value is required to quickly supply the gate charge, reducing the switching losses through fast rise/fall times.

The fastest rise/fall times are 18/20 ns according to the IPT012N08N5 datasheet. Using Equation 7.3.4 and assuming Q_g to be $1.5 \cdot 223 \text{ nC}$ as the value is specified from 0 to 10 V,

returns a current of $16.7 A_{pk}$. From Equation 7.3.4 the gate resistor should be about 0Ω , which is close to the internal resistive value. Selecting a three times slower rate of 60 ns returns acceptable values:

$$I_{Gate} = \frac{Q_g}{t} = \frac{1.5 \cdot 223 \text{ nC}}{60 \text{ ns}} = 5.575 \text{ A} \quad (7.3.14)$$

$$R_{Gate} = \frac{V_{high} - V_{Low}}{I_{Gate}} = \frac{15 \text{ V} - (-8.7 \text{ V})}{5.575 \text{ A}} - 1.6 \Omega = 2.65 \Omega \quad (7.3.15)$$

Selecting a 2.7Ω resistor results in a total damping of $2 \cdot 2.7 \Omega + 2 \cdot 1.6 \Omega = 8.6 \Omega$, and a gate current of $5.5 A_{pk}$. This is chosen as an initial acceptable compromise, but a redesign may be required if test later show issues with gate ringing.

The gate driver must hence be able to source and sink a minimum of $11 A_{pk}$.

Driver circuit

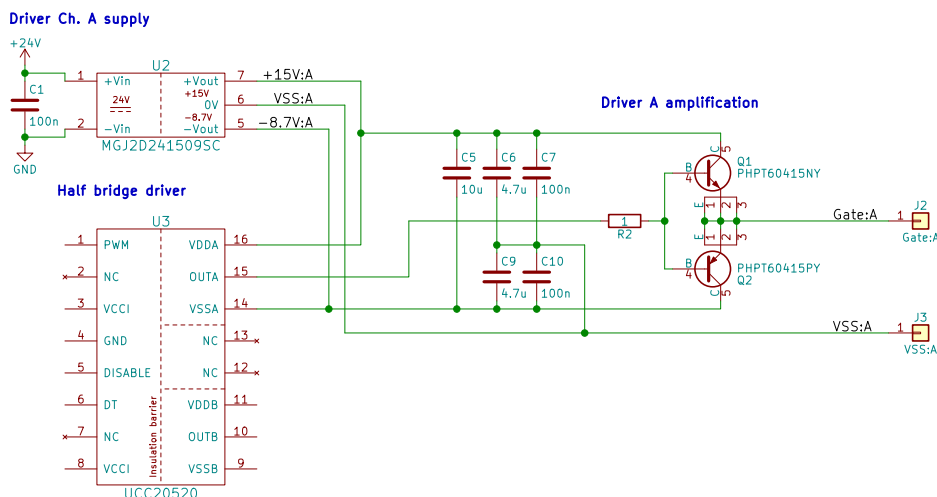


Figure 7.11.: Segment of the gate driver schematic from subsection A.1.3, showing the high side channel, which is identical to the low side.

As the $11 A_{pk}$ rating is quite high, a single half-bridge Integrated circuit (IC) driver can not be used. This leaves two possible approaches; Either using two drivers, one for the high side and one for the low side devices. This however requires the controller to handle the gate drive PWM signals for both high and low side, while ensuring a dead-time period. The other option is to use a half-bridge driver, and add an external totem-pole

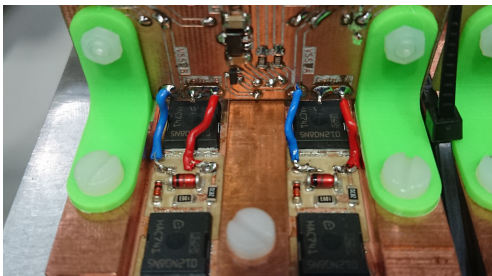
amplifier to both channels.

For the project, the latter option has been chosen as partially shown in Figure 7.11. The chosen gate driver IC handles dead-time generation and generates the inverted signal for the low side channel internally. This simplifies the requirements for the motor-controller and adds to the reliability of the project by preventing shoot-through due to unintended overlap of high and low side signals.

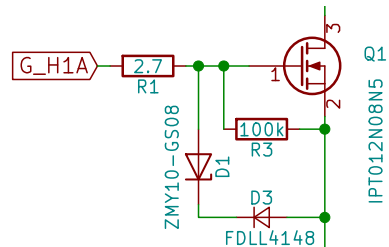
Amplification stage

The amplification stage is based on a Bipolar junction transistor (BJT) push-pull stage using high frequency power BJTs. The choice PHPT60415NY/PHPT60415PY for NPN/PNP is based on the transition frequency rating above 100MHz, as well as a current rating of 15A. The transition rate is important as a slow transition would propagate to the driven MOSFETs thereby preventing the intended switching characteristics.

Gate driver connection



(a) Board interconnections.



(b) Gate drive components on the inverter phase board

Figure 7.12.: The gate resistor and clamp are placed on the inverter phase board

As the gate driver boards and modular inverter phase boards are connected by wires, an inductance is introduced in the gate drive loop. To prevent this making a resonant tank with the gate inductance, the gate resistor is placed directly at the MOSFET, together with the pull-down resister and gate clamp.

7.3.5. DC-Link Capacitor bank

DC-link capacitor has a big role in power conversion electronics. Choosing right DC- link capacitor is extremely important on lifetime and efficiency of the system. The main role

of DC-link capacitors in inverter are to provide low impedance path for ripple current, to provide almost constant DC voltage and reducing leakage inductance of the inverter. In electronic devices like inverters, the ripple currents can lead to degradation of devices by raising their internal temperature. Ripple currents are effects of the load inductance (motor), bus voltage and PWM frequency of the inverter.

DC-link capacitor also reduces leakage inductance in the inverter which can cause high voltage spikes and damage the device. Therefore, designing a DC-link capacitor with right capacity and low impedance is crucial for efficiency of the inverter. In order to find out the DC-link capacity, the ripple current needs to be calculated.

Ripple current is maximum when duty cycle is at 50 %. Derived equation for calculating maximum ripple current is obtained from paper[20].

$$\Delta I_{0.5t} = \frac{0.5 \cdot (1 - 0.5) \cdot V_{bus}}{f \cdot L} \quad (7.3.16)$$

Where V_{bus} is DC-link voltage, f is minimum switching frequency and L is inductance of the load[20].

The DC-link voltage is 36 V(subsection 2.4.1), Inductance of the motor is $31.16 \mu H$ [21], while minimum switching frequency in a inverter is 3 kHz. Including this in Equation 7.3.5 the ripple current is $96.27 A_{pp}$ or $34.03 A_{rms}$. Adding safety margin of 10 % to maximum ripple current yields $37.4 A_{rms}$. The DC-link bus capacitor has to be sized to meet current ripple requirements and at the same time, to keep ripple voltage at level desired for system. Before choosing right capacitors to meet this requirements, it is necessary to determine which value of capacitors is needed.

$$C = \frac{V_{bus}}{32 \cdot L \cdot V_{bus} \cdot f^2} \quad (7.3.17)$$

Equation 7.3.17 is obtained from a paper[20], Where L is inductance of the load, $\Delta V_{0.5t}$ is a desired voltage ripple across capacitor at 50 % duty cycle and f is minimum switching frequency. Desired $\Delta V_{0.5t}$ in this case is $2 V_{pp}$. Adding this value into Equation 7.3.17, and yields a desired capacitance of DC-link capacitor around $2000 \mu F$. Choosing a right template has to be done so that the capacitor bank meet the capacity and ripple current

requirements. Good capacitors can handle around 1.5 Arms and in order to handle ripple current, a big number of capacitor will be added in parallel.

The chosen capacitor is hybrid polymer capacitor ZA series [22] which has capacity of $56\ \mu F$. The capacitor can handle ripple current of $1.8\ A_{rms}$ at $100\ kHz$, has a low Equivalent Series Resistance (ESR) of $30\ m\Omega$ and a low Mean Time To Failure (MTTF) of 10000 hours.

This hybrid capacitor offers some advantages over electrolytic capacitors like high ripple current handling, higher MTTF and lower ESR which makes it suitable for motor drives applications[22]. Designing $2000\ \mu F$ capacitor bank yields that the needed number of ZA series capacitors is 36. This means that capacitor bank can handle $64.8\ A_{rms}$, which is above the maximum ripple current calculated to be $37.4\ A_{rms}$. Each capacitor size is $1.02\ cm^2$ which means capacitor bank size is will be approximately $37\ cm^2$. Therefore, capacitor bank has a high ripple current handling and it is not too bulky.

7.4. Simulation

As part of designing the phase leg and gate driver and to verify the final design before building a physical copy, the joined system has been simulated in LTSpice. Spice is beneficial as a tool, as Infineon provides models of the MOSFETS, and NXP of the BJTs used for the push-pull stage. The simulation models can be found in the attached folder that came with this report under *Appendix >LTSpice*. The system is simulated for a single phase with an inductive load in the *Gate_drive_fixed_PWM_80V* model shown in Figure 7.13. To investigate the issues of parallel connection and high current switching as mentioned in section 7.3.4 and section 7.3.4, the two right MOSFETS, M_H2 and M_L2 have been changed from nominal to maximum values for gate charge, gate voltage threshold and R_{DS_ON} .

Chapter 7. Inverter hardware

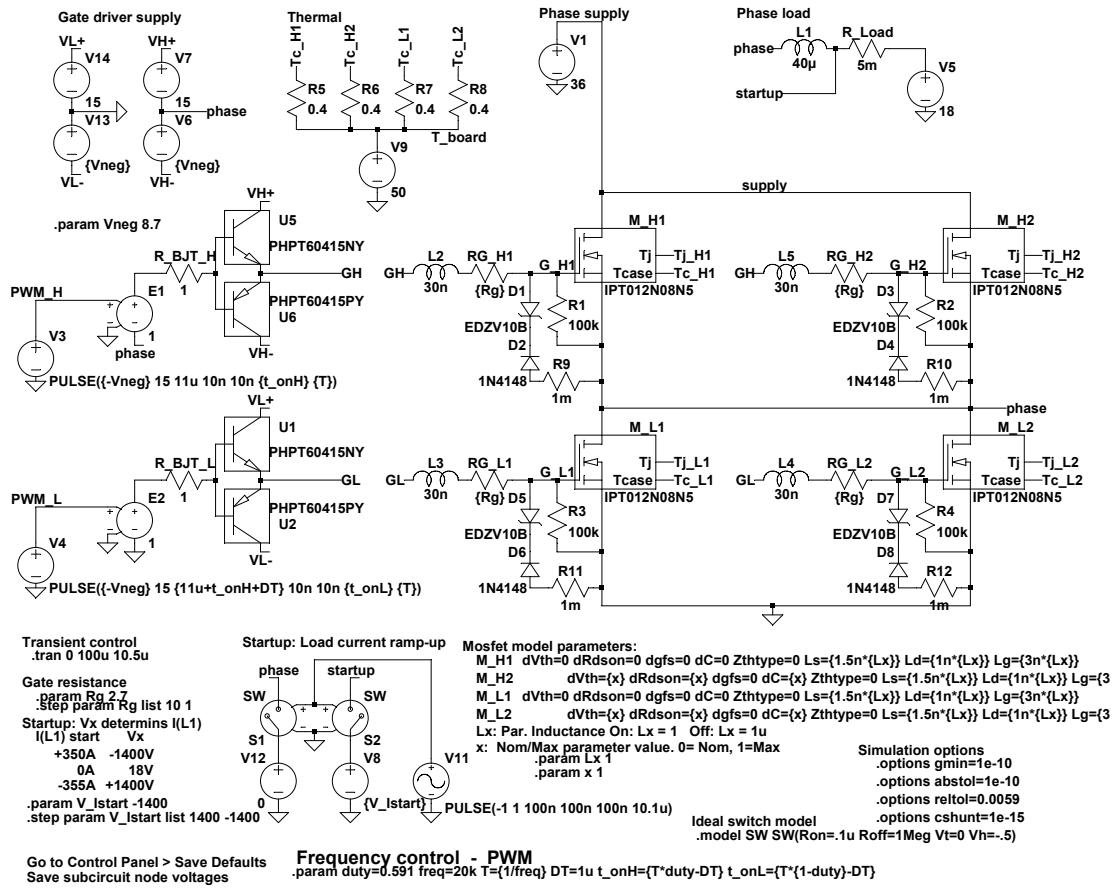


Figure 7.13.: Gate_drive_fixed_PWM_80V.asc

Even though a model of the half-bridge gate drive IC exists, it has been replaced by a Pulse differential supply to speed up the simulation. The startup circuit at the bottom of Figure 7.13 precharges the inductive load to the rated current of the motor (371 A). The resulting switching waveforms are shown on the following page in Figure 7.14.

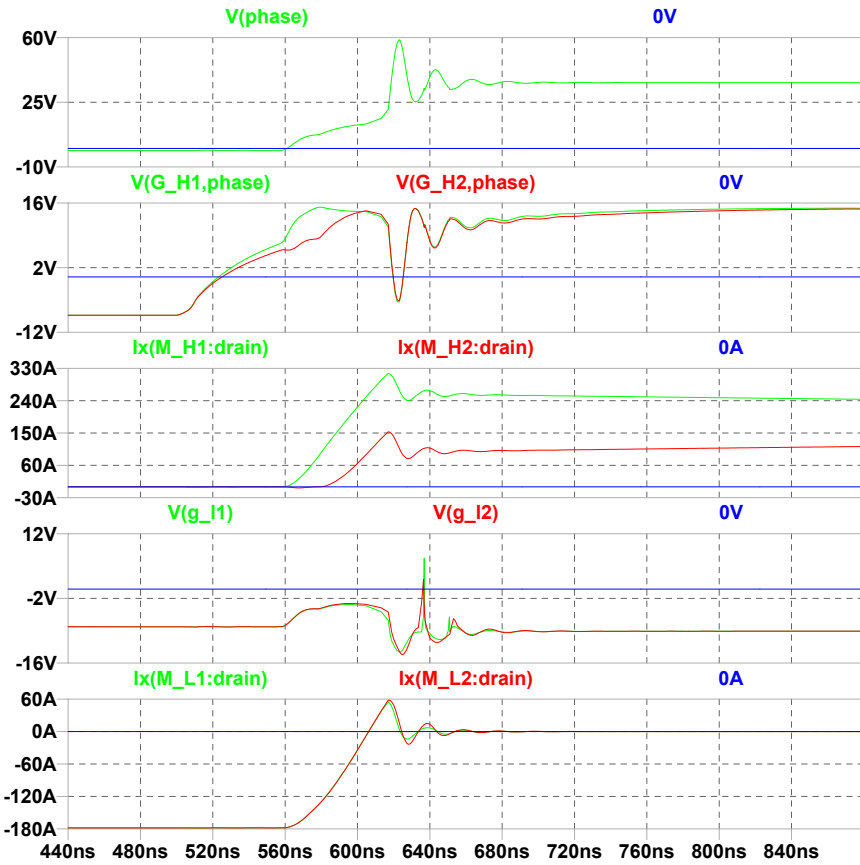


Figure 7.14.: Gate_drive_fixed_PWM_80V.asc waveforms for a 371 A phase current

As the left high side device has a lower C_{gs} and gate threshold than the right, the left one will turn on first, as the required gate charge will be lower. This will further slow down the right device, due to the Miller effect as the phase voltage is increasing. Comparing the drain current for all four MOSFETs with the timing of the phase voltage rise between t:560 ns and 620 ns it is clear that the increase in voltage must be due to the di/dt causing a voltage potential across the parasitic inductances.

The result of this is a delay of about 30 ns difference in turn on time for the left and right devices.

7.5. Test and verification

Double pulse test

In this section describes the experiment, which examines the dynamic performance of the selected MOSFET for the inverter.

The idea behind the experiment is to investigate the parasitic element on the printed circuit board, affecting the dynamic performance of the MOSFET. A double pulse test setup has been constructed for a single phase of the inverter, where the high side MOSFET is the Device under Test (DUT) and the low side MOSFET is working as a freewheeling diode. The test setup for the double pulse test is shown in Figure 7.15

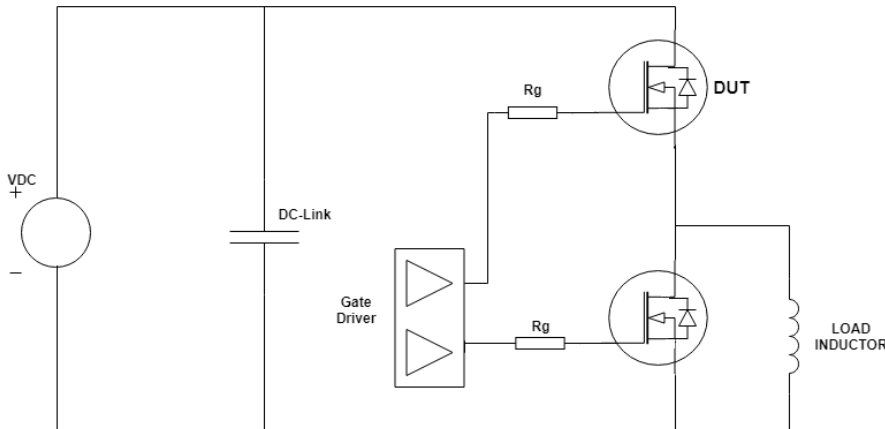


Figure 7.15.: Double pulse test setup

The operation principle of the double pulse test is illustrated in Figure 7.16. The DUT is turned on at t₁, where the load inductor is getting charged to the desired current, at t₂ the DUT is turned off and the MOSFET on the low side is conducting the inductor current as a freewheeling diode. At t₃ the DUT is turned on again, but the conduction period is less than the first one. Finally, at t₄ the DUT is turned off. The pulse width is controlled by a Digital signal processor (DSP), where the desired current can be achieved by adjusting the pulse width. The operation frequency of the double pulse test is low, since the discharge time for the inductor is very large as the $V = L \cdot \frac{di}{dt}$ is limited by the forward voltage of the diode, thereby the discharge time must be very long.

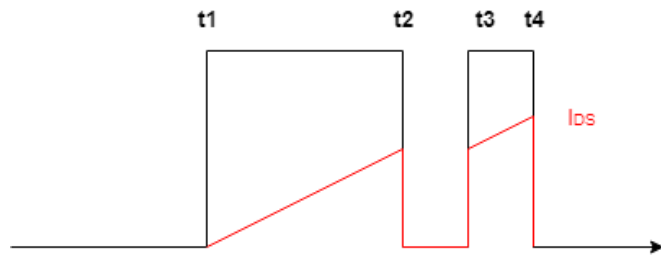


Figure 7.16.: Double plus signal

Experimental test setup

This section describes the result from the laboratory experiments, as well as the LTspice simulation of the double plus test. An investigation of the results from the experiment and simulation will be made. The experimental test setup of the double pulse test is made using two different inductive loads, due to current limitation of the first load, a different inductor is needed to get higher current. The physical test setup is seen in Figure 7.17

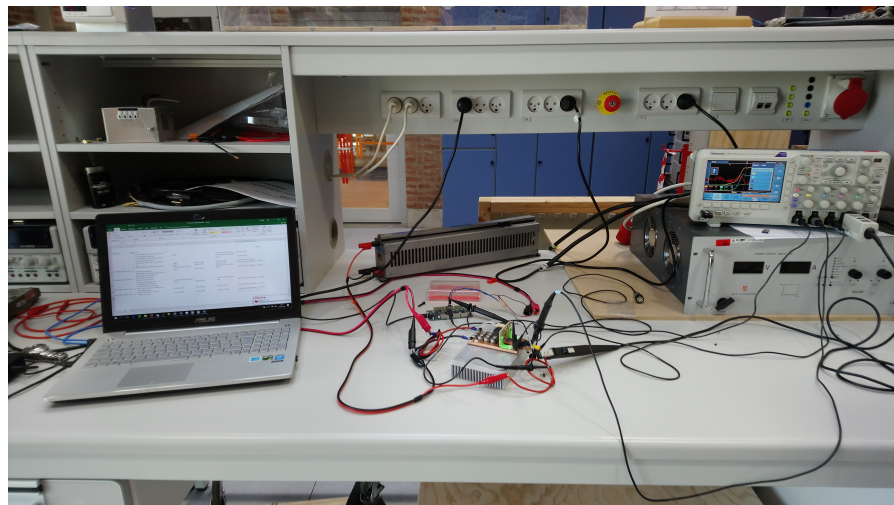


Figure 7.17.: Experimental test setup

Equipment	Type
COMP.Motor	Thrige-Titan Electric
Inductor 1.8mH	NORATEL
6 Power resistor 1.4Ω	
Power supply	SM 45-140
Lab DC power supply	GW instek GPS-4303
DSP	Arduino Due
Oscilloscope	Tektronix TBS1064

Table 7.4.: Test equipment

The experimental test of the double pulse test is based on two different inductive load, as mentioned earlier. The sequence for the test is based on a variation in load current, to investigate the transients that may occur in switching moment t3 at turn off and t4 at turn on. The sequence for the test is described in tabel Table 7.5

Parameter	Inductive Load						
	1.8mH			244uH			
Vdc	36V	36V	36V	30V	30V	30V	30V
I Drain-Source	6.08A	8.56A	27.7A	60A	76.8A	81A	83A
1.Puls	250us	400us	1400us	400us	520us	560us	600us
Break	40us	40us	40us	40us	40us	40us	40us
2.Puls	50us	40us	40us	40us	40us	40us	40us
Frequency	1Hz	1Hz	1Hz	1Hz	1Hz	1Hz	1Hz

Table 7.5.: The sequence for the double pulse test

Practical and simulated results

The voltage waveform of the gate and the phase, as well as the load current in the switching transition is compared for the different conditions. The duty cycle of the switches is the varying factor, for the comparison. The practical and simulated switching dynamic of the switches are illustrated in Figure 7.18- Figure 7.21.

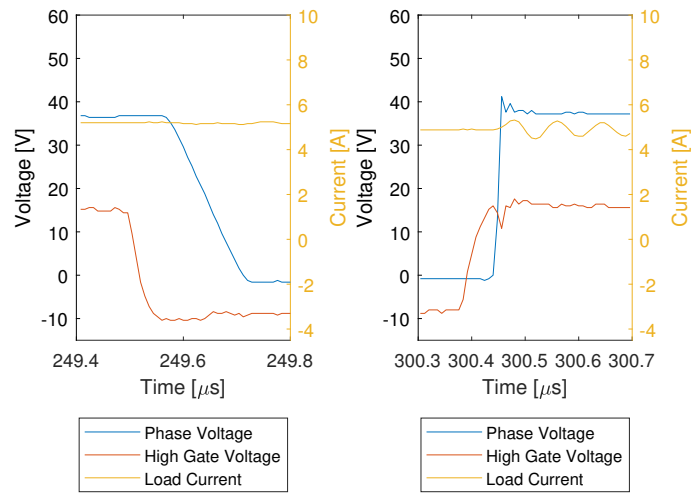


Figure 7.18.: 30V 6.08A turn off and on practical

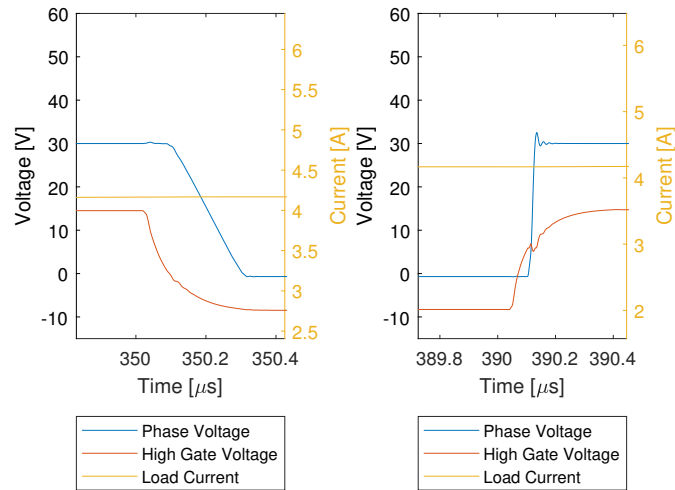


Figure 7.19.: 30V 6.08 turn off and on simulated

Figure 7.18 and Figure 7.19 illustrated the double pulse test for the inductive load of 1.8 mH, with a duration of 250 μ s of the 1.pulse and 50 μ s for the 2.pulse.

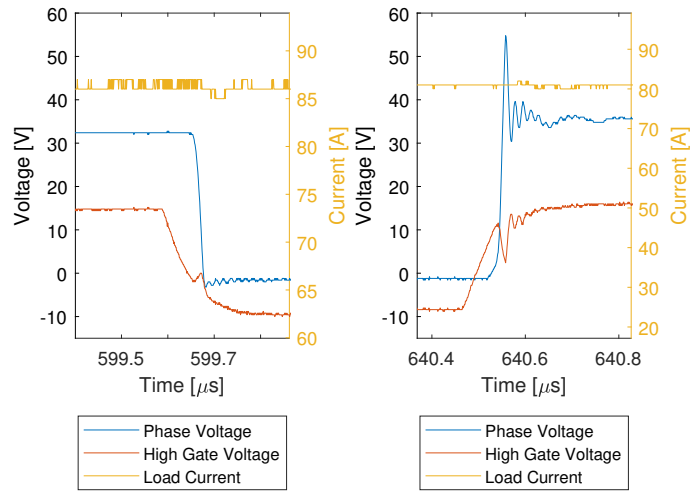


Figure 7.20.: 36V 83A turn on and off practical

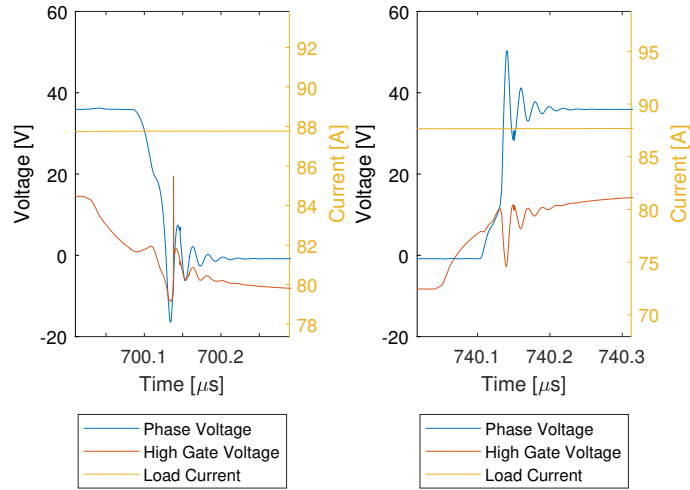


Figure 7.21.: 36V 83A turn on and off simulated

Figure 7.20 and Figure 7.21 illustrated the double pulse test for the inductive load of $244 \mu\text{H}$, with a duration of $600 \mu\text{s}$ of the 1.pulse and $40 \mu\text{s}$ for the 2.pulse.

From the double pulse test, it is seen that there is some transient on the gate and phase voltage. The transient are more significant in the turn on transition, due to the stray inductance in the circuit. The overshoot of the phase voltage is increasing for a higher load current in the test. This is illustrated in Figure 7.20 and Figure 7.21, where the overshoot for load current of $6.08A$ is less than the load current of $83A$. For the gate voltage, there is a drop of the voltage and this is due to the miller effect of the MOSFETs. The voltage transient can cause damage on the transistor, thereby it is important to reduce this parasitic element in the layout design of the circuit. To reduce the parasitic element effect on the circuit, a snubber circuit can be implementing in the circuit and a modification of the gate driver can be done.

DC-test of the single phase inverter

This section describes the experiment, which examines the thermal condition of the modular single-phase board. The background for the experiment is to investigate the thermal condition of the different component on the single-phase inverter. A DC-test setup has been made for the single-phase inverter which is showing Figure 7.22.



Figure 7.22.: DC-test setup

The test setup for the DC-test is similar to the double pulse test, with the difference that the inductive load is connected in series with a resistor bank, to burn the power on. The

sequence for the dc-test is showing in Table 7.7

Equipment	Type
COMP.Motor	Thrige-Titan Electric
6 Power resistor 1.4Ω	
Power supply	SM 45-140
Lab DC power supply	GW
Function generator	Instek GFG-8216
Oscilloscope	Tektronix TBS1064
Thermal imaging camera	Fluke e40

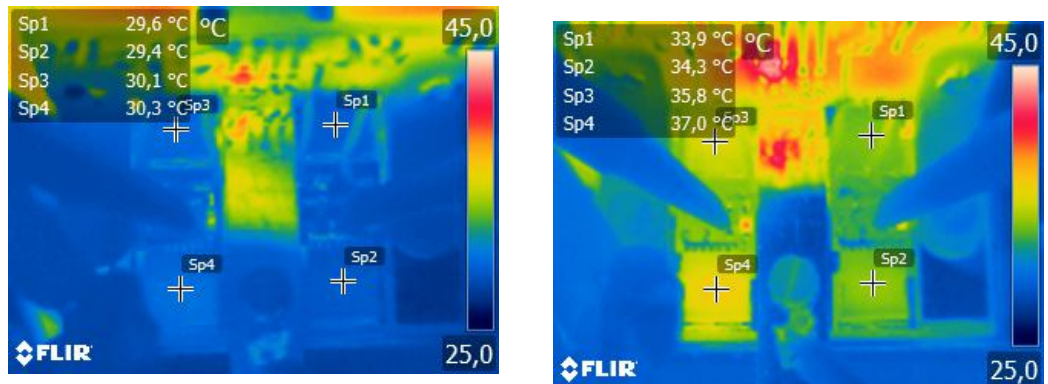
Table 7.6.: Test equipment

Practical results

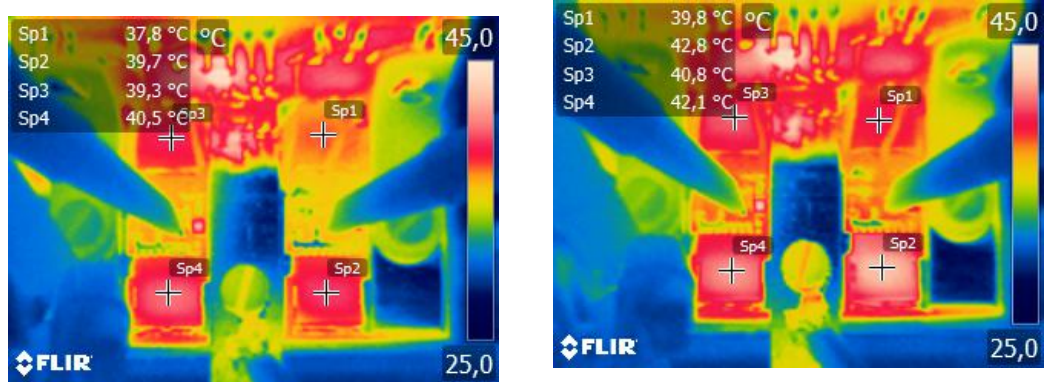
There has been made different test on the single-phase inverter board, with different current levels. The temperature condition of the DUT has been examined by a change of the current. In the DC test, it was not possible to make a test of the maximum current for the system, which is 263 A_{rms} , since there was a current limitation on the power resistor bank. The maximum current that could be achieved for the test was 90 A_{rms} . The results of the temperature measurement of the MOSFETs is illustrated in Table 7.8 and Table 7.7

Test	V supply	Duty cycle	I Average	I Peak	Frequency
1	36V	20%	21.1A	23.8A	20kHz
2	36V	40%	44.7A	47.2A	20kHz
3	36V	53%	60A	62.8A	20kHz
4	36V	61%	70.3A	72.8A	20kHz
5	36V	70%	80A	84A	20kHz
6	36V	77%	89.8A	92.4A	20kHz

Table 7.7.: the sequence for the DC-test



(a) Temp. measurement of the inverter for 44,7 A (b) Temp. measurement of the inverter for 60 A



(c) Temp. measurement of the inverter for 80 A (d) Temp. measurement of the inverter for 89,8A

Test	Q1	Q2	Q3	Q4	Theoretical	Unit
1	29.5	29	30	30.5	30	°C
2	31.8	31.9	33.4	34.5	31	°C
3	33.6	34	35.7	36.8	31	°C
4	35.7	36.6	37.5	38.8	32	°C
5	38.1	39.7	39.7	41	32	°C
6	40.2	43	41	42	33	°C

Table 7.8.: The Practical and theoretical Temperature

The results of the temperature form the DC-test is very close to the theoretical results. Although the measurements are from the surface of the MOSFETS, the should not be a big difference compared to the junction temperature. The different between the practical

and theoretical temperature, start to increase in higher current level. The relationship between the power dissipation and the temperature is linear, thereby the maximum theoretical temperature can be calculated based on the equation in the subsection 7.3.3. The maximum theoretical temperature, based on the functional requirements, which is $263A_{rms}$ and $371A_{rms}$ is $71^{\circ}C$. This temperature is acceptable as it do not exceed the maximum junction temperature of the MOSFETs, which is $175^{\circ}C$.

8. Additional hardware

8.1. DC Chopper

It is well known fact that induction machine is a device that converts electrical energy into mechanical energy and visa versa. When mechanical energy is applied to the rotor, the machine behaves as a generator and produces electrical energy. This characteristic of an electrical machine is commonly used and known in electric car industry as a regenerative braking. Using the kinetic energy stored in the car when in motion can be converted back into electrical energy and stored back into the batteries. This can lead up to more efficient energy management of the car.

While conventional mechanical braking is more efficient solution for braking, the regenerative braking provides an alternative for non-emergency braking, leading to less wear out of the mechanical brakes and improves the overall energy efficiency of the vehicle. This application introduces new problems, that has to be taking into consideration. When the system is turned off and there is applied force on rotor, machine will be in generator mode, starting building up a potential which could lead to damage of the batteries. If the build up voltage, is going into the DC link through the inverter is higher than the charging voltage of a batteries, the batteries will heat up, which could lead to failure.

In order to protect the batteries, a DC chopper circuit will be used. A simple DC chopper circuit is shown in Figure 8.1.

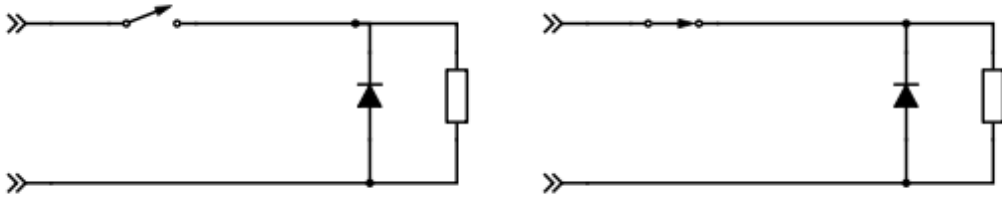


Figure 8.1.: DC Chopper On and Off State

A DC chopper contains a controllable switch, a power resistor which main goal is to dissipate energy and cut off voltage. It also consist of a flyback diode to protect the switch. When the DC-link voltage is lower then the charging voltage for the batteries, the switch will be off and there will be no current going through the power resistor.

The circuit to the right in Figure 8.1 represent the state of the circuit when the switch is on and current going through the resistor which is going to dissipate the energy as heat. This is the basic circuit used in designing DC chopper. It is important that the DC chopper has its own controller circuit due to its main purpose of protecting the batteries when system is in off state.

8.1.1. Controller circuit design for DC chopper

A requirement for the DC chopper controller is to be powered without any supply from the main supply and its functionality is not affected by the main supply being connected to the system or not. According to Figure 2.3, the maximum charging voltage of a single battery is 14.7V which yields 44.1V for all three batteries. It is a requirement for the system that when there is a DC link voltage over 44V, switch should be ON and DC chopper should chop the voltage down. When the DC Chopper chop voltage under 42V, the switch should turn off. The switch-on voltage is the highest voltage the batteries can be charged before increasing the risk of damaging the batteries. The turn off voltage is a design choice taking in account battery discharge voltage. Therefore, desired controller would control the switching between this dual threshold.

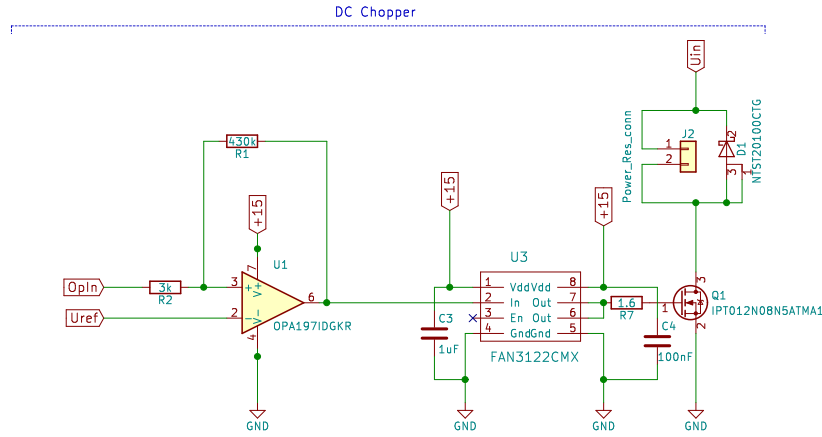


Figure 8.2.: DC Chopper circuit

In Figure 8.1.1 a circuit for DC Chopper is provided. Circuit is based around operational amplifier which acts as schmitt trigger. When logical output from schmitt trigger is +15 V, gate driver is driving MOSFET which is then conducting. Using Schmitt trigger hysteresis characteristics, it is possible to adjust the threshold DC chopper needs. The designed threshold can be seen in Figure 8.3.

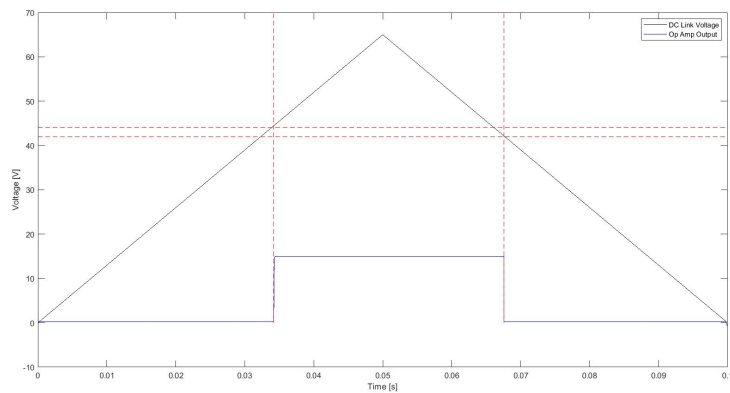


Figure 8.3.: Schmitt trigger hysteresis

The black line represent a ramp input on the DC link, while the blue represent the logical output of operational amplifier which will be used to control the gate driver resulting in a switching of the power MOSFET. Area between 42V and 44V represents hysteresis of Operational amplifier. The gate driver and operational amplifier will be powered from linear regulator circuit shown in Figure A.1.4 connected to the DC link. When the components tolerances are included, the schmitt trigger hysteresis will be approximately 43.5-44.5 V for high and 41.5-42.5 V for low side, which provides good enough threshold for the requirements of the system.

The whole schematic of a DC chopper circuit is provided in Figure A.1.4.

8.1.2. Components selection

Components are chosen based on requirements of the design circuit. As a controller, operational amplifier with specific feedback resistors is used to provide schmitt trigger behaviour. The power MOSFET used for dc chopper is the same one used for inverter and it is selected due to stock availability. While for this application, power MOSFET is over dimensioned, due to higher drain current rating than needed, it still provides good solution for dc chopper switch. Gate driver is selected based on MOSFET gate charge, turn on and turn off time. Power resistor value is 4Ω and rated for 500 W. Other components are chosen solely to provide desired hardware functionality.

8.1.3. Layout design

DC Chopper PCB layout can be seen in Figure A.8. PCB consist of 2 copper layers where all components are soldered. During layout design, some consideration which can affect circuit functionality were taken. Trace width between power resistor, diode and MOSFET had to meet width requirement for current. Because current going through MOSFET and resistor will be around 12 A, required trace width should be more than 10 mm. Other important consideration during layout design was that gate driver is close as possible to MOSFET to reduce a stray inductance. As current going through PCB is not big enough compared to inverter max current, there is no need for external heat sink. Power resistors are usually big and bulky components. Adding 2 connectors to PCB allows power resistor to be connected externally. This makes PCB more compact and easier to integrate into a system.

8.1.4. DC Chopper Test

In order to test a DC Chopper circuit, a simple test setup will be implemented. Main goal is to test controller circuit, schmitt trigger turn on and turn off switch voltage.

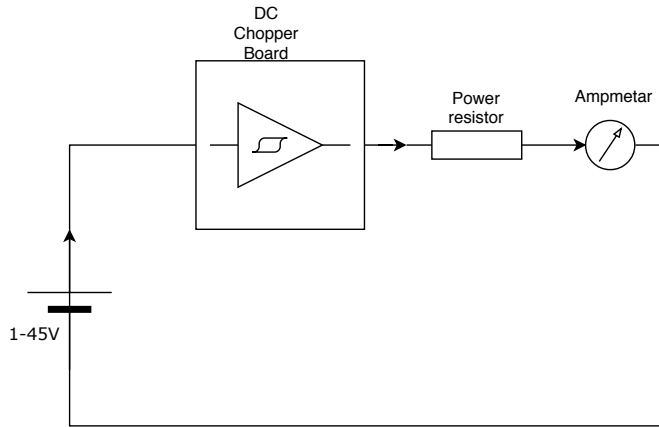


Figure 8.4.: DC Chopper Test

Figure 8.1.4 shows test setup for testing DC Chopper. Setup consist of 2 bench power supply connected in series, power resistor connected externally to DC Chopper circuit and ammeter connected in series with a resistor to measure a current. Power supply is supplying voltage ramp to 45 V to a DC Chopper board. When voltage level applied is higher than 44 V, switch should turn on and there should be current going through resistor measured by the ammeter. Unfortunately, due to lack of time the mistake was not found and proper testing could not be done. While simulation provides good results, soldering provided unexpected problems which exceeds the time limit for testing.

8.2. Interface board

8.2.1. Supply

The interface board is supplied by two 12 V lead acid batteries, which are coupled in series giving a total supply voltage of 24 V. This supply is only used to supply the interface board, which then supplies to internal circuits, cooling fan, gate drives, MCU and current measurement board.

To keep a stable supply to the components varies of linear voltage regulators are used.

Component	Supply
Cooling fan	12 V
Current transducers	± 15 V
Voltmeter High Side	5 V
Voltmeter Low Side	5 V
Auxiliary circuits	± 15 V

Table 8.1.: Supply voltage

8.2.2. Main supply voltage measurement

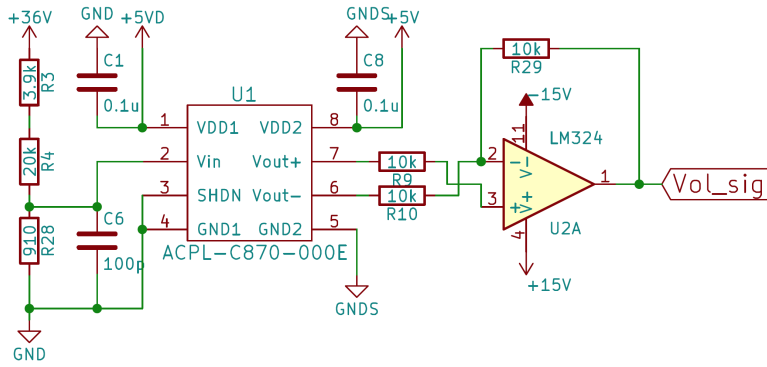


Figure 8.5.: Voltage measurement circuit

Parameter	Notation	Value
Supply voltage	VDD1+2	5 V
Maximum input voltage	V_{in}	VDD1+0.5 V
Withstand voltage	V_{iso}	5000 V

Table 8.2.: Isolation amplifier data [23]

The component "U1" shown on Figure 8.5, is an Broadcom ACPL-C870-000E optical isolation amplifier. Because the interface board is supplied by its own battery package, the main supply measurement for the system has to be galvanic isolated. By using the optical isolation amplifier the measured voltage on the main supply side be transferred to the 24 V side without any electrical connections and thereby obtaining the needed galvanic isolation. The maximum input of the amplifier is 0.5 V above the supply voltage, which here is 5 V, giving a total maximum input 5.5 V. The measured voltage has to be

scaled down by a voltage divider. The ADC in the MCU is a 12-bit, allowing a resolution of $2^{12} = 4096$. Because the voltage measurement do not need a precise measurement, when it is used to determine when the batteries are depleted, the resolution is divided into 20mV/step, allowing voltage measurement up to 81.92 V.

The configuration of the isolation amplifier is chosen base on recommendations from vendor [23].

8.2.3. Inverter output current measurement

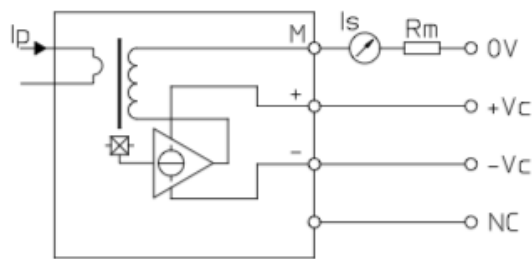


Figure 8.6.: Current transducer [24]

Parameter	Notation	Value
Supply voltage	V_C	$\pm 15 \text{ V}$
Measuring range	I_s	$\pm 300 \text{ A}$
Conversion ratio	K_N	1 : 2000

Table 8.3.: Current transducer data [24]

The current transducer is a LEM LA 200-P, which can measure between $\pm 300 \text{ A}$, see Table 8.3. These transducers were available at the university and due to budget limitation these were chosen. The measuring range limit the maximum output of the inverter, which is taken into consideration. The resistor "R_m" is the resistor used to convert the output signal of the transducers into a voltage signal, which can be used as input for the MCU. The current transducers are located at the output of the inverter to measure the current, making the signals vulnerable to disturbance. The measuring resistor is chosen to be located at the interface, making the transferred signal from the current transducer board to the interface board a current signal. This makes the signal less affected by the electrical

field emitted from the phases.

The measuring resistance is calculated based on the ADC input range of the MCU of 0 – 3 V. The current input measuring range for the transducers are ± 300 A giving a peak to peak of 600 A.

$$R_m = \frac{ADC_{max}}{2} \cdot \frac{CT_{ratio}}{I_{in_{pp}}} = \frac{3}{2} \cdot \frac{2000}{600} = 5[\Omega] \quad (8.2.1)$$

As shown in Equation 8.2.3, the resistor is 5Ω giving a peak voltage signal of 1.5 V. Because the input range of the ADC in the MCU is 0 - 3 V the signal has to be shifted by 1.5 V, giving a signal with peak to peak of 3 V with a DC of 1.5 V.

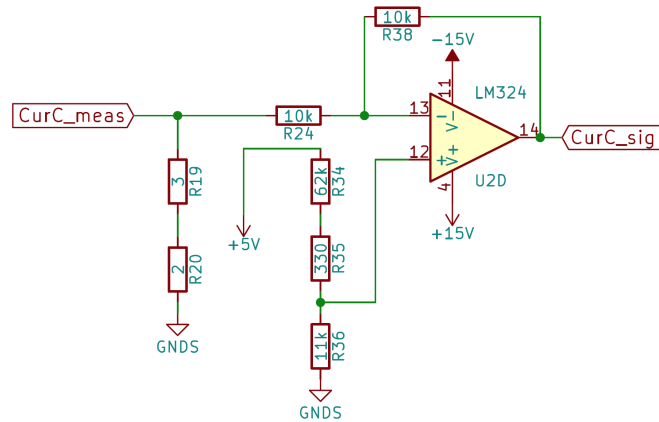


Figure 8.7.: Level shifter circuit

The level shifter circuit is shown in Figure 8.7. It consists of an operational amplifier with a unity gain and the negative input at the voltage signal and the positive input at the DC voltage.

8.2.4. Torque pedal command

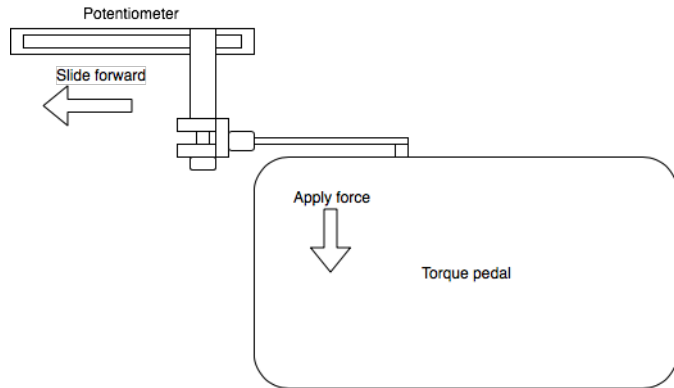


Figure 8.8.: Sliding potentiometer for torque pedal

To control the torque, a torque command given by the driver by applying force to the torque pedal. To measure the torque command, a sliding potentiometer is used.

The potentiometer resistance range is $0.5 - 925 \Omega$ and by making it a part of a voltage divider, the voltage level can be controlled by the potentiometer. The voltage range for the torque command is from approximately 0-3 V.

8.2.5. Signal scaling

For down scaling signals to fit the 0-3 V range of the ADCs, a simple voltage divider is used.

9. System Test and Validation

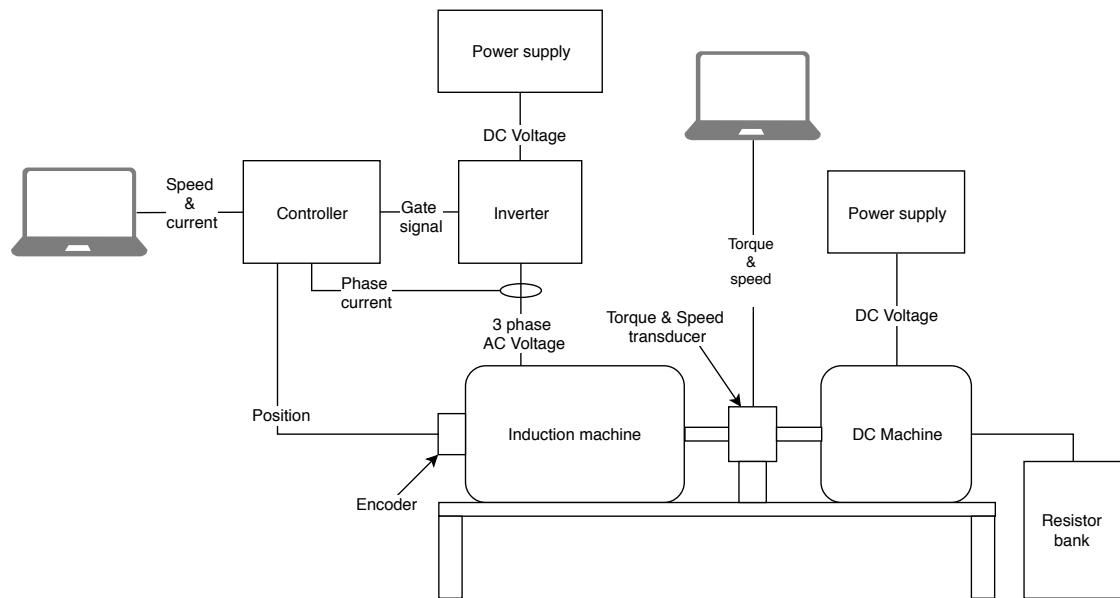


Figure 9.1.: System validation test setup diagram

To validate the system in a controlled environment, the induction machine is placed on a test bench. To represent the load that the Go-Kart and driver would provide to the system, a DC Machine and a resistor bank is used. By increasing the resistance on the resistor bank, the DC machine is applying a load torque on the rotor axis. This way the load can be controlled.

No information about the torque is given to the system, so to verify that the system can provide the expected torque, a torque and speed transducer is installed. The transducer is providing information about the applied torque and can be compared with the given torque command from the torque pedal.

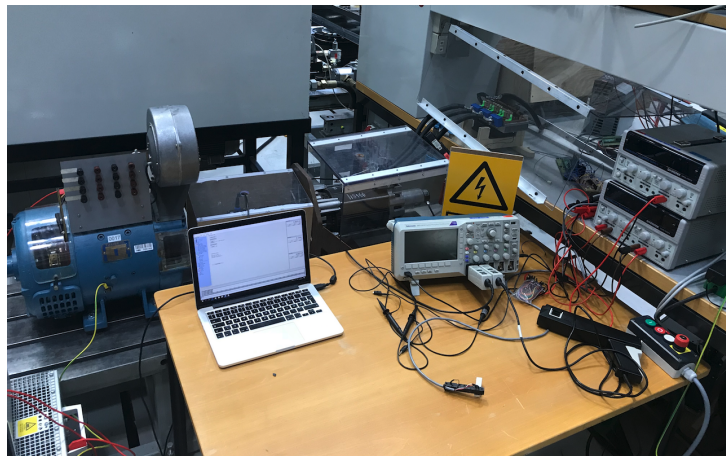


Figure 9.2.: System validation test setup

Equipment	Type
DC Machine	Thrigé LAT 160
Resistor bank	Danoetherm ZRF 55/600 914
Main power supply	LAMBDA ESS 50-300-2-D
Torque transducer	Lorenz DR-3000
Lab DC power supply	GW Instek GPS-4303
Oscilloscope	Tektronix TBS1064

Table 9.1.: Test equipment

Req#	Test	Status
1.1	Drive the car manually	The powertrain needs to be installed on the Go-Kart platform
1.2	Apply a torque on the rotor, from an external machine without supplying the IM	The controller needs to be setup for generative mode
1.3	Apply load torque on the rotor and give a torque command higher than the load torque	Test can be conducted on a test bench
1.4	When driving the machine, press emergency button	Emergency button needs to be installed, but can be tested on test bench
1.5	Add variable power supply, and lower the voltage to the lower limit of the batteries	Test can be conducted on a test bench
2.1	Full load test, measure speed and applied torque to determine the power output	Test can be conducted on a test bench
2.2	Drive the Go-Kart with mixed driving, until the lower voltage levels of the batteries are reached	The powertrain needs to be installed on the Go-Kart platform
2.3	Drive the car and measure the top speed in a straight line	The powertrain needs to be installed on the Go-Kart platform

Table 9.2.: Functional- and performance requirements, from Table 1.5.1 and Table 1.5.2

9.1. Conclusion on system validation test

The system start-up is conditioned by a speed limitation. If the speed is not beneath the given speed limit, the enable output for the gate drivers will be false. The measured speed was exceeding the limit, when the system was turned on and thereby not allowing the gate drives to run. The problem was found to be a loose connection making the input floating, which could cause the misreading due to disturbance. The three current sensors used for the controller as a reference, was showing unwanted behaviour for two of the three phases. Phase "a" showed the maximum current for the sensors, which is 300 A. Phase "b" showed around 150 A where Phase "c" showed the expected value of 0 A. The current sensors were dismounted but the current reading was unchanged. Unfortunately we did not have time to debug the system, and find the root-cause of the problem due to time limitation.

10. Conclusion

The transition from combustion engine to an electrical machine requires implementation of the objectives stated in the system requirements. The main objective of the project was to develop a 3-phase inverter capable of supplying an induction machine at full power, bi-directional power flow and a induction motor controller capable of providing stable dynamic torque control using sensor vector control. Comparing final state of the system with project objective leaves the control of bi-directional power flow to be fulfilled, because it was not implemented. Even though bi-directional power flow control is not implemented, the inverter is design to be of bi-directional power flow which leaves the possibility for improvement in the future. The inverter was designed as planned, and verified with various test that proved to be satisfactory. As for induction motor controller, simulation provided satisfied results but due to time constraints, proper validation could not be done. Same applies with safety management, which is not implemented because of time constrains mentioned before. At the end, it can be concluded that for this kind of task, more time for developing and testing is needed before system can be used in reliable and safe manners.

11. Future work

Motor controller

The motor controller is only capable of running the machine in motor mode. For future work, the controller should also be able to control the machine in generative mode. This is needed to be able to use the bi-directional capability of the inverter, as intended.

Inverter optimisation

The inverter including the gate drivers layout is prototype layouts, making it easier to access the points for measuring and verifying the design functionality. The overall size can be reduced by changing the positioning of the gate drivers and reducing the footprint size by producing the inverter on a single board, instead of three separate phase legs.

Safety

According to the requirement 1.4 in Table 1.5.1, the system should be able to disconnect battery in case of emergency. If the powertrain will be installed back on the Go-Kart chassis, this has to be implemented as a protection.

System validation

The system was not validated in the time frame of the project, but a full setup was built, ready for testing. A couple of tests need to be conducted to validate the system according to the functional- and performance requirements by testing according to ??

Bibliography

- [1] Scancon Encoders. *Encoder Datasheet*. 2009.
- [2] Optima. *Optima Batteries Users Guide*. 2005.
- [3] Mathworks. *Generic Model of a Battery in Simscape*. 2018. URL: <https://se.mathworks.com/help/physmod/sps/powersys/ref/battery.html>.
- [4] Thomas A Lipo. *Vector control and dynamics of AC drives*. Vol. 41. Oxford university press, 1996.
- [5] Mohd Hadi Anuar Mohd Fakharuzi et al. “Design and testing of inertia dynamometer for prototype fuel cell electric vehicle”. In: *ARPN Journal of Engineering and Applied Sciences* 10.17 (2015), pp. 7416–7422.
- [6] PTB-Braunschweig. 2007. URL: www.ptb.de/cartoweb3/SISproject.php.
- [7] G Kohlrusz and D Fodor. “Comparison of scalar and vector control strategies of induction motors”. In: *Hungarian Journal of Industry and Chemistry* 39.2 (2011), pp. 265–270.
- [8] Charles L Phillips and Royce D Habor. *Feedback control systems, 4th Edition*. Simon & Schuster, 2000.
- [9] Zulkifilie Bin Ibrahim et al. “Simulation investigation of SPWM, THIPWM and SVPWM techniques for three phase voltage source inverter”. In: *International Journal of Power Electronics and Drive Systems* 4.2 (2014), p. 223.
- [10] John A Houldsworth and Duncan A Grant. “The use of harmonic distortion to increase the output voltage of a three-phase PWM inverter”. In: *IEEE Transactions on Industry Applications* 5 (1984), pp. 1224–1228.
- [11] Marko Kettunen Mika Ikonen Ossi Laakkonen. “TWO-LEVEL AND THREE-LEVEL CONVERTER COMPARISON IN WIND POWER APPLICATION: choose wisely”. In: *Department of Electrical Engineering Lappeenranta University of Technology* (2001).

Chapter Bibliography

- [12] Josef Lutz et al. *Semiconductor Power Devices*. Springer, 2011. Chap. Chapter 9.
- [13] Carl Blake and Chris Bull. “IGBT or MOSFET: choose wisely”. In: *International Rectifier* (2001).
- [14] NXP Semiconductors. *Power MOSFET Selecting MOSFFETs and Consideration for Circuit Design*. Visit date: 27-05-2018. <https://toshiba.semicon-storage.com/info/docget.jsp?did=13416>, 2018.
- [15] Paul Horowitz, Winfield Hill, and Ian Robinson. *The art of electronics*. Vol. 2. Cambridge university press Cambridge, 1980.
- [16] Infineon. *PT007N06N, Datasheet*. Visit date: 04-05-2018. Farnell. http://www.farnell.com/datasheets/1932532.pdf?_ga=2.144156147.752691451.1525433148-1457305428.1519985450, 2018.
- [17] Infineon. *PT012N08N5, Datasheet*. Visit date: 04-05-2018. Farnell. http://www.farnell.com/datasheets/2117680.pdf?_ga=2.211764563.752691451.1525433148-1457305428.1519985450, 2018.
- [18] nexperia. *AN11158, Understanding power MOSFET data sheet parameters*. Visit date: 09-12-2017. NXP Semiconductors. <https://assets.nexperia.com/documents/application-note/AN11158.pdf>, 2017.
- [19] Andreas Kiep Dr.Dusan Graovac Marco Purschel. “MOSFET POWER Losses Calculation using the data-sheet parameter”. In: (2006).
- [20] Michael Salcone and Joe Bond. “Selecting Film Bus Link Capacitors For High Performance Inverter Applications”. In: (2009).
- [21] Sauer Danfoss. *Motor Datasheet*. 2004.
- [22] Panasonic. *Conductive polymer hybrid aluminum electrolytic capacitors*. 2018.
- [23] Broadcom. *ACPL-C870-000E, Datasheet*. Visit date: 18-04-2018. Broadcom. <https://docs.broadcom.com/docs/AV02-3563EN>, 2018.
- [24] LEM. *LA200-P, Datasheet*. Visit date: 02-04-2018. elfadistrelec. https://www.elfadistrelec.dk/Web/Downloads/_t/ds/LA200P_eng_tds.pdf, 2018.

A. appendix

A.1. Schematics and PCB-layout

This first appendix sections contain the wiring diagram for the hardware, followed by the board layout, schematics and BOM for each of the boards in the project. Presented in the following order:

1. Wiring diagram
2. Modular Inverter Phase
3. Gate driver
4. DC chopper
5. Interface
6. Current measurement board

Each section contains in order:

1. Board photo
2. Bill of materials
3. Schematic
4. PCB layout

A.1.1. Wiring diagram

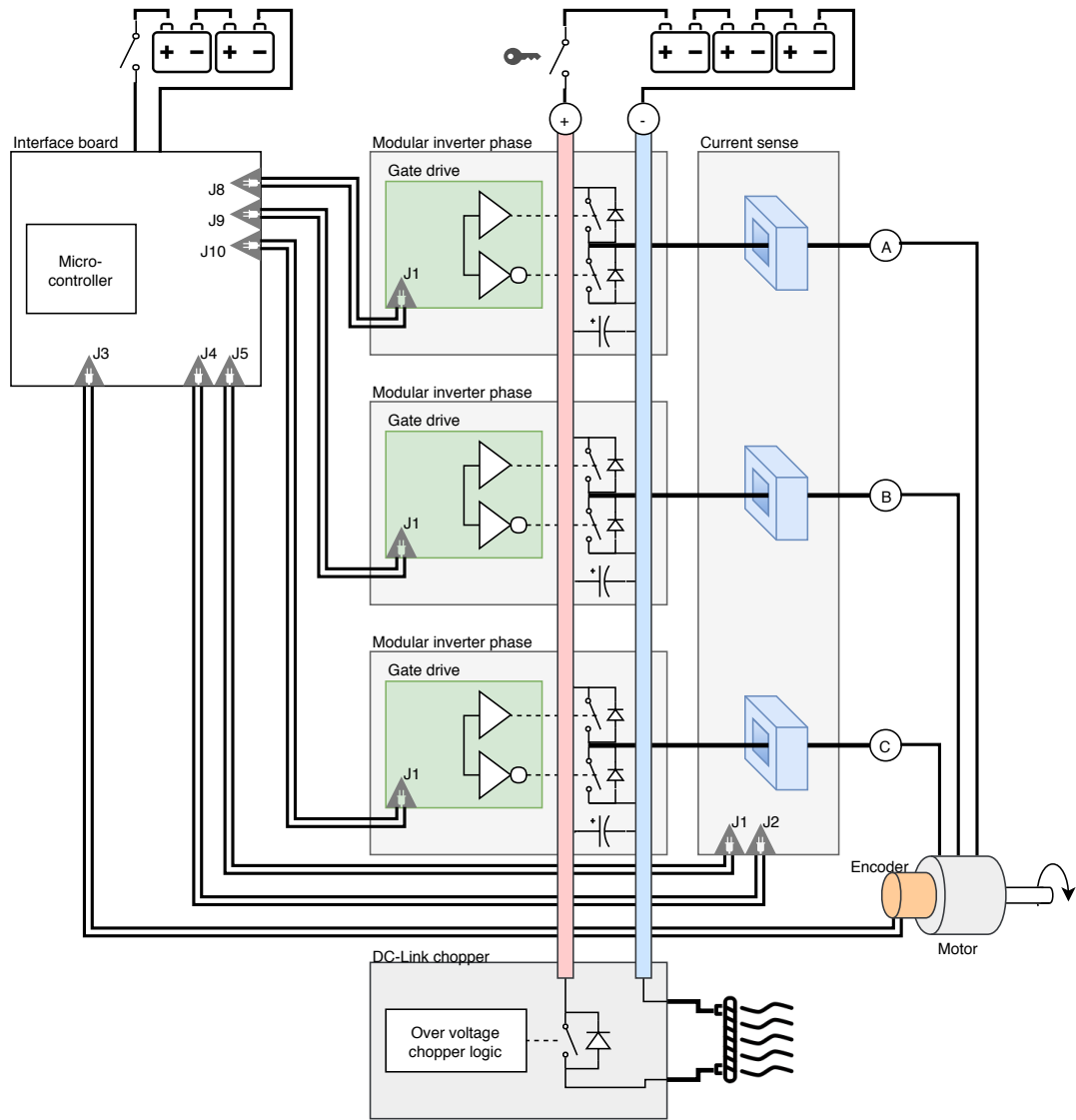


Figure A.1.: Wiring diagram

A.1.2. Modular Inverter Phase

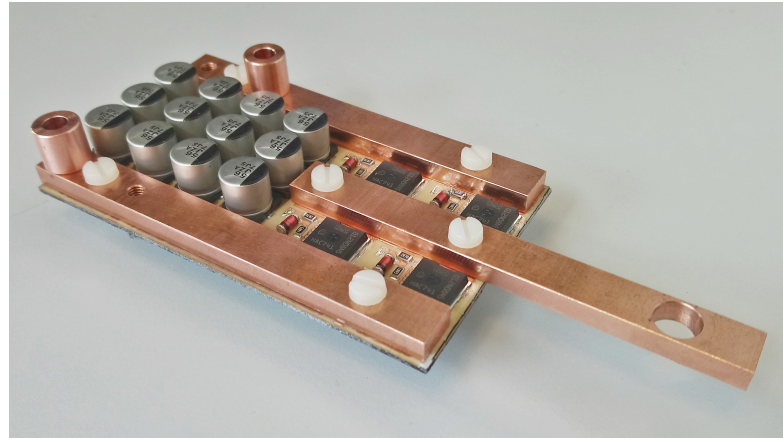


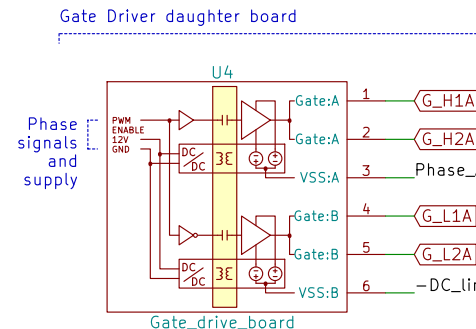
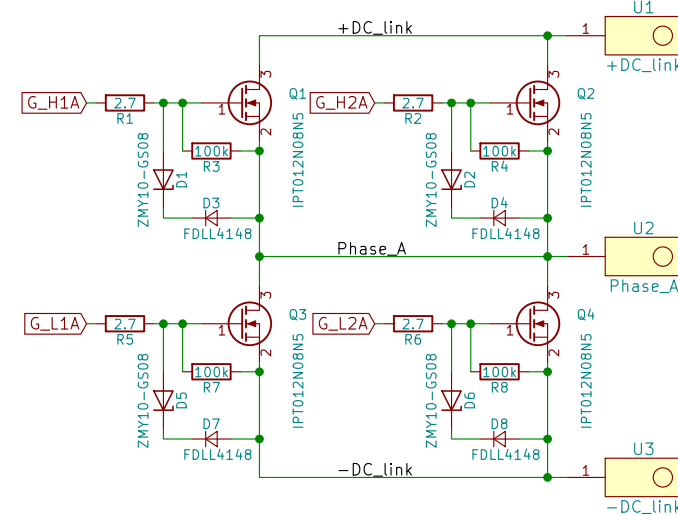
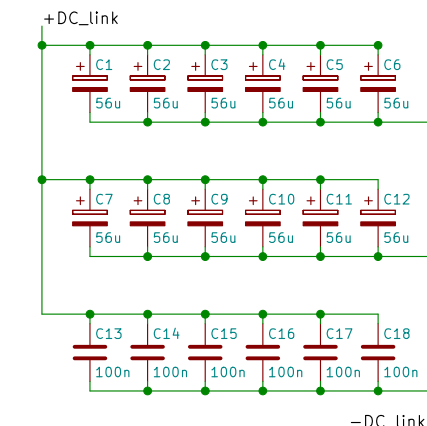
Figure A.2.: Modular Inverter Phase

Ref	Qnty	Value
C1, C2, C3, C4, C5, C6, C7, C8, C9, C10, C11, C12	12	56u
C13, C14, C15, C16, C17, C18	6	100n
D1, D2, D5, D6	4	ZMY10-GS08
D3, D4, D7, D8	4	FDLL4148
Q1, Q2, Q3, Q4	4	IPT012N08N5
R3, R4, R7, R8	4	100k
R1, R2, R5, R6	4	2.7
U1	1	+DC_link
U2	1	Phase_A
U3	1	-DC_link
U4	1	Gate_drive_board

Table A.1.: BOM for single inverter phase leg

1 2 3 4 5 6

A

**Phase leg****DC-Link Cap. bank**

B

C

D

Two level inverter with DC-Link capacitor bank
Designed for <45VDC input, and up to 355A peak output current
A custom gate driver board designed for this application is used



AALBORG UNIVERSITET

Appendix A.1.2

File: Inverter.sch

Title: Modular Inverter Phase

Size: A4 Date: 2018-04-13

KiCad E.D.A. kicad 4.0.7

Rev: 1.0

Page: 1/1

1 2 3 4 5 6

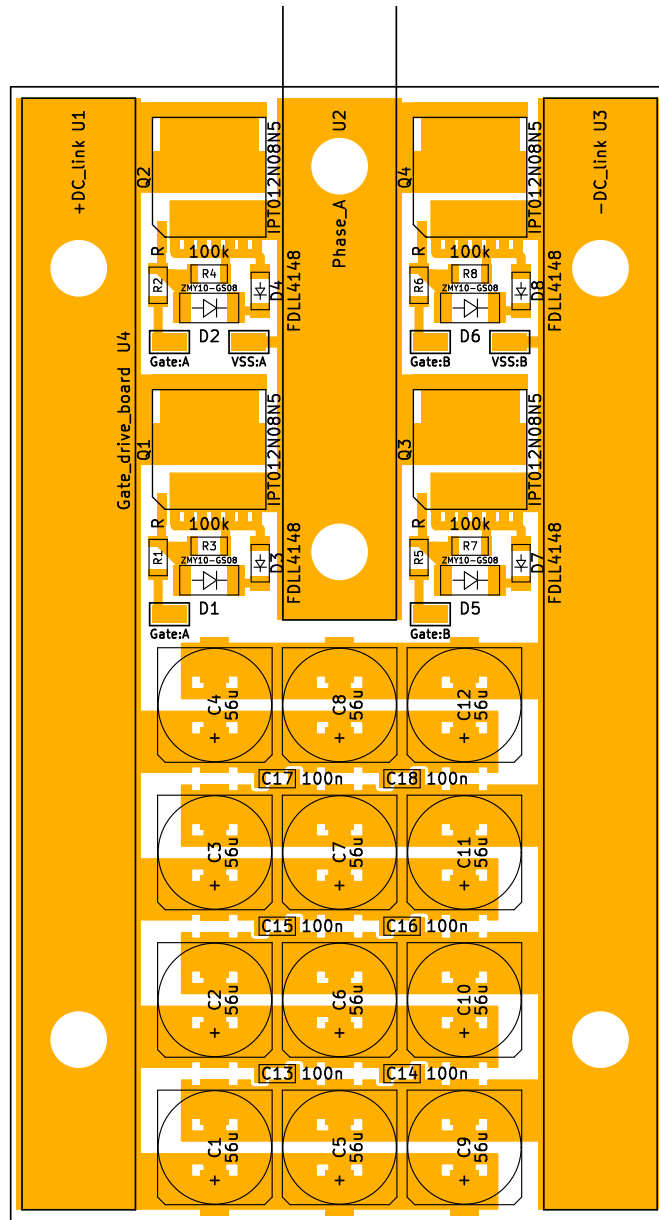


Figure A.3.: PCB layout for the Modular inverter. Top view, Scale: 3:2

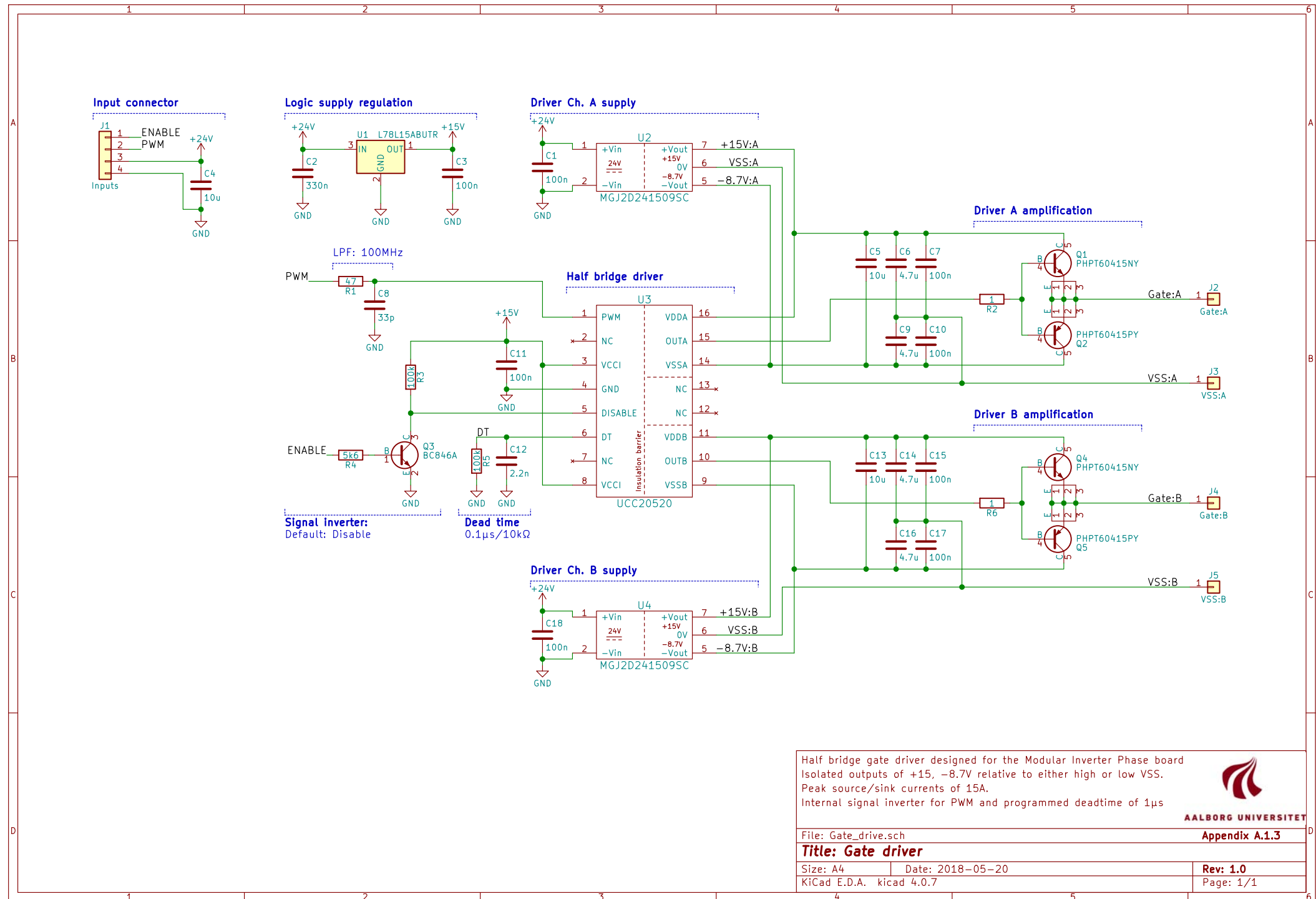
A.1.3. Gate drive



Figure A.4.: Gate driver board

Ref	Qty	Value
C2	1	330n
C8	1	33p
C1, C3, C7, C10, C11, C15, C17, C18	8	100n
C12	1	2.2n
C4, C5, C13	3	10u
C6, C9, C14, C16	4	4.7u
J1	1	WR-WTB 4 pin
Q3	1	BC846A
Q4, Q1	2	PHPT60415NY
Q5, Q2	2	PHPT60415PY
R1	1	47
R4	1	5k6
R3, R5	2	100k
R2, R6	2	1
U1	1	L78L15ABUTR
U2, U4	2	MGJ2D241509SC
U3	1	UCC20520

Table A.2.: BOM for a single gate driver board



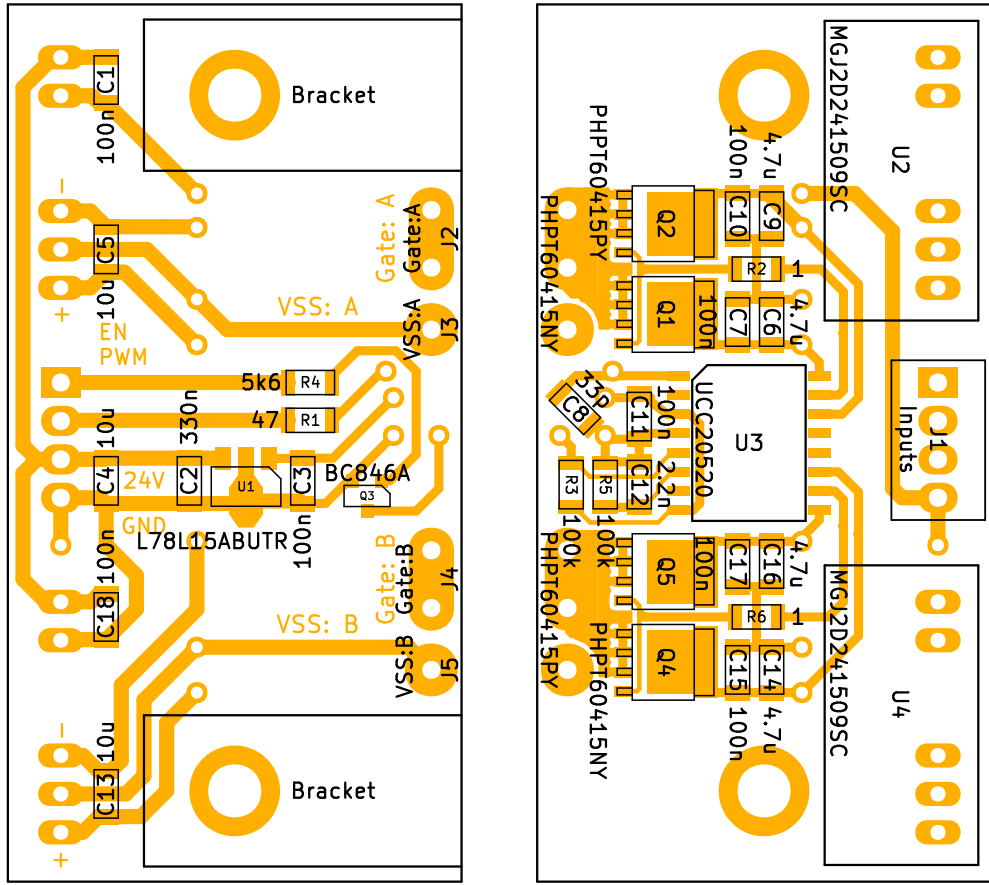


Figure A.5.: PCB layout for the Gate drive board. Left: Top view, Right: Bottom view,
Scale: 2:1

A.1.4. DC Chopper



Figure A.6.: DC Chopper Board

Ref	Qnty	Value
R1	1	430k
R2	1	3k
R3	1	39k
R4	1	5.1k
R5	1	30k
R6	1	15k
R7	1	1.6
R8	1	220
R9	1	2.4k
C1,C4	2	0.1u
C2,C3	2	1u
U1	1	OPA197IDGKR
U2	1	LM317HV
U3	1	FAN3122CMX
D1	1	NTST20100CTG
Q1	1	IPT012N08N5ATMA1

Figure A.7.: BOM for a DC Chopper board

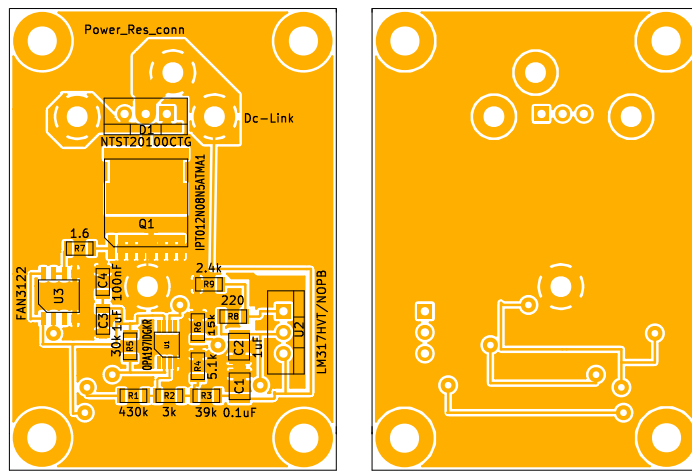
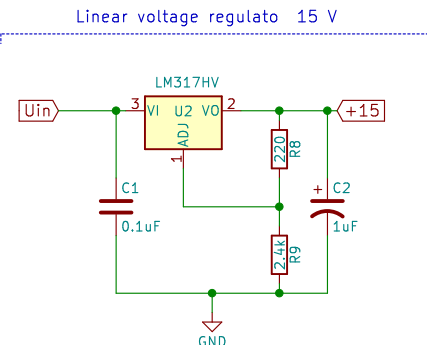
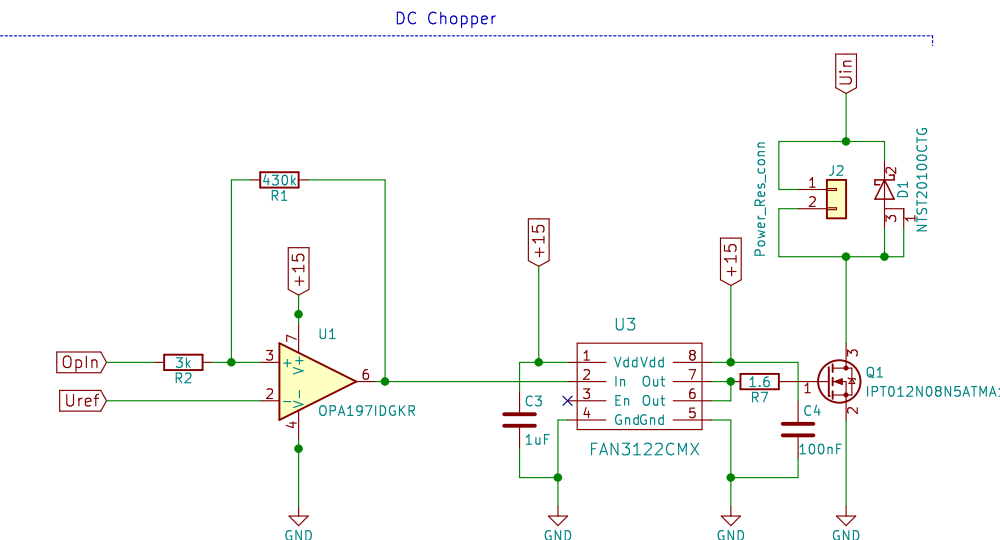
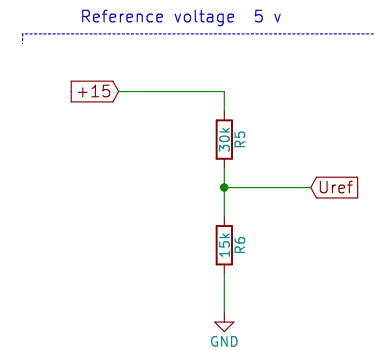
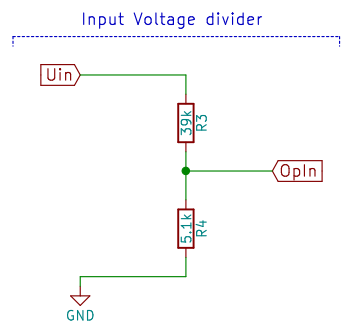
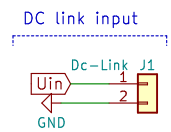


Figure A.8.: PCB layout for the DC Chopper. Left: Top view, Right: Bottom view,
Scale: 3:2



Dc Chopper circuit using schmitt trigger as a controller



AALBORG UNIVERSITET

Appendix A.1.4

File: Ucenje.sch

Title: Dc Chopper

Size: A4 Date: 2018-05-01

KiCad E.D.A. kicad 4.0.7

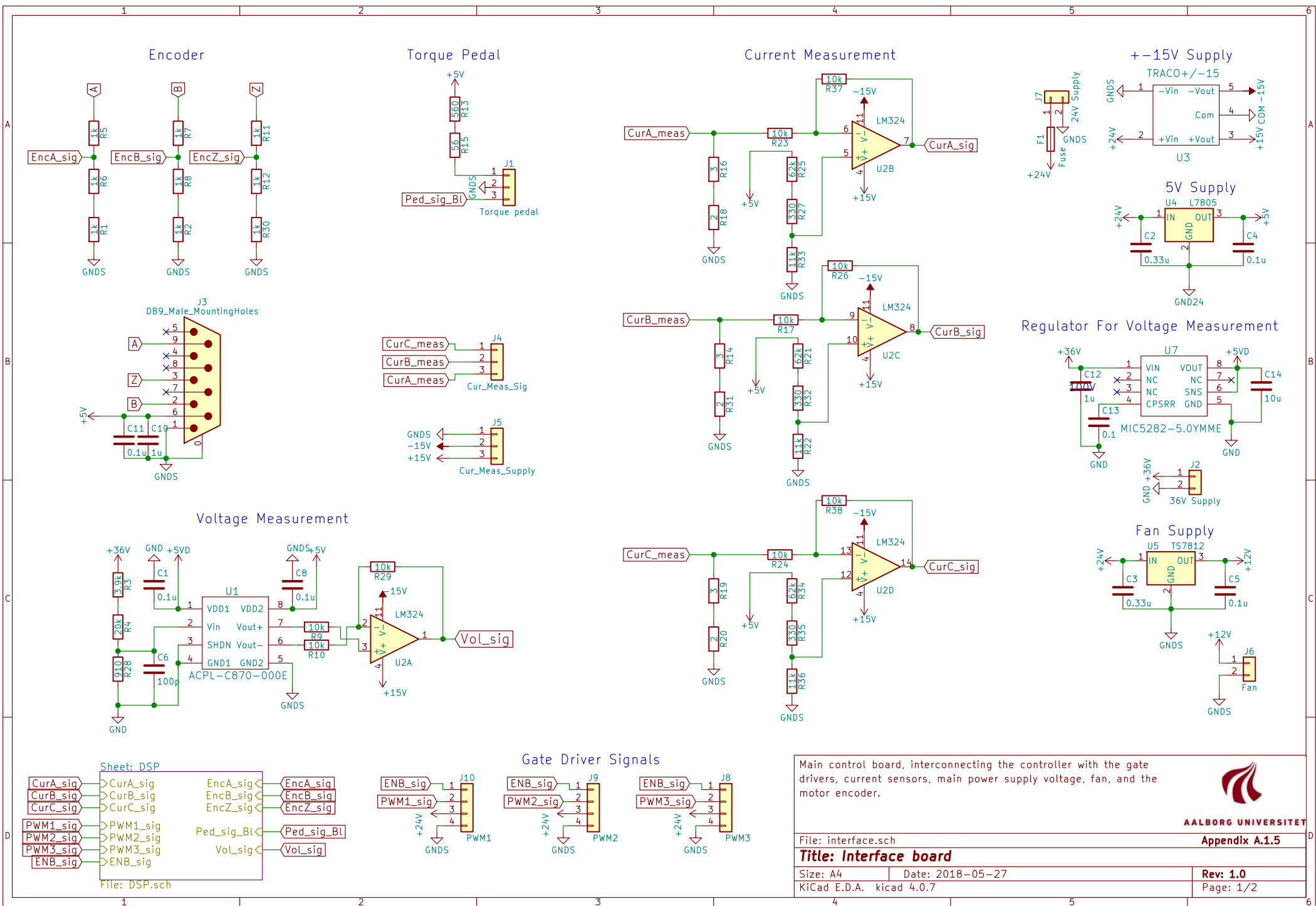
Rev: 1.0

Page: 1/1

A.1.5. Interface board

Ref	Qty	Value
R1, R2, R5, R6, R7, R8, R11, R12, R30	9	1k
R9, R10, R17, R23, R24, R26, R28, R29, R37, R38	10	10k
R15	1	56
R13	1	560k
R22, R33, R36	3	11k
R18, R20, R31	3	2k
R14, R16, R19	3	3k
R27, R32, R35	3	330
R21, R25, R34	3	62k
R4	1	68k
R3	1	4.7k
C1, C4, C5, C8, C11	5	0.1u
C10, C12, C13	3	1u
C6	1	100p
C2, C3	3	0.33u
U1	1	ACPL-C870-000E
U2	1	LM324 4xOpAmp
U3	1	TRACO TEL 15-2423
U4	1	L7805
U5	1	TS7812
U6	1	F28075 Socket
U7	1	MIC5282-5.0YMME
F1	1	800mA Glass fuse
J2, J6, J7	3	WR-WTB 2 pin
J1, J4, J5	3	WR-WTB 3 pin
J8, J9, J10	3	WR-WTB 4 pin
J3	1	RS422 male-connector

Table A.3.: BOM for Interface board



A

B

C

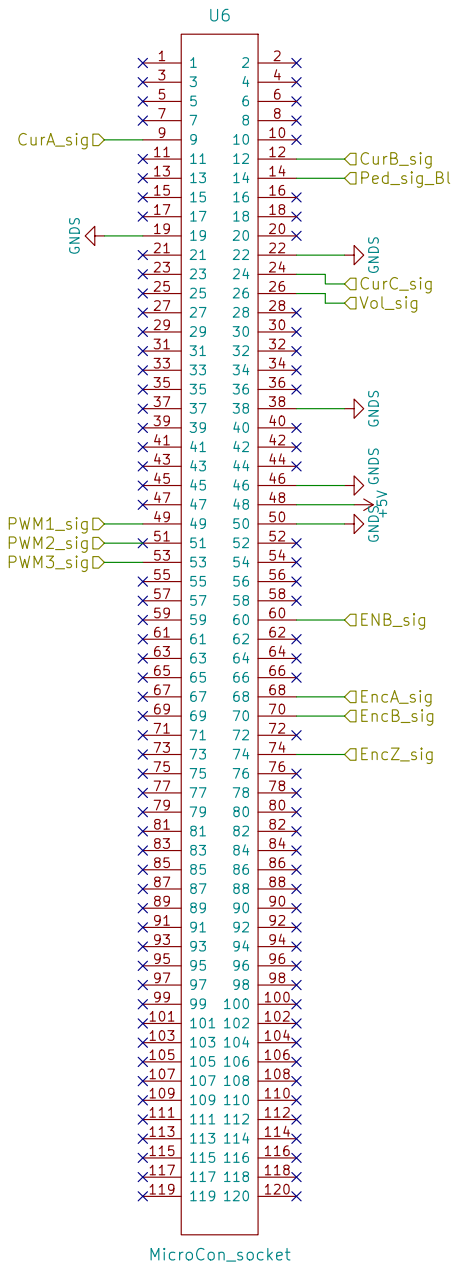
D

A

B

C

D



Connector for a Texas Instruments Picolo F28075 ControlCard



AALBORG UNIVERSITET

Appendix A.1.5

File: DSP.sch

Title: Interface board

Size: A4 Date: 2018-05-27

KiCad E.D.A. kicad 4.0.7

Rev: 1.0

Page: 2/2

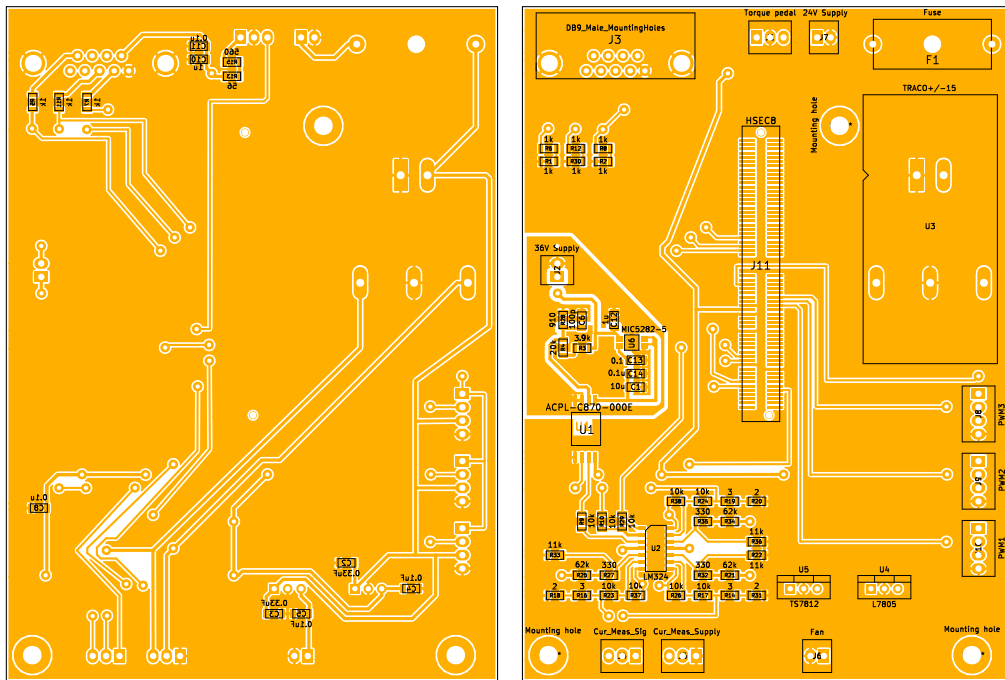


Figure A.9.: PCB layout for the Interfaceboard. Left: Bottom view, Right: Top view,
Scale: 4:5

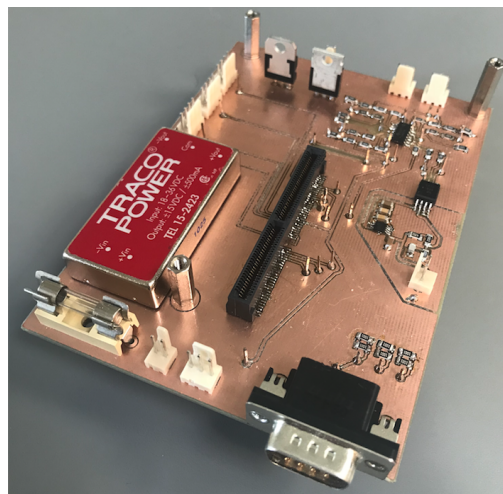


Figure A.10.: Interface board

A.1.6. Current measurement board

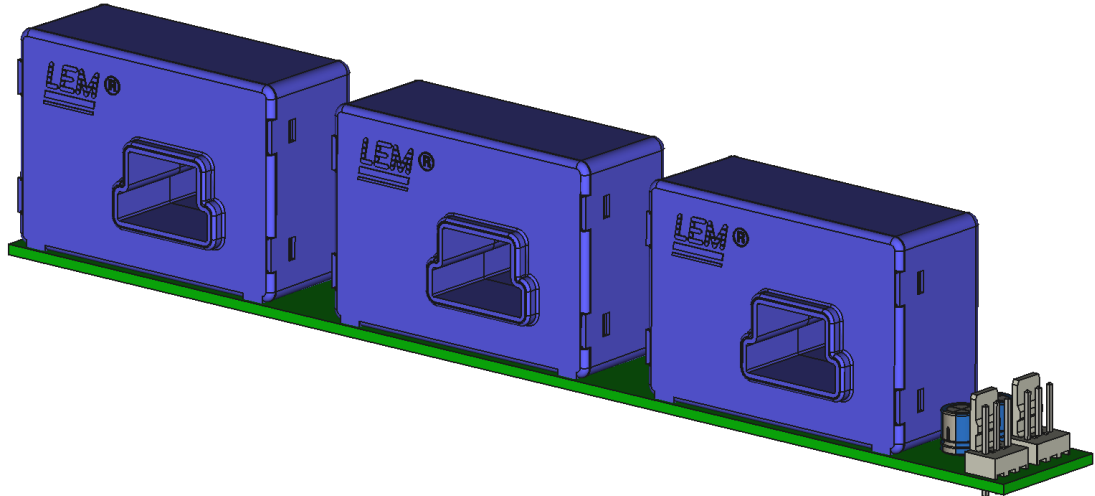
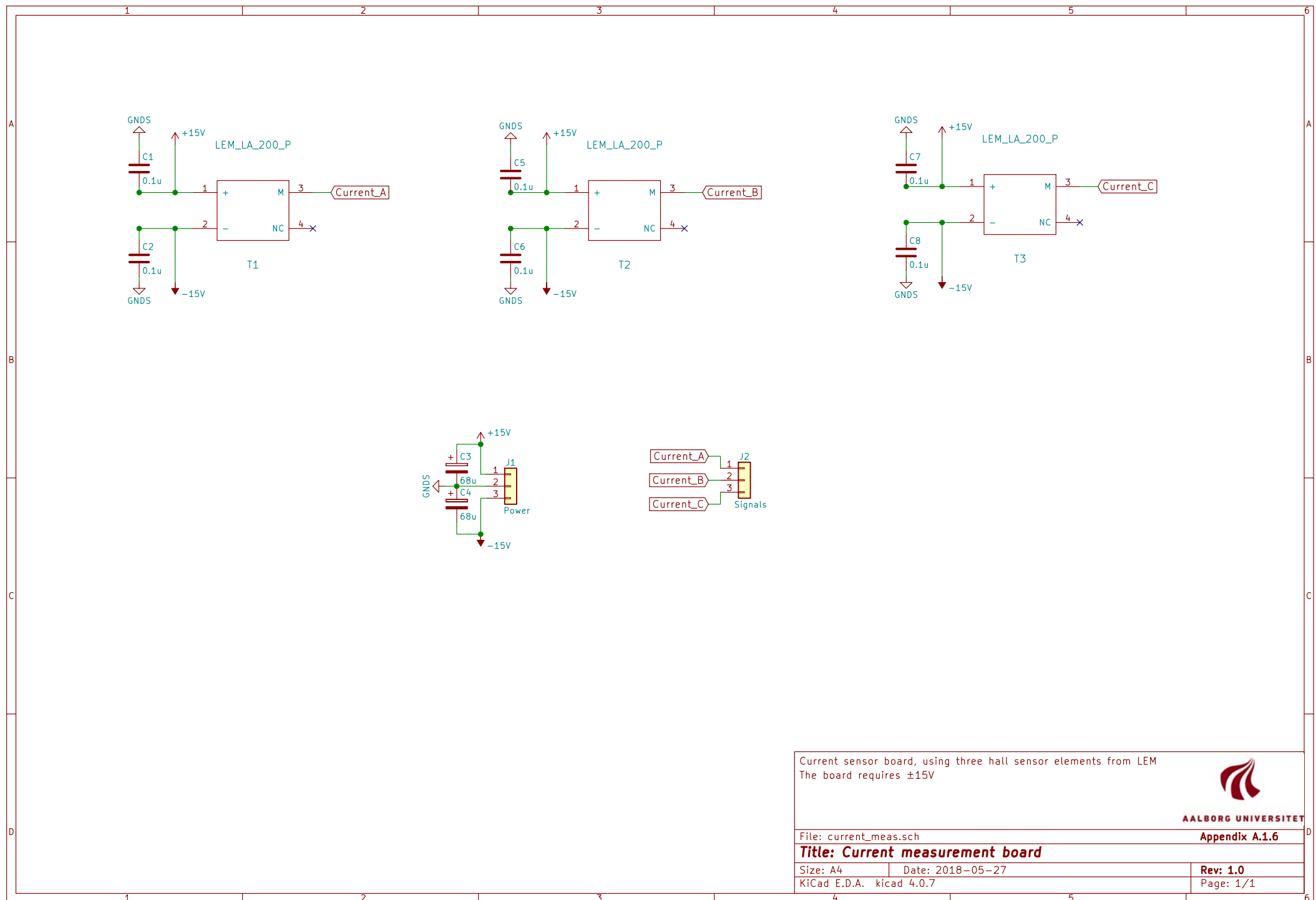


Figure A.11.: Current measurement board

Ref	Qty	Value
C1, C2, C5, C6, C7, C8	6	0.1u
C3, C4	2	68u
J1, J2	2	WR-WTB 3 pin
T1, T2, T3	3	LEM LA-200P

Table A.4.: BOM for Current measurement board



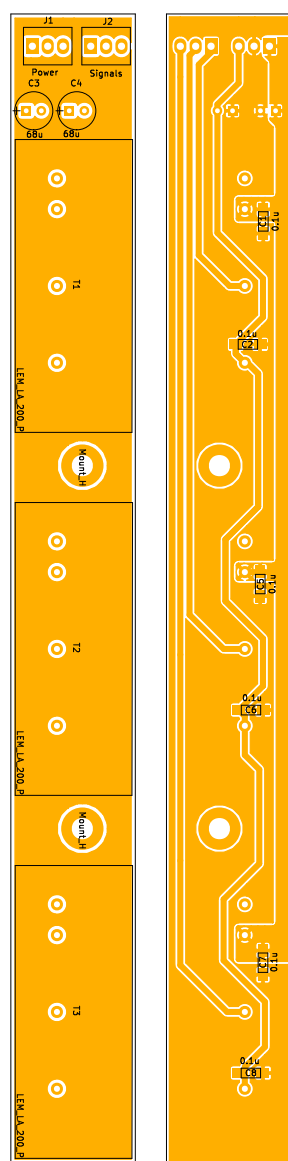


Figure A.12.: PCB layout for the Current measurement board. Left: Top view, Right: Bottom view, Scale: 4:5

A.2. Mechanics

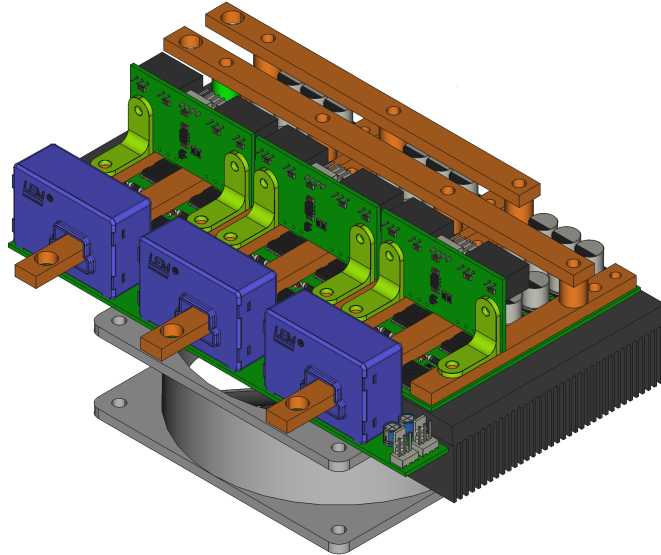
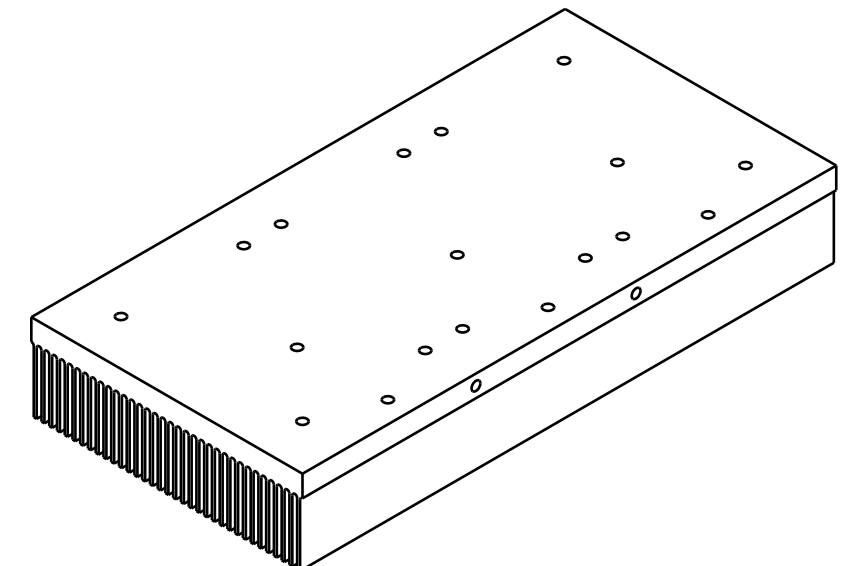
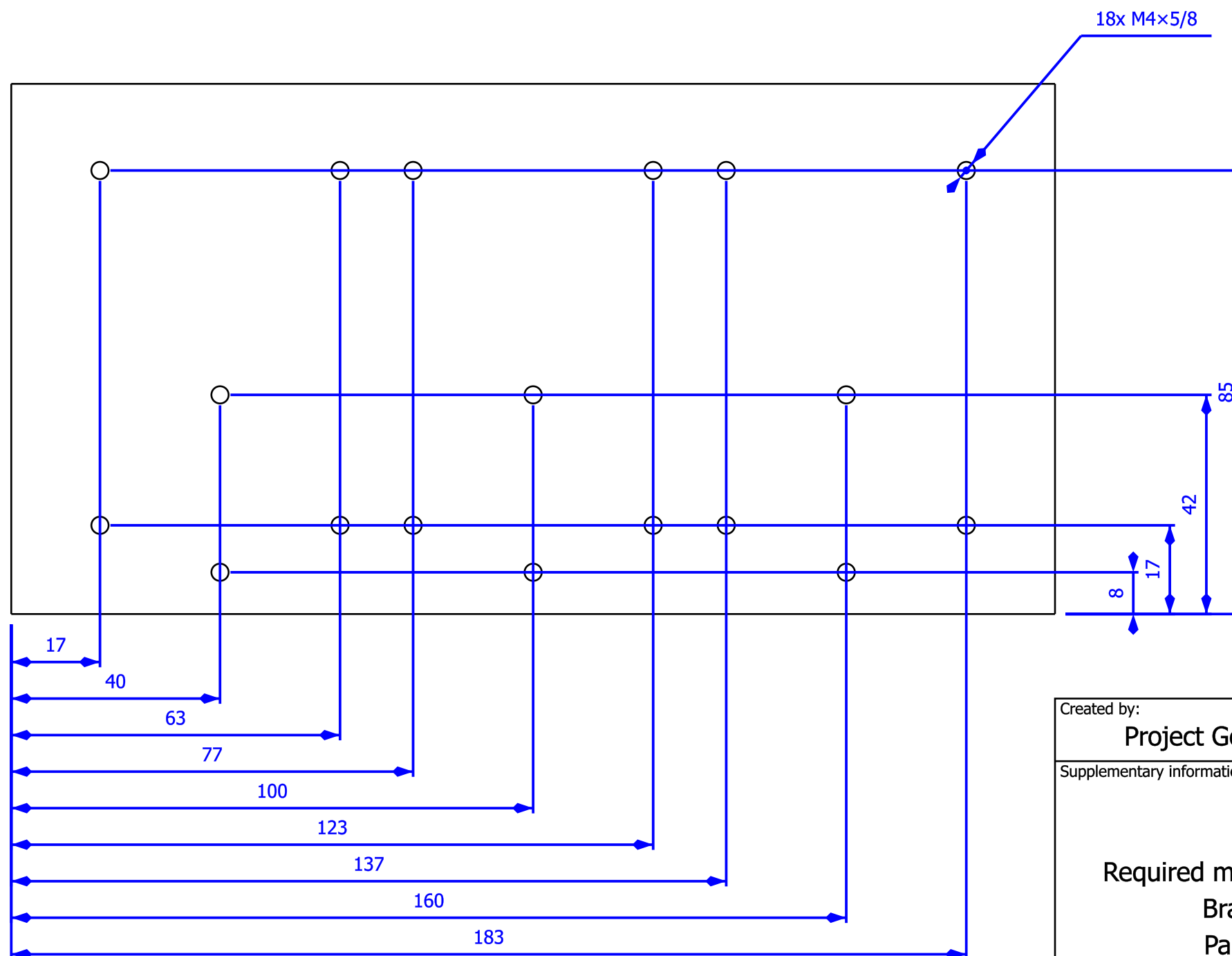
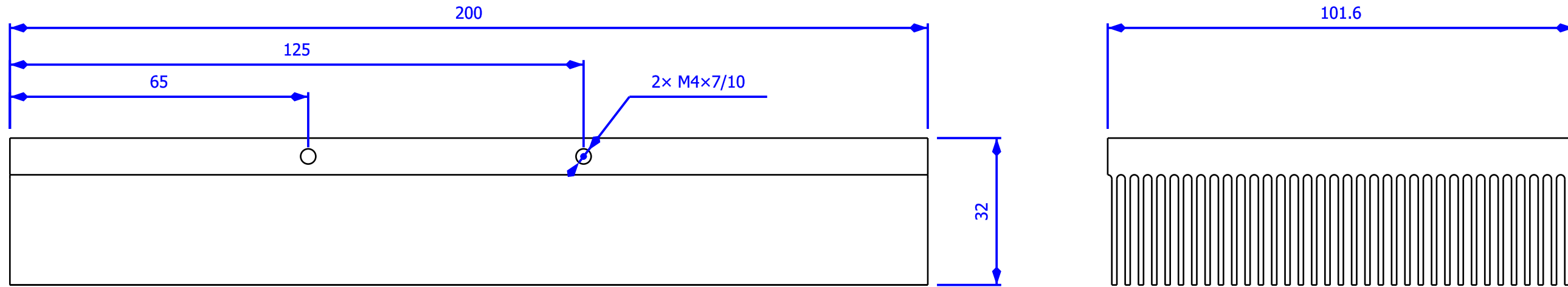


Figure A.13.: Assembled inverter

This appendix contains the mechanical parts required for the inverter. Presented in the following order:

1. Bus bar: Rail
2. Bus bar: Phase
3. Bus bar: Supply +
4. Bus bar: Supply -
5. Bus bar: Spacer
6. Heat sink



Created by:
Project Go-Kart

Supplementary information:

Inverter heat sink
Required modifications to the bought heatsink
Brand: HS Marton Aerospace
Part no: 890SP-02000-A-100



13/05/2018 REV A

Size: A3 Sheet: 1 / 1 Scale: 1:1

Part number: 6

Drawing number: 6

Date: 13/05/2018 Revision: REV A

A.3. Calculation

A.3.1. Calculating I_{dRef}

The rated peak current:

$$I_p = I_n \cdot \sqrt{2} = 267.49 \text{ A} \quad (\text{A.3.1})$$

The stator voltage in dq reference frame:

$$\bar{u}_{dqs} = U_n \cdot \sqrt{2} = 34 \text{ V} \quad (\text{A.3.2})$$

The stator current in dq reference frame:

$$i_{dqs} = I_p \cdot e^{-j\phi} = 203.2 - j173.84 \quad (\text{A.3.3})$$

where $\phi = 0.707$ is the power factor angle.

The synchronous speed in *rad/sec* is $\omega_\theta = 2 \cdot \pi \cdot f_n = 364.4 \text{ rad/sec}$.

The stator flux in dq can be calculated from Equation 4.1.17:

$$\bar{\lambda}_{dqs} = (0.001703 - j0.09114) \text{ Wb.}$$

Then the rotor flux in dq can be calculate from Equation 4.1.21:

$$\bar{\lambda}_{dqr} = (-0.01134 - j0.0873) \text{ Wb, and in magnitude } |\bar{\lambda}_{dqs}| = 0.084415 \text{ Wb}$$

Finally i_{dRef}

$$i_{dRef} = \frac{|\bar{\lambda}_{dqs}|}{L_m} = 222.14 \text{ A} \quad (\text{A.3.4})$$

In the same way, $i_{dRef} = 222.27 \text{ A}$ for $P_n = 7.3 \text{ kW}$.